

AD NO. AD623050

DDC FILE COPY



THE GENERAL MILLS ELECTRONICS GROUP

December 1, 1961

~~FIELD PROJECTS RESEARCH FILE COPY~~

"GUSSES" F-2

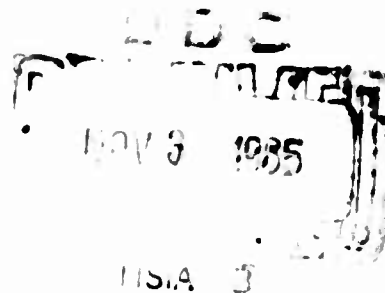
COMMUNICATION VIA  
ARTIFICIAL SCATTERERS  
PLACED BELOW THE  
IONOSPHERE

REPORT NO. 2245

NONR 1589127

Prepared for:

Department of the Navy  
Office of Naval Research  
Washington 25, D.C.



Submitted by:

*Roy P. Schindler*  
Roy P. Schindler  
Senior Engineer

Approved by:

*O. Stuetzer*  
O. Stuetzer  
Director of Development

Project No. 85043

*John E. Barkley*  
John E. Barkley  
Technical Director

Research and Development  
2003 East Hennepin Avenue  
Minneapolis 13, Minnesota

**Reproduction in whole or in part is permitted  
for any purpose of the United States Government.**

**Prepared by:**

**H. Raabe  
S. Steinberg  
S. P. Jones  
G. Witnah  
B. Schmidt  
A. Belmont  
D. Dartt  
O. Stuetzer**

## TABLE OF CONTENTS

Section	Title	Page
I	INTRODUCTION AND SUMMARY	1-1
II	SCATTERING BY ARTIFICIAL DEVICES	2-1
	A. The Scatter Communication Path	2-1
	1. Scatter Path Geometry	2-1
	2. Scatter Path Efficiency	2-3
	B. Artificial Scatterers with Random Spacing	2-6
	1. Small Metallized Bubbles	2-7
	2. Large Metallized Balloons	2-9
	3. Resonating Devices	2-10
	C. Coherent Scattering by Diffraction Gratings	2-11
	D. Coherent Scattering in a Refractive System	2-14
	E. Practical Scattering Systems	2-21
	1. Characteristics of a Ten-Meter System	2-21
	2. Characteristics of a One-Meter System	2-24
	F. Scatter Experiments	2-32
	1. Backscatter from Spheres	2-35
	2. Forward Scatter from Spheres	2-35
	3. Forward Scatter from Dipole Arrays	2-43
	G. Conclusions	2-46
III	DELIVERY AND SUPPORT OF SCATTERING ELEMENTS	3-1
	A. Experimental Study of the Radiometer Effect to Prevent or Retard Gravitational Settling of Small Particles in the Stratosphere	3-1
	1. Natural Settling of Small Particles	3-1
	2. Studies on the Radiometer Effect	3-5
	a. Background	3-5
	b. Special Particles having a Radiometer Effect	3-8
	c. Experimental Study	3-11
	d. Results of the Experimental Study	3-15
	e. Conclusions of the Experimental Study	3-19
	B. Delivery and Support of Large Scattering Elements	3-19
	1. Introduction	3-19
	2. Support of the Scattering System in the Atmosphere	3-20
	a. Aerodynamic Systems	3-20
	b. Buoyancy Systems	3-22
	3. Delivery of Balloon-Supported Scattering Systems	3-29



## TABLE OF CONTENTS (Continued)

Section	Title	Page
	C. The Effect of Meteorology on the Useful Life of Scattering Elements	3-31
	1. Introduction	3-31
	2. Discussion of Zonal Wind Speeds at 30 km	3-31
IV	BRIEF DESCRIPTION OF THE PROPOSED SYSTEM	4-1
V	PROPOSED PROGRAM	5-1
VI	REFERENCES	6-1
APPENDIX A.	GEOMETRY OF SPACE WITHIN WHICH SCATTERERS WOULD BE USEFUL	A-1
APPENDIX B.	AVERAGE ZONAL COMPONENT OF PREVAILING WIND IN KNOTS BY MONTH AT 10 mb (30 km)	B-1

## LIST OF ILLUSTRATIONS

<b>Figure</b>	<b>Title</b>	<b>Page</b>
2-1	Scatter Path Geometry	2-2
2-2	Locus of Scatterers for Phase Enhancement	2-12
2-3	Spacing of Planes	2-14
2-4	Dipole with Phase Shift	2-15
2-5	Phasor Diagram of Scattered Wave	2-17
2-6	Dipole Equivalent Circuit	2-17
2-7	Scattering Factor versus Normalized Dipole Length	2-20
2-8	Scattering System for Ten-Meter Wavelength	2-23
2-9	Scattering System for One-Meter Wavelength	2-27
2-10	Backscatter Power versus Angle $\theta$	2-29
2-11	Change in Field Pattern for Three Configurations of 3/8-inch Spheres (Forward Scatter)	2-30
2-12	Change in Field Pattern for Two Configurations of 3/8-inch Spheres (Forward Scatter)	2-31
2-13	Change in Field Pattern for Several Arrangements of Dipole Pairs (Forward Scatter)	2-33
2-14	Block Diagram of X-Band Electromagnetic Scattering Facility	2-34
2-15	Diagram of Backscatter Measurement Facility	2-36
2-16	Number of 3/8-inch Spheres (N) versus Back-scattered Power	2-37
2-17	Arrangement No. 1	2-38
2-18	Arrangement No. 2	2-39
2-19	Diagram of Forward Scatter Facility	2-40

## LIST OF ILLUSTRATIONS (Continued)

Figure	Title	Page
2-20	Arrangement of Scattering Spheres for Results of Figures 2-11 and 2-12 with Phase Reinforcement at 20 Degrees	2-42
2-21	Placements of Dipoles for Phase Reinforcement at 20 Degrees	2-44
2-22	Cylindrical Polystyrene Foamed Plastic Model for Mounting of 24 Dipole Pairs	2-45
3-1	Variation of Slip Coefficient	3-2
3-2	Settling Velocity in the Stratosphere	3-3
3-3	Settling at 30 km for Spheres, Bubbles, and Cylinders	3-6
3-4	Radiometer Effect on Micron-Size Particles. Data taken from Rosenblatt	3-9
3-5	Radiometer Force on Particles of Various Sizes	3-10
3-6	Particle which would Exhibit Negative Photo-phoresis or Motion toward the Sun	3-11
3-7	Experimental Set-Up Used to Study the Radiometer Effect	3-12
3-8	Schematic Diagram of Experimental Set-Up Used to Study the Radiometer Effect	3-13
3-9	Effect of Varing Radiation Intensity on a 13-mm Diameter, Thin-Walled Hollow Quartz Sphere	3-16
3-10	Effect of Varying Size and Shape on Force Exerted by the Radiometer Effect	3-17
3-11	Natural-Shape Balloon	3-27
A-1	Geometry of Space Useful for Scattering	A-3

## I. INTRODUCTION AND SUMMARY

The possibility of creating a stable, efficient scatter propagation communication path below the ionosphere has been investigated by General Mills, Inc. This communication path would be free from interruptions due to ionospheric storms. Quite often communication by sky wave propagation is made impossible at any frequency and only ground waves and tropospheric scatter are useful for propagation beyond line-of-sight. Neither the low frequency channels, which must be resorted to for efficient ground wave transmission, nor tropospheric scatter circuits are very useful for tactical communication purposes. Both require high power, and elaborate antenna structures. Communication by tropospheric scatter is normally limited to a few hundred miles.

At present it is possible to re-establish high frequency communication paths by using high flying aircraft as radio relay stations. Two points 630 miles apart can be linked by one aircraft flying at 50,000 feet at the path midpoint. This solution is quite expensive. Also, because it would very likely take an hour or two to get an aircraft at the proper location it is not feasible in coping with a sudden ionospheric disturbance which may only last 30 minutes.

The general approach taken in this study was suggested by Dr. William J. Thaler of the Office of Naval Research. Efficient scattering elements are to be generated and placed in the lower stratosphere within line of sight of two stations wishing to communicate.

The majority of the work on this contract has centered on two important considerations; one, what will do the job of scattering, and two, how can we place the scatterers in the proper position and maintain them there. To be considered workable the scattering system must be capable of fulfilling the requirements of both considerations.

From the investigation of forward scatter theory an efficient scattering system was developed. This scattering system consists of a number of tuned dipoles tied together such that scattered energy from each is in phase at the receiver. Because of this coherence effect the number of dipoles required is so small that it is feasible to consider using only one dipole network as the scattering medium. This network could be suspended from or printed on the surface of a balloon.

By utilizing a relatively sophisticated scattering system such as the above, the mass of the scattering system to be sent aloft is minimized. This is very important when one realizes that in many cases the scattering system would have to be replaced every few hours due to weather conditions.

Delivery by rocket appears feasible because the scattering system would be light in weight and collapsible for packaging in a small space. Also, the likelihood of frequent scatterer replacement make rocket delivery attractive. This possibility is examined for the proposed system.

The proposed program includes development of techniques for release and inflation of the scattering system from a small rocket and the conduction of field tests for verification of the theoretical and laboratory work on scatterers performed on this contract.

This study is to some extent incomplete in that a portion of the proposed study was not funded. The unfunded portion of the study was to be an investigation of scatterers whose electrical scatter cross section is large compared to their mechanical cross section. Results of such a study might naturally change our present views.

## II. SCATTERING BY ARTIFICIAL DEVICES

In application to radar, scattering by artificial devices has been given considerably attention, whereby such devices, mostly of the shape of tuned dipoles, are dispersed in the atmosphere as a countermeasure against the operation of a radar set. Since, in general, such radars are monostatic we have a highly special case of back scattering. The theory of back scattering holds, even for bistatic radar systems, because the angle formed by the incident and scattered ray paths is rarely greater than 90 degrees. In application to communication one would like to provide a propagation path beyond the horizon. Therefore, the angle between the incident and the scattered ray paths is sometimes close but never equal to 180 degrees, especially if the scatterers are dispersed at lower altitudes. It will be shown that in this case of forward scattering, special phenomena can be explored which would lead to a greatly increased effectiveness of the scatterers. This is of vital importance to make long range communication by means of artificial scatterers feasible at all.

### A. The Scatter Communication Path

#### 1. Scatter Path Geometry

It is assumed that a single-hop transmission according to Figure 2-1 must be achieved between the transmitter T and the receiver R. To be effective at all, scatterers must be dispersed within the space that is above the two planes which are tangential to the earth at the locations of T and R and below the D layer of the ionosphere. For a detailed discussion of this volume refer to Appendix A. The optimum location is near the intersection S of the two tangential planes and the plane through T, R and the center of the earth because the total propagation distance  $2r$  is a minimum and approximately equal to the total ground distance  $d$ . The angle between the ray paths and the horizontal plane through S is  $\theta$ , and the minimum height

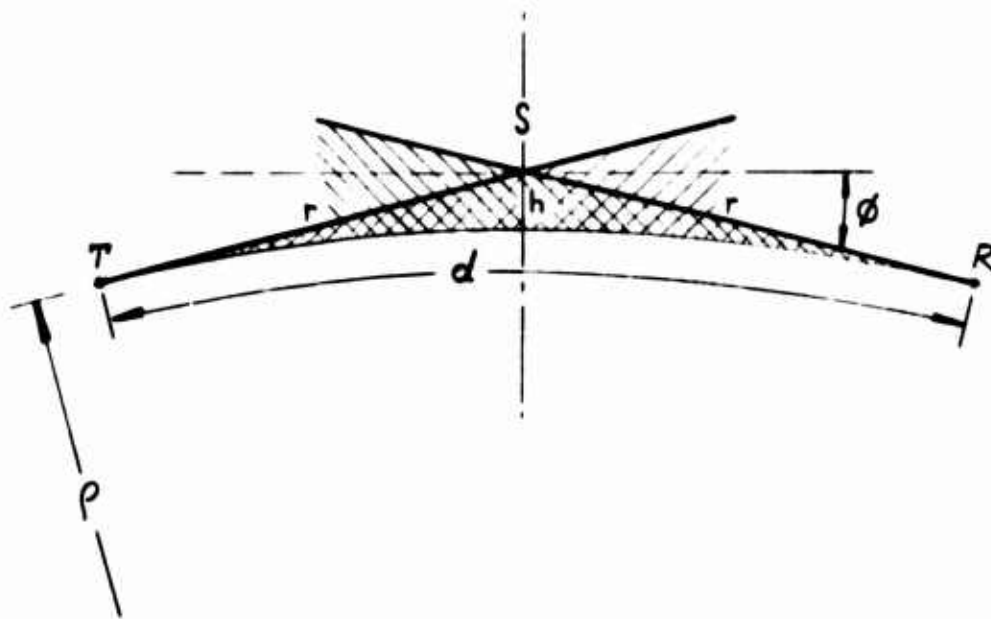


Figure 2-1. Scatter Path Geometry

of scatterers is  $h$ , which is always very small compared to the radius of the earth  $\rho$ . Therefore the simplified relations apply

$$r = \sqrt{2 \rho h} , \quad (2-1)$$

$$\phi = \sqrt{2 h / \rho} = \frac{2 h}{r} . \quad (2-2)$$

We learn from Equation (2-1) that little range can be gained from an increase of the height. On the other hand an increase of height rapidly increases the problem of dispersion and suspension of scatterers; therefore, some reasonable assumption of the height will correspond to a total



propagation range which cannot be greatly extended without requiring tremendous efforts in the deployment of scatterers. It seems that an assumption of

$$h = 30 \text{ km (} \sim 100,000 \text{ feet)} \quad (2-3)$$

is very reasonable so that

$$r = 715 \text{ km (445 miles) ,} \quad (2-4)$$

$$d = 1430 \text{ km (890 miles) ,} \quad (2-5)$$

and

$$\theta = 0.084 \text{ rad. (4.8 degrees)} \quad (2-6)$$

if a modified earth radius of  $\rho = 8500 \text{ km}$  is used to take refraction of the rays into account.

## 2. Scatter Path Efficiency

The propagation efficiency of the entire path can be defined by the ratio of the received and the transmitted powers  $P_R$  and  $P_T$ :

$$e = \frac{P_R}{P_T} = \frac{G_T}{4\pi r^2} \cdot \frac{\Sigma}{4\pi r^2} \cdot \frac{G_R \lambda^2}{4\pi} \quad (2-7)$$

Thereby, the first term describes the normalized intensity at the scatterers, the second adds the effect of the transmission from the scatterers to the ground, while the third term shows how much power is admitted by the receiving antenna. Specifically,  $G_T$  and  $G_R$  are the gains of the transmitting and receiving antennas, respectively,  $\Sigma$  is the integrated bistatic

scattering cross section of all scatterers and  $\lambda$  the wavelength. If we compare the efficiency of the scatter propagation with that of the direct transmission

$$e_o = \frac{G_T}{4\pi d^2} \cdot \frac{G_R \lambda^2}{4\pi} \quad (2-8)$$

we obtain the scatterer efficiency

$$e_s = \frac{e}{e_o} = \frac{\Sigma}{\pi r^2} \quad (2-9)$$

which shows the immense disadvantage of any scatter propagation over a direct propagation as  $\Sigma$  will always be many orders of magnitude smaller than the area of  $\pi r^2$ . The scatterer efficiency also shows that multiple hop scatter propagation is highly unfeasible.

Although no specific system requirements were given, some numerical data may help to illustrate the scatter problem. We assume

$$\left. \begin{array}{l} \lambda = 10 \text{ m ,} \\ G_T = 25 , \\ G_R = 4 , \\ d = 1430 \text{ km .} \end{array} \right\} \quad (2-10)$$

Hence we obtain for (2-7)

$$e_o = 0.31 \cdot 10^{-10} \text{ (-105 db) .} \quad (2-11)$$

At a wavelength of 10 meters the primary system noise source is cosmic noise. In a recent tutorial article on sky-noise temperature<sup>1</sup>, Hogg and Mumford arrived at the following simple relationship between wavelength and average effective sky-noise temperature due to cosmic noise;

$$\frac{T_c}{290} = \lambda^2, \quad (\lambda \text{ in meters}). \quad (2-12)$$

The sky-noise temperature may be as high as five times the average and as low as one-fifth this average depending on antenna orientation. Hence the maximum noise temperature may reach

$$T_c = 5 \times 290 \times 10^2 = 145,000^\circ\text{K}. \quad (2-13)$$

If it is assumed that all antenna side lobes are also affected by this same cosmic noise, the noise at the antenna terminal  $P_N$  is independent of the antenna characteristic:

$$P_N = kT_c B, \quad (2-14)$$

where:

$B$  = system bandwidth ,

$k$  = Boltzmann's constant ,

For a 3-kc noise channel the cosmic noise at the antenna terminals is

$$P_N = 60 \times 10^{-16} \text{ watts}. \quad (2-15)$$

If it is assumed that a unity signal-to-noise ratio is sufficient to establish communication, the received signal power could also be  $60 \times 10^{-16}$  watts.

If we finally assume a transmitted power level of

$$P_T = 2.5 \text{ kw} , \quad (2-16)$$

the propagation efficiency must be according to (2-7)

$$e = 2.4 \cdot 10^{-18} \text{ (-176 db)} . \quad (2-17)$$

Hence the scatterer efficiency must be at least

$$e_s = 7.75 \cdot 10^{-8} \text{ (-71 db)} . \quad (2-18)$$

and the total scattering cross section should be according to (2-9).

$$\Sigma = e_s \pi r^2 = 12.4 \cdot 10^4 \text{ m}^2 . \quad (2-19)$$

#### B. Artificial Scatterers with Random Spacing

When large numbers of individual scatterers are employed we may conservatively assume that each scatterer contributes a randomly phased wave at the receiver. We may further assume that the scatterers are dispersed so widely that no near-field coupling exists and that the cloud of scatterers remains highly transparent so that each scatterer can contribute its full share to the scattered signal. This means that the field strength at the receiver is determined by the Rayleigh distribution and the average intensity is the sum of the intensity of all  $n$  scatterers or

$$\Sigma = n \sigma , \quad (2-20)$$

where  $\sigma$  is the cross section of an individual scatterer and  $\Sigma$  is the cross section of the large population of scatterers.

### 1. Small Metallized Bubbles

Spherical conductive scatterers as obtainable by metallization of small plastic bubbles have a radius  $a$ , which is small compared with the wavelength, so that Rayleigh's law can be applied. Accordingly, the scattering characteristic is that of a dipole with a cross section of

$$s = 9 \left( \frac{2\pi a}{\lambda} \right)^4 \pi a^2 = k \pi a^2. \quad (2-21)$$

Since the dipole characteristic affords a gain of 1.64 in the plane normal to the polarization vector the scattering cross section in the vicinity of this plane is about

$$\sigma = 1.6 s = 14.4 \left( \frac{2\pi a}{\lambda} \right)^4 \pi a^2. \quad (2-22)$$

This law describes the cross section fairly well up to an  $a/\lambda$  ratio of 0.1. Expression (2-22) indicates the advantage of large spheres from the view point of electromagnetic scattering properties. However, within the range of sizes of plastic bubbles which can be fabricated by proven methods, a radius of 1 mm is on the large end.

Laboratory experience shows that a dependably conductive metal film should be

$$\delta = 10^{-8} \text{ m} \quad (2-23)$$

thick. Therefore, the volume of the metal film of one sphere is

$$m = 4 a^2 \pi \delta . \quad (2-24)$$

With the aid of (2-24) we can express (2-22) in terms of  $m$  and obtain

$$\zeta = 3.65 \frac{\pi^2 m^3}{\lambda^4 \delta^3} . \quad (2-25)$$

Again, we see that the larger spheres produce a rapidly increasing advantage in the utilization of the metal as long as Rayleigh's law applies. Therefore, the largest bubbles should be considered.

From (2-20) and (2-22) we derive

$$n = \frac{\sum \lambda^4}{14.4 (2\pi a)^4 \pi a^2} . \quad (2-26)$$

With  $\Sigma$  as in (2-19),  $a = 10^{-3}$  m and  $\lambda = 10$  m we obtain

$$n = 1.76 \cdot 10^{22} . \quad (2-27)$$

The total volume of the metal coating becomes according to (2-24) and (2-27)

$$M = n \cdot m = 22.1 \cdot 10^8 \text{ m}^3 . \quad (2-28)$$

This figure shows that the uncontrolled dispersal of such small bubbles has absolutely no chance of success.

## 2. Large Metallized Balloons

Rayleigh's law indicates that small spheres have a scattering cross section which is much smaller than their physical cross section  $\pi a^2$  due to the factor of  $k$  in (2-21). For large spheres, i.e.,  $a/\lambda \ll 1$  the two cross sections can be set equal. In the intermediate range resonance effects can even give an increase of the scattering cross section over the value of the physical cross section. For large spheres the reflection characteristic is isotropic. In this case

$$\sigma = \pi a^2. \quad (2-29)$$

Again, we assume an uncontrolled dispersal for which random phasing of the contributions of individual spheres applies. Thus, we may write

$$n = \frac{\Sigma}{\pi a^2} \quad (2-30)$$

and

$$M = n \cdot m = 4 \sigma \Sigma = 4.96 \cdot 10^{-3} \text{ m}^3. \quad (2-31)$$

This figure is quite reasonable and means a total weight of 13.5 kg of aluminum. However, if the number of spheres is determined, this approach is no longer appealing. For example, if balloons with a diameter of 20 m (66 feet) are used, 395 of these balloons are required.

The optimum size of a spherical scatterer is

$$a = 0.17 \lambda_r \quad (2-32)$$



so that

$$k = 3.75 \text{ ,} \quad (2-33)$$

In this case

$$n = \frac{2.94 \Sigma}{\lambda_r^2} \text{ .} \quad (2-34)$$

This leads to 3650 balloons of 3.4 m (11 feet) diameter.

Although a system with large balloons would be technically feasible, it cannot be recommended because of the high cost of the continuous replacement which is required for a reliable communication system. Moreover, the straying balloons will also impose a major problem.

### 3. Resonating Devices

By far the lowest weight penalty is associated with resonating devices. The simplest and best understood form is the half-wavelength dipole. Although a resonating device leaves no choice of the frequency, there is a sufficient bandwidth for any signal spectrum. The natural mode of radiation for which a dipole can be matched as a link between the dipole and a load is the spherical wave. However, if the matched dipole is coupled to a plane wave system, only half of the intercepted energy will be received while the other half is scattered into the spherical wave. If the dipole is short circuited all of the intercepted energy will be found in the scattered wave. The amount of intercepted energy is determined by the intercepting cross section or scattering cross section of the short circuited loss-less dipole

$$\sigma = 0.238 \lambda^2 \text{ .} \quad (2-35)$$

In contrast to this value one frequently finds the receiving cross section given as  $0.119 \lambda^2$ .

With (2-35) we can derive the minimum number of scattering dipoles according to (2-20) and find for the above situation

$$n = \frac{12.4 \cdot 10^4}{0.238 \cdot 10^2} = 5220 . \quad (2-36)$$

Since the matched impedance of a dipole is 73 ohms, a considerable resistance can be tolerated in the dipole before the scattering cross section is appreciably reduced. This means that an extremely thin wire is all that is needed. Because of the skin effect a metallized plastic strip should be considered. However, one must make sure that the dipoles maintain an outstretched position parallel to the polarization vector to be fully effective.

### C. Coherent Scattering by Diffraction Gratings

The random dispersion of scatterers results in an inefficient forward propagation because the phases of the individual contributions are also randomized. In the case where the number of scatterers is large, the pay-off would be tremendous if scatterers could be dispersed in controlled locations so that phase coherence of the forward propagation could be achieved. Actually, there is always perfect phase coherence for the forward scatter propagation if the receiver is located along the straight line from the transmitter through the scattering cloud. This is because the total propagation distance from the transmitter to the receiver via the scatterer is independent of the location of the scatterer provided the lateral width of the scatterer cloud is within certain limits. It is also important that the scatterers shift the phase by the same amount, which could be expected from identical artificial scatterers. Thus, the question may be posed whether there is a locus where scatterers should be placed so that all individual contributions are phase coherent at the receiver.

Figure 2-2 illustrates the answer to this question. It shows the two terminals and the cross section of an ellipsoid whose two foci coincide with the terminals. Since the sum of the distances of any point on an ellipse to the foci is constant, we should disperse scatterers over that part of an ellipsoid which has the two terminals as foci and which extends into the common space above the two horizontal planes through the terminals. Since a phase shift of a not too large multiple of  $2\pi$  has no effect on the transmitted signal we can also include a number of adjacent concentric ellipsoids as permissible locations for our scatterers. If the phase difference becomes a large number of cycles the delay difference could reduce the useful signal spectrum.

An arrangement of scatterers along the ellipsoidal surface is in principle a three-dimensional diffraction grating with a major lobe directed toward the receiver. The side lobes of this diffraction pattern are at the low level of the back and bistatic scattering due to random build-up.

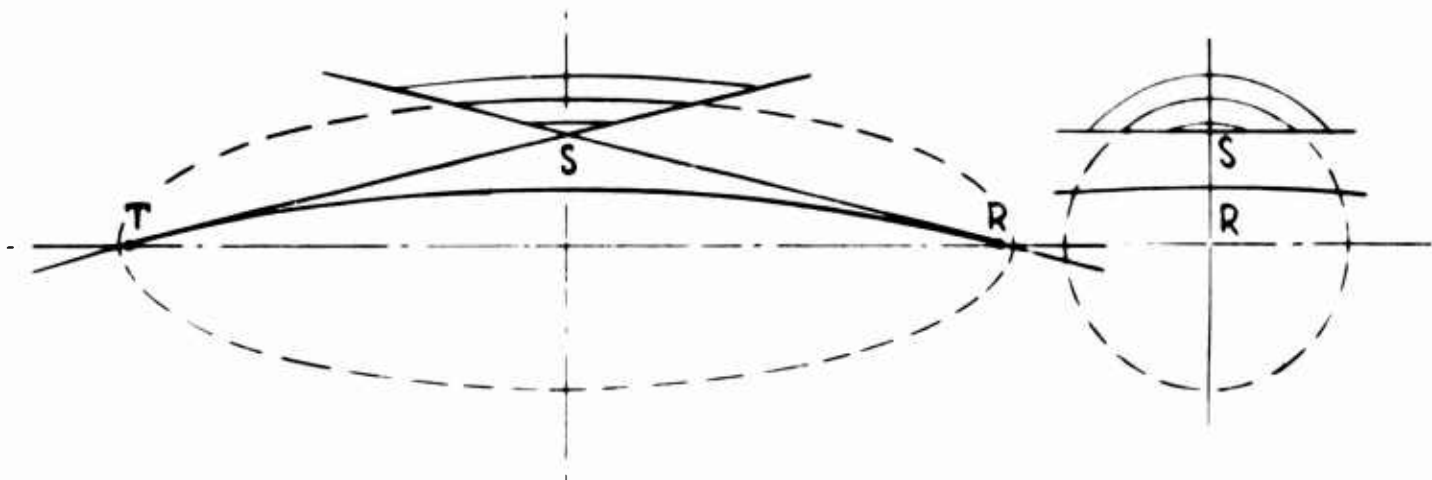


Figure 2-2. Locus of Scatterers for Phase Enhancement

Since the geographical dimensions of the propagation path are very large in terms of the wavelength, we can assume for all practical arrangements that the diffraction grating is formed by a set of parallel equidistant planes. The spacing of these planes can be derived from Figure 2-3. It shows two adjacent planes, m and n, on which two scatterers,  $S_m$  and  $S_n$ , are located above each other. Two parallel rays, 1 and 2, whose phase fronts are parallel to  $X S_m$  are scattered at  $S_m$  and  $S_n$  respectively so that in the direction of rays 1' and 2' phase coherence parallel to  $Y S_m$  results. Since the two scatterers are alike, the delay of ray 2-2' over ray 1-1' amounts to a full cycle. This means

$$\overline{X S_n} + \overline{S_n Y} = 2 \overline{S_n Y} = \lambda . \quad (2-37)$$

Hence from triangle  $S_m S_n Y$  we derive

$$S = \frac{\lambda}{2 \sin \emptyset} \approx \frac{\lambda}{2 \emptyset} ; \quad (2-38)$$

with  $\emptyset$  as in (2-6) we get

$$S = 5.95 \lambda \approx 6 \lambda . \quad (2-39)$$

While the lateral distribution of the scatterers within the planes of the grating can be absolutely uncontrolled provided enough spacing is allowed to maintain a maximum contribution by each scatterer, vertical deviation from the plane should be limited to a range such that a positive contribution to the signal strength is assured. This corresponds to a phase delay of  $\pm \pi/2$ . In other words, the scatterers may occupy layers of  $s/2$  or  $3 \lambda$  thick. A more conservative requirement would keep the contribution of each scatterer within 3 db of the maximum value which corresponds to layers of  $s/4$  or  $1.5 \lambda$  thick.

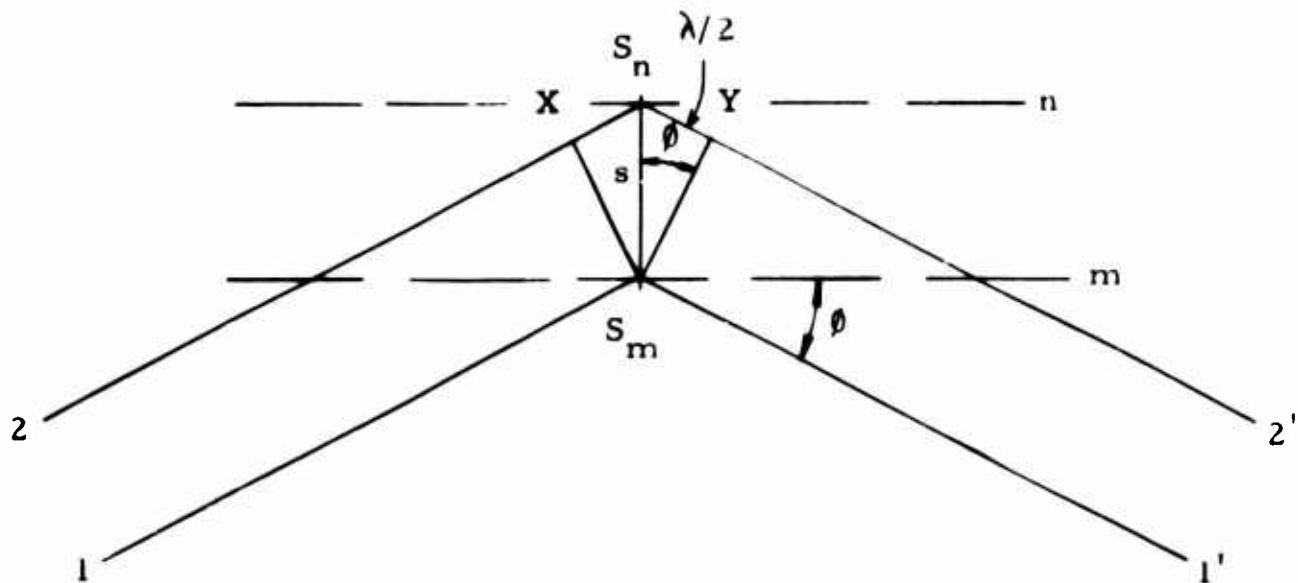


Figure 2-3. Spacing of Planes

#### D. Coherent Scattering in a Refractive System

If a scattering system can be devised so that phases are advanced by a linearly increasing amount for rays arriving in a higher level or that phases are retarded for rays arriving in a lower level, we would have a refractive system which can be compared to a prism except that the effect is caused by individual scatterers rather than by a continuous medium. Therefore, part of the radiation will go straight through.

A dipole can be modified so a positive or negative phase shift is affected. The principle is illustrated in Figure 2-4. The half-wavelength dipole is not directly short circuited but connected to a transmission line on which a movable short is located at a distance of one-half wavelength. If the characteristic impedance of this transmission line is matched to the 73.5 ohms of the dipole impedance, half of the power intercepted by the dipole will be scattered immediately, while the other half travels down the

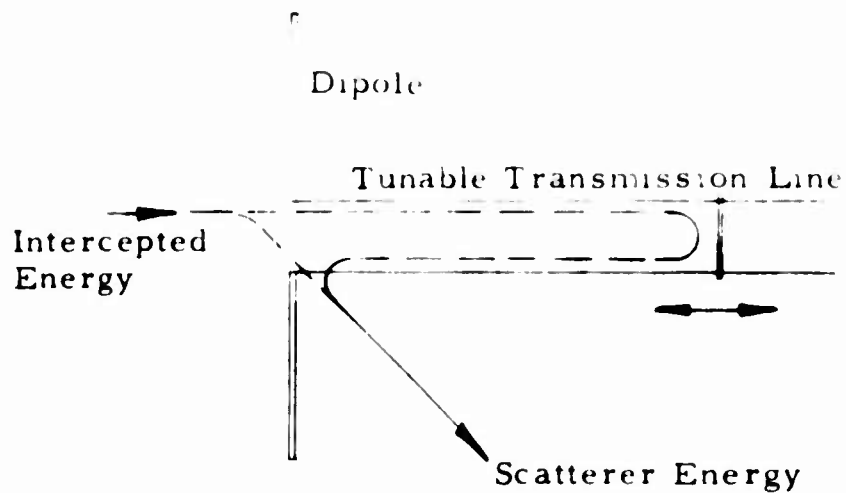


Figure 2-4. Dipole with Phase Shift

line to the short where it is reflected back to the dipole and then radiated with a phase delay of one cycle. Thus, the circuit 2 is equivalent to the short-circuited dipole over a certain bandwidth. If, however, the short on the transmission line is moved forward or backward, the phase of the reflected wave is advanced or retarded respectively. The effect on the resulting scattered wave is illustrated by the phasor diagram of Figure 2-5. Phasor A symbolizes the immediately scattered wave, while B symbolizes the wave transmitted by the dipole after having travelled twice through the transmission line. Although the phase shift  $2\psi$  of B is unlimited, the resulting phase shift of the sum phasor C is limited to  $\pm \pi/2$  whereby the amount of C varies as

$$|C| = C_0 \cos \psi . \quad (2-40)$$

Because of this phase limitation, the refractive effect is limited to layers of scatterers of a thickness of  $s/2$ .

A more practical form of a phase shifting scatterer is a one-half-wave-length dipole with a reactive load, either a capacitance to advance the phase or an inductance to retard the phase. But the most attractive is a short-circuited dipole whose length is varied. The equivalent circuit of a dipole is illustrated in Figure 2-6. It describes the characteristics of a dipole in the vicinity of the fundamental resonance fairly well. The dipole is assumed to be loss-less so that  $R_a$  is the radiation resistance. According to Jordan<sup>2</sup>, the relations exist

$$L_a = \frac{Z_o}{8f_r} , \quad (2-41)$$

$$C_a = \frac{2}{\pi^2 f_r Z_o} , \quad (2-42)$$

$$Q = \frac{\pi Z_o}{4 R_a} , \quad (2-43)$$

$$R_a = \left( \frac{4H}{\lambda} \right)^2 R_o , \quad (2-44)$$

$$Z_o = 120 \left[ \ln \left( \frac{2H}{a} \right) - 1 \right] . \quad (2-45)$$

Hereby, most of the quantities are explained by Figure 2-6 and

$$\lambda_r = 4H , \quad (2-46)$$

$$f_r = \frac{c}{\lambda_r} = \frac{c}{4H} . \quad (2-47)$$



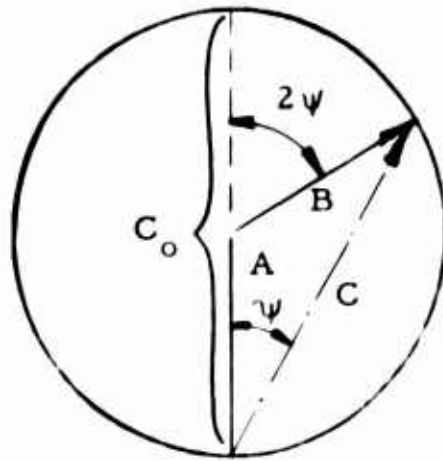


Figure 2-5. Phasor Diagram of Scattered Wave

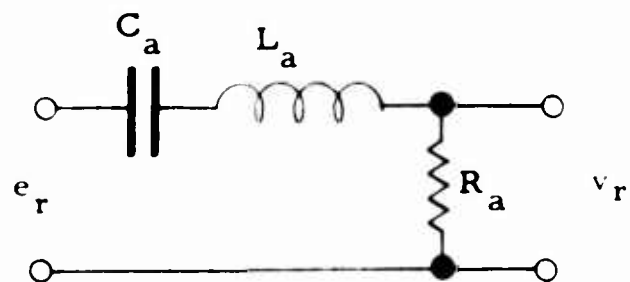


Figure 2-6. Dipole Equivalent Circuit

Hence (2-41) and (2-42) become

$$L_a = \frac{4H}{8c} Z_o, \quad (2-48)$$

$$C_a = \frac{8H}{\pi^2 c} \cdot \frac{1}{Z_o}. \quad (2-49)$$

Now (2-44), (2-45), (2-48), and (2-49) define the circuit of Figure 2-6 in terms of the dipole length  $H$ . The input voltage  $e_r$  is the electromotive force due to the incident radiation, while the voltage  $v_r$  across the radiation resistance generates the scattered spherical wave. Thus we are interested in the complex scattering factor

$$k = \frac{v_r}{e_r} = \frac{R_a}{R_a + j(\omega L_a - \frac{1}{C_a})} = |k| e^{j\psi} \quad (2-50)$$

as a function of the dipole length  $H$ . From (2-50) we derive

$$|k| = \frac{R_a}{\sqrt{R_a^2 + (\omega L_a - \frac{1}{C_a})^2}} \quad (2-51)$$

and

$$\psi = \arctan \frac{\omega L_a - \frac{1}{C_a}}{R_a} \quad (2-52)$$

If we introduce the expressions (2-44), (2-45), (2-48), and (2-49) and normalize the antenna length with respect to the length of the tuned antenna according to

$$h = \frac{4H}{\lambda} \quad (2-53)$$

we obtain

$$|k| = \frac{h^2 R_o}{\sqrt{h^4 R_o^2 + \left\{ 30\pi \left[ \ln \left( h \frac{\lambda}{2a} \right) - 1 \right] \left( h - \frac{1}{h} \right) \right\}^2}} \quad (2-54)$$

and

$$\psi = \arctan \left\{ \left( h - \frac{1}{h} \right) 30\pi \left[ \ln \left( h \frac{\lambda}{2a} \right) - 1 \right] / h^2 R_o \right\} . \quad (2-55)$$

Numerical evaluation was carried out for

$$R_o = 73.5 \text{ and } \frac{\lambda}{2a} = 20,000 . \quad (2-56)$$

This means that for a wavelength of 10 m as in the above example the antenna would have a tuned length of 5 m and a diameter of 0.5 mm (AWG 24). The result is shown in the diagram of Figure 2-7. The sinusoidal shape of  $|k| = f(\psi)$  indicates that the effectiveness of the phase shifting dipoles follows the same trend regardless of whether the length is varied or the length of a short-circuited transmission line is changed. The curve  $h = f(\psi)$  shows that the linear relation between dipole length and phase is restricted to  $\pm 45$  degrees and that phase shifts near  $\pm 80$  degrees and more cannot be realized regardless of how long the dipole is made. In addition, one must be cautious in applying the theory for dipoles which are 150% and more of the tuned length.

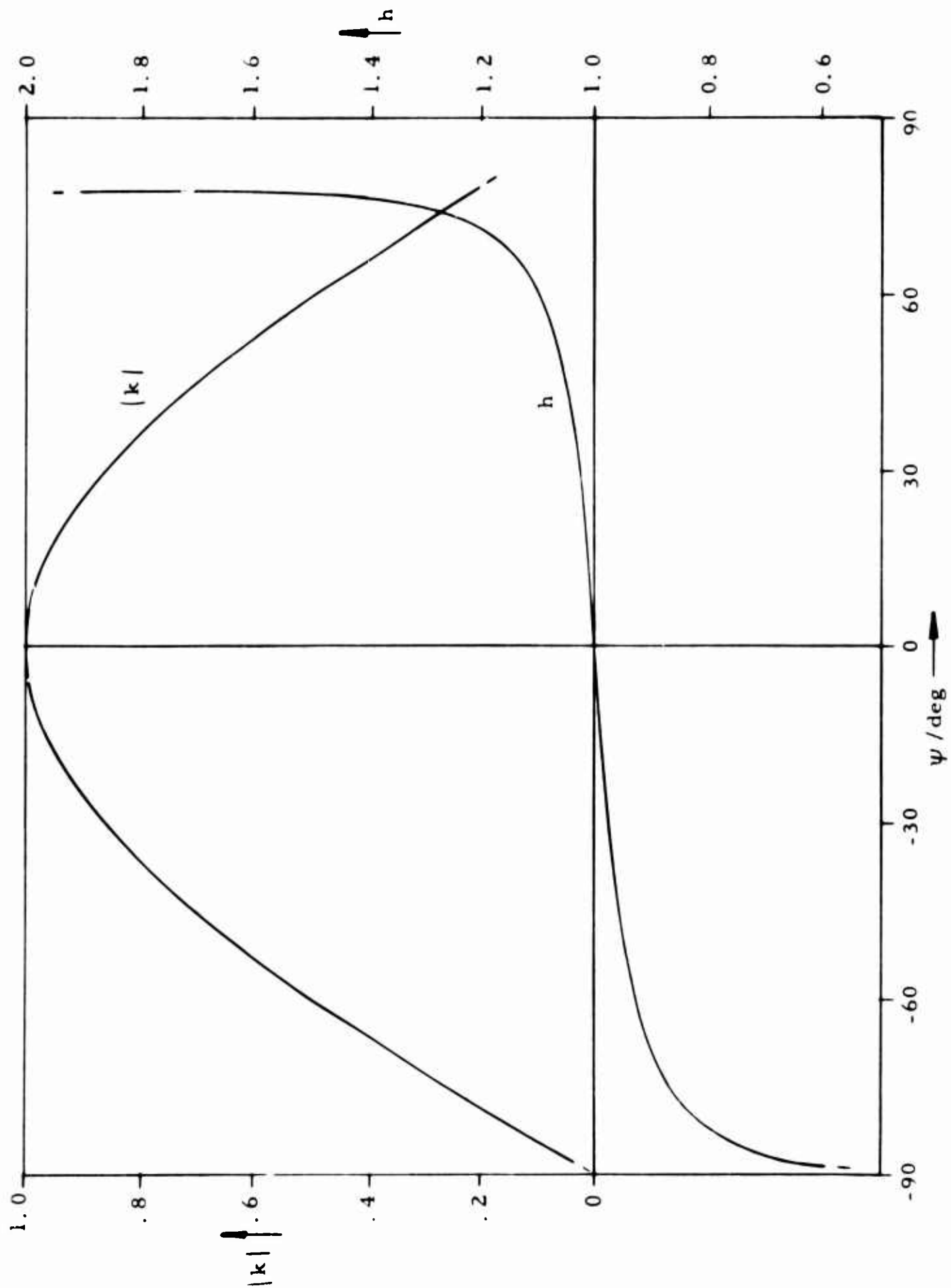


Figure 2-7. Scattering Factor versus Normalized Dipole Length

It is quite obvious that the diffraction grating can be combined with the refractive effect so that refractive layers are repeated to form a diffractive grating.

In paragraph C (coherent scattering by diffraction gratings), we found that dipoles are not uniformly effective if they are spread out above or below the surface of an ellipsoid and we also determined the thickness of a layer over which any positive contribution could be made by a scatterer. From Figure 2-5 we can derive that the contribution varies as the cosine of the phase error. Now we see that by means of phase shifting scatterers we can eliminate the phase error, but found that the amplitude drops off as the cosine of the phase shift. Thus, it seems that we have not gained anything. This is true if we weigh scatterer against scatterer. However, if we compare the scattering cross section, we see that the tuned dipole maintains a full scattering cross section while that of the phase shifting dipole changes as indicated by its contribution. Thus, we could compensate for this effect by packing the phase shifting dipoles more densely than the tuned dipoles since more radiation is transmitted straight through a cloud of phase shifting or detuned scatterers than through a cloud of tuned scatterers.

## E. Practical Scattering Systems

### 1. Characteristics of a Ten-Meter System

Without tying the scatterers together mechanically, it does not seem possible to maintain them in the proper vertical relation while they may be free to shift laterally. First, let us see how many dipoles are needed if they are arranged to give maximum phase coherent scattering. As in the previous examples, system wavelength is 10 meters. Since the received signal power increases as the number of the non-coherent scatterers (while it increases as the square of the number of coherent scatterers), we can start from the previously computed example of the non-coherent system,

which required 5220 dipoles as in (2-36) and find the number of coherent dipoles required as

$$n' = \sqrt{5220} = 73. \quad (2-57)$$

If the dipoles are distributed over the maximum thickness of a layer providing positive contribution, the average contribution drops to the average of a cosine distribution, namely  $2/\pi$ . Therefore, one should use

$$n = \frac{\pi n'}{2} = 114 \quad (2-58)$$

dipoles.

Unless there is strong objection against vertical polarization, it should be used as dipoles can easily be oriented vertically by the aid of gravity. Horizontal polarization would require crossed dipoles or other arrangements with twice the number of dipoles unless some technique can be applied which keeps the dipoles in transversal orientation with respect to the propagation path.

The easiest way to control the proper relative position of a number of vertical dipoles is to connect them in a chain. If all dipoles were included in a single chain a length of  $116 \lambda / 2 = 57 \lambda = 570$  meters would result. Since we can occupy only layers of  $3 \lambda$  thick with equally wide empty spaces, the total length of the scattering system would be 1140 m. The disadvantage of such arrangements is the extremely narrow vertical beamwidth of about 0.5 degree. This may require a control of the altitude to prevent the beam from missing the receiver location. Therefore, several parallel chains would be more attractive. For example, 5 chains of 24 dipoles distributed over 4 diffraction layers of 6 dipoles per layer per chain offer an attractive system. All 5 chains could be suspended on a balloon of 5 meters radius as illustrated in Figure 2-8. Such a balloon

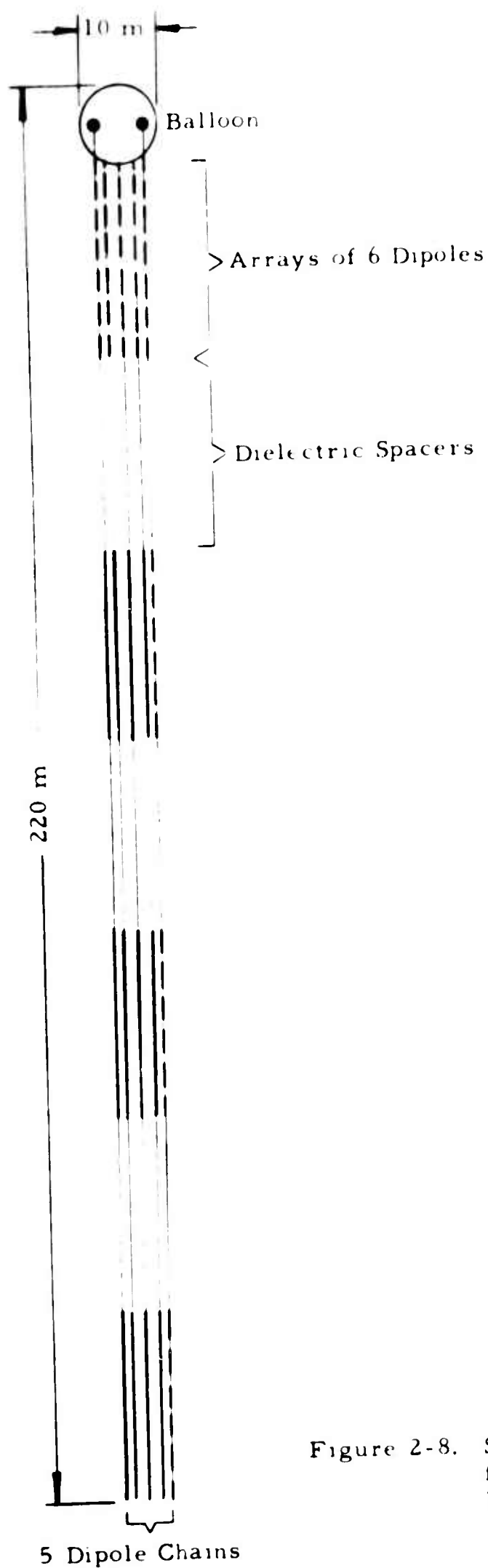


Figure 2-8. Scattering System for Ten-Meter Wavelength



could lift 4 pounds payload to an altitude of 30 km. If the chains are made of metallized Mylar strips, spaced and insulated by strips of clear Mylar, one could easily stay within the payload. The distance between chains is  $\lambda/2$  and should be sufficient to give each chain its full share of illuminating power. The vertical beamwidth of 210 meters long scattering system becomes about 2.7 degrees while the horizontal beam would cover at least 60 degrees so that the receiver can be reached over a wide geographical area. Thus one simple and inexpensive balloon-borne scattering system would suffice to provide a communication link between the ground stations over about 900 miles. In contrast to other non-coherent scatter propagation systems, this coherent system does not cause scintillation of the signal.

## 2. Characteristics of a One-Meter System

No attempt was made to determine the optimum frequency for this technique, since many operational factors would enter the picture. However, from the technical point of view, it is interesting to see how some parameters would change so that one would be in a better position to appraise the value of an artificial scatter communication system.

To investigate longer wavelengths did not seem to be rewarding because of the increased dimensions of the scattering array. Also, less gain can be expected for the antennas at the terminals. Therefore, some advantage was expected only from a system operating at shorter wavelength.

The following specifications were assumed.

$$\left. \begin{aligned} \lambda &= 1 \text{ m} , \\ G_T &= 250 , \\ G_R &= 10 . \end{aligned} \right\} \quad (2-59)$$

Hence, we obtain for (2-7)

$$e_o = 7.74 \times 10^{-12} \text{ (-111 db)} . \quad (2-60)$$

At a wavelength of one meter, the average effective sky-noise temperature is according to (2-12) only 290°K or room temperature. While the receiver noise should be stronger by about 3 db, the highest sky-noise level will be higher yet due to a factor of 5 or 7 db. This means that we are safe to assume a noise temperature of

$$T_c = 5 \cdot 290 = 1450^\circ\text{K} . \quad (2-61)$$

In this case, the noise power and hence the received signal power become

$$P_N = P_R = 60 \cdot 10^{-18} \text{ watts} . \quad (2-62)$$

If we now assume a transmitted power level of

$$P_T = 0.5 \text{ kw} \quad (2-63)$$

the propagation efficiency must be according to (2-7)

$$e = 12.0 \cdot 10^{-20} \text{ (-189 db)} . \quad (2-64)$$

Hence, the scatterer efficiency must be at least

$$e_s = 1.55 \cdot 10^{-8} \text{ (-78 db)} \quad (2-65)$$

and the total scattering cross section should be according to (2-9)

$$\Sigma = 2.49 \cdot 10^4 \text{ m}^2. \quad (2-66)$$

The scattering cross section of a dipole is according to (2-35)

$$\sigma = 0.238 \text{ m}^2. \quad (2-67)$$

Hence, the number of coherently scattering dipoles becomes

$$n' = \sqrt{\frac{\Sigma}{\sigma}} = 324. \quad (2-68)$$

This number increases if the dipoles are distributed over a layer  $3\lambda$  thick to

$$n = \frac{\pi n'}{2} = 510. \quad (2-69)$$

To maintain a vertical beamwidth of 2.7 degrees we restrict the array to 4 layers of 6 dipoles high. Thus, the number of dipole chains becomes  $510/24 = 22$ .

Although the number of dipoles is considerably greater than that for the 10-m wavelength system, they take much less space and can be printed or taped on the surface of a cylindrical balloon. If we choose a diameter of 7 m, the circumference of 22 m could accommodate 22 dipole chains at 1-wavelength lateral spacing; therefore, good transparency can be assumed for uniform illumination of all dipoles. The length of the array becomes 21 m so the overall length of the balloon is 28 m. A small weight should be fastened to one end to keep the balloon in a vertical position. The balloon is illustrated in Figure 2-9. The larger horizontal aperture of the 1-m system reduces the horizontal beamwidth to about 9 degrees.

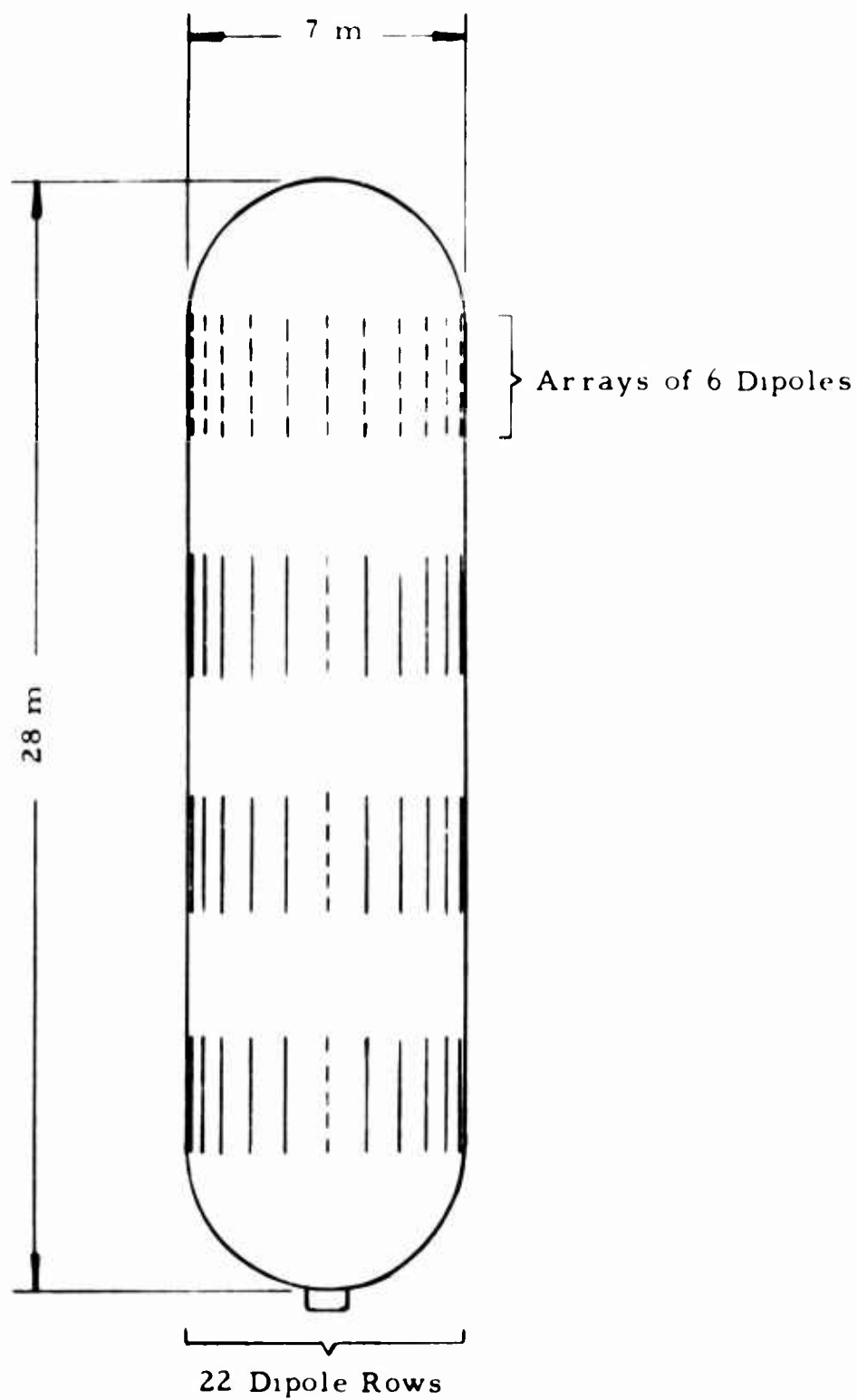


Figure 2-9. Scattering System for One-Meter Wavelength

The length of the balloon of the 1-m system can be reduced considerably if dipoles were placed in the center in the form of vertical chains. For reasons discussed above, the density of the phase shifting dipoles can also be increased. Some reduction of the average share of each scatterer will result from the concentrated array so that the total number of scatterers should be increased accordingly. Since the dipoles, however, contribute very little to the weight and cost of the system, the smaller overall size of the balloon will nevertheless reduce the cost of the system.

The two studied scattering systems are by no means optimized designs. They disclose, however, features of such systems from which a more intelligent approach can be started. More definite operational considerations must be included in a future study as well as logistics and the cost of maintaining such communication channels operative.

The soundness of the physical principle has been proven in a number of experiments as described in the next section. The communication path was scaled down so that the experiments could be performed in an anechoic room of the microwave laboratory. The wavelength was scaled down to 3 cm because sufficient test equipment was available for this band. The difference between non-coherent back scattering and coherent forward scattering is demonstrated by Figures 2-10 and 2-11. Forward scattering by a random array of spherical scatterers was compared with coherent forward scattering when the spheres occupied only the Fresnel zones of in-phase contributions as illustrated in Figures 2-11 and 2-12. Because of the wide aperture and relatively short range between scatterers and the communication terminals, the zones were determined for a close focus. Such an arrangement can be compared with a collecting Fresnel lens. However, in contrast to the latter, the phasing of the radiation from the different zones is controlled to produce the desired ray path rather than the refractive effect, which is of secondary importance.

That scatterers can be placed at random positions with respect to the longitudinal dimension is demonstrated in Figure 2-11. The effect of dipole scatterers and their superiority over spheres is shown in

Figure 2-10. Backscatter Power vs Angle  $\theta$

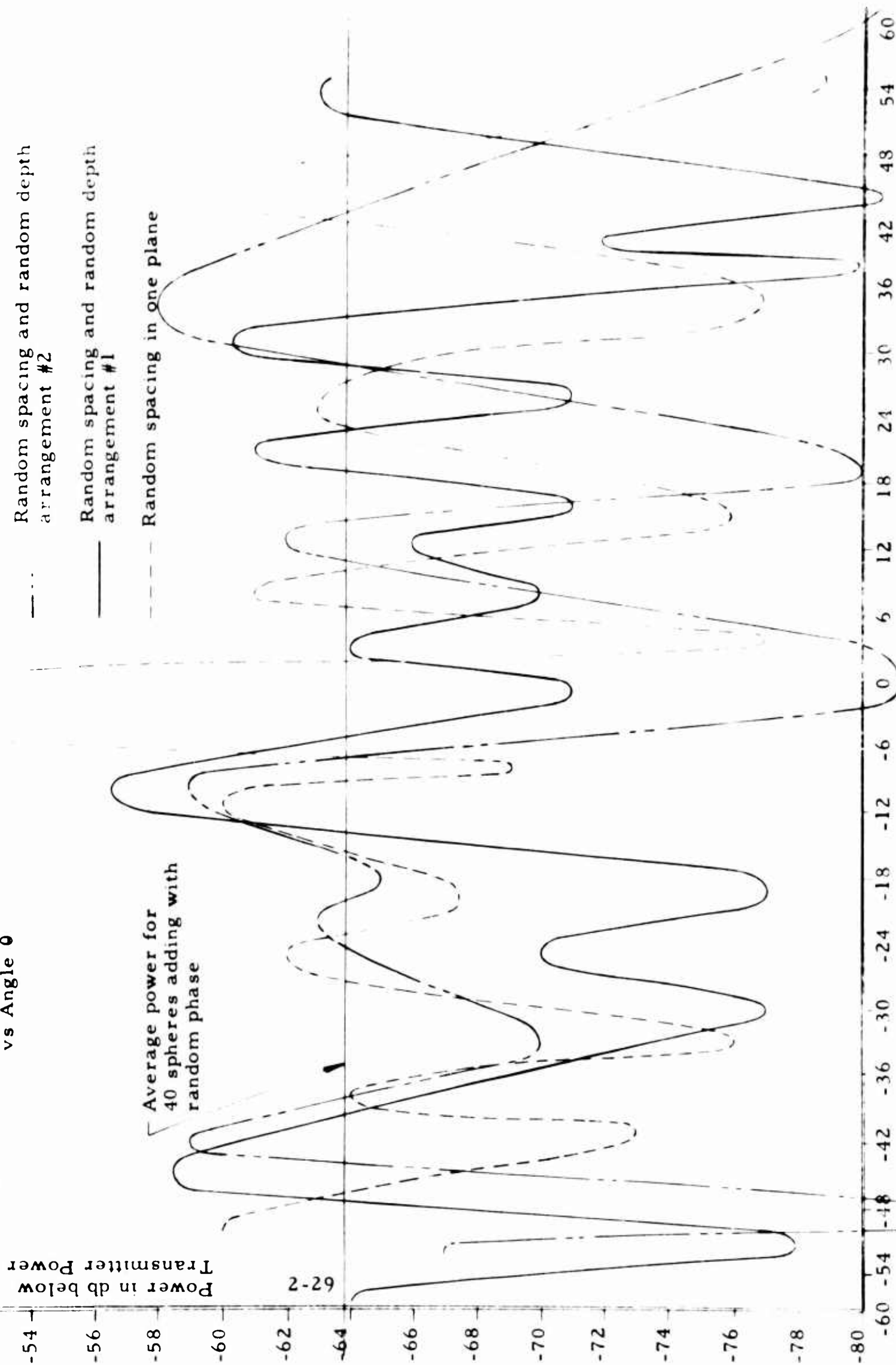


Figure 2-11. Change in Field Pattern for Three Configurations of 3/8-inch Spheres (Forward Scatter)

Power in db below Transmitter Power

- Pattern with no scattering elements in field
- △— Pattern with ninety 3/8-inch spheres in positions indicated by crosshatched area of Figure 2-20, randomly spaced in one plane
- Pattern with ninety 3/8-inch spheres in same positions as above but distributed in random depth
- Pattern with ninety 3/8-inch spheres in positions indicated by curved areas in Figure 2-20, randomly spaced in the same place

$\beta$  in Degrees

-5

0

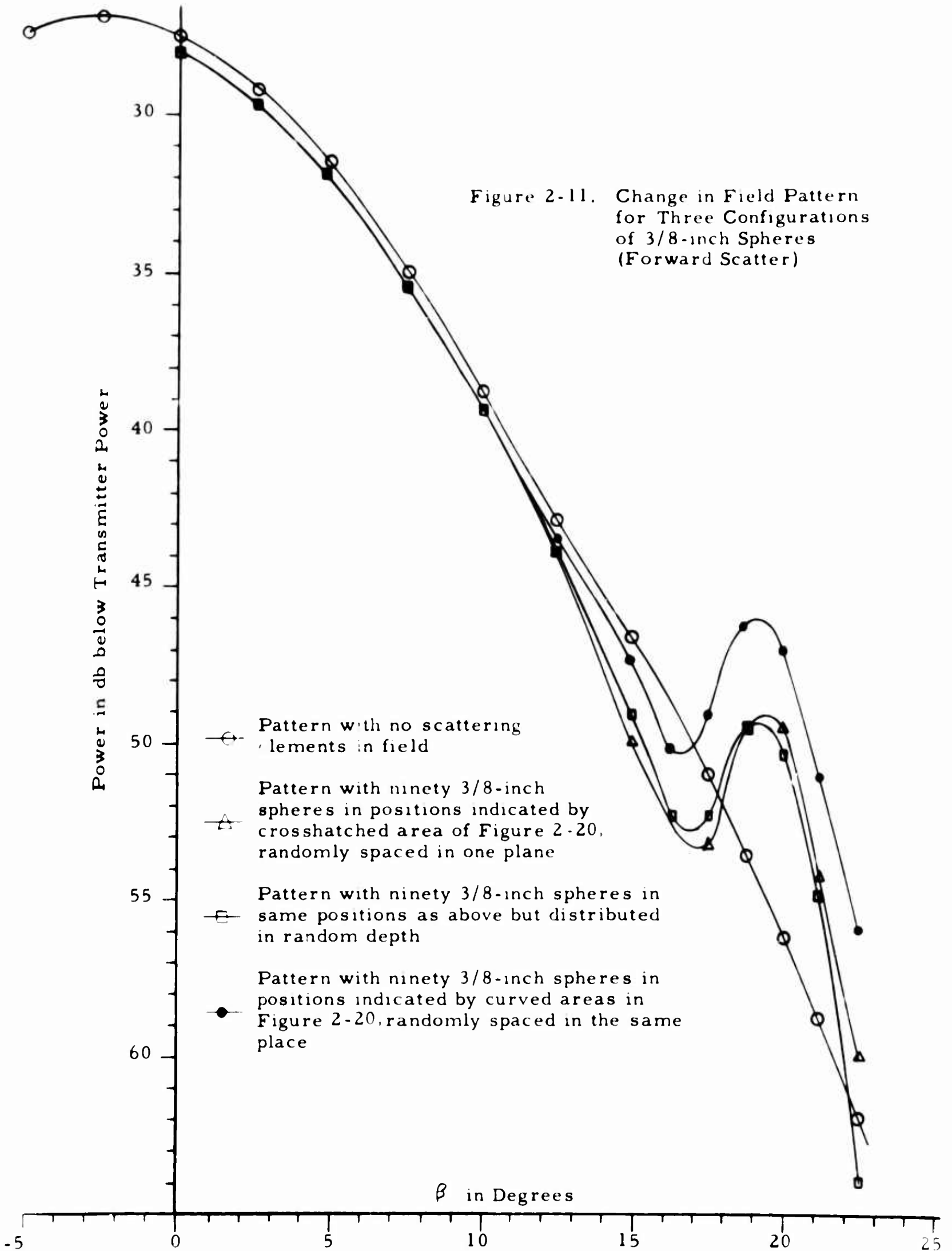
5

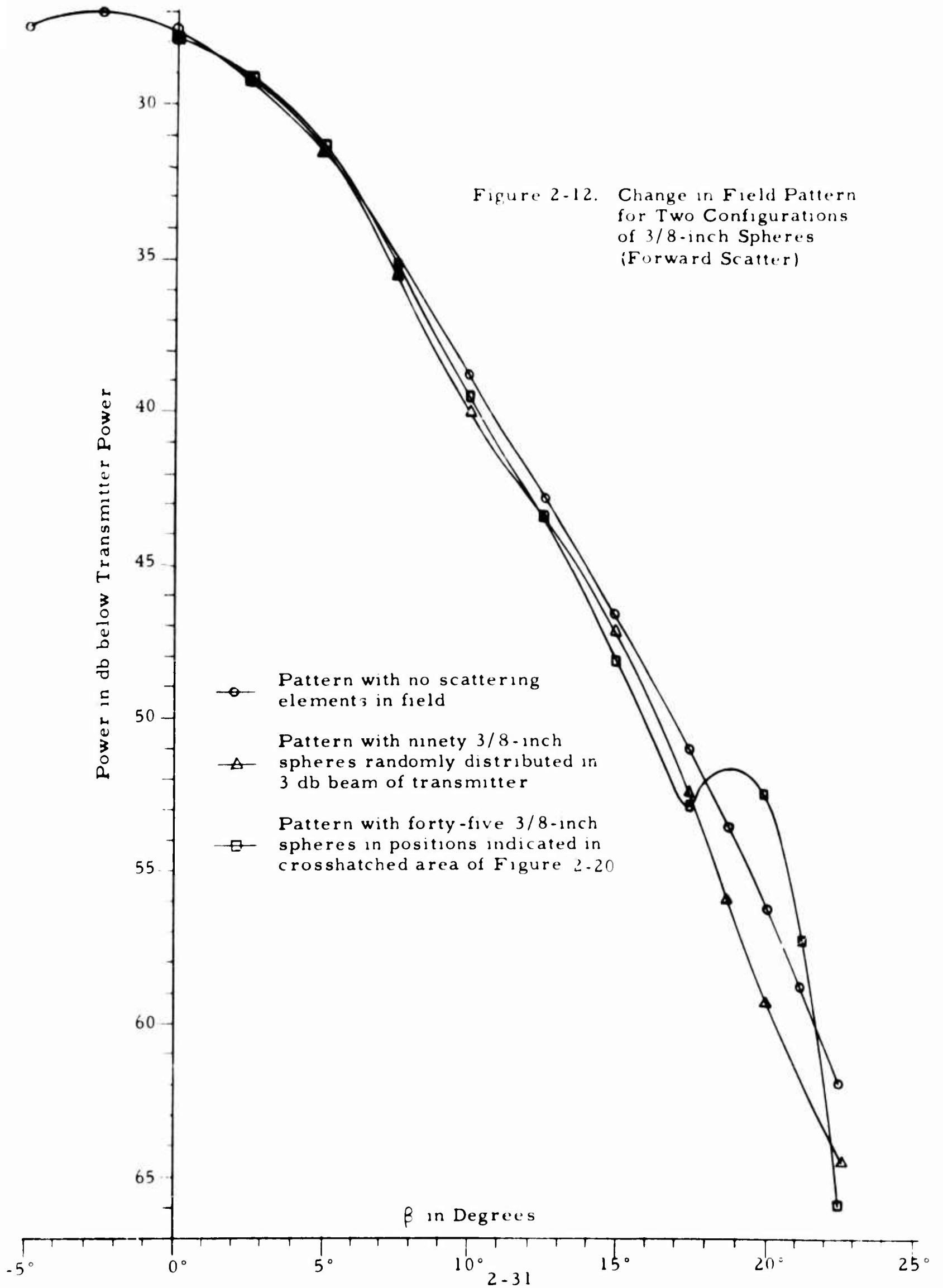
2-30

15

20

25







Figures 2-11 and 2-13. Two arrangements are compared in Figure 2-13, a two-dimensional arrangement of 24 dipoles in focusing Fresnel zones and a three-dimensional arrangement of the same number of dipoles but unfocused. The three-dimensional distribution follows a cylindrical surface to simulate the proposed configurations. The dipoles were shaped for the refractive effect. This shows up clearly when the array is upside down.

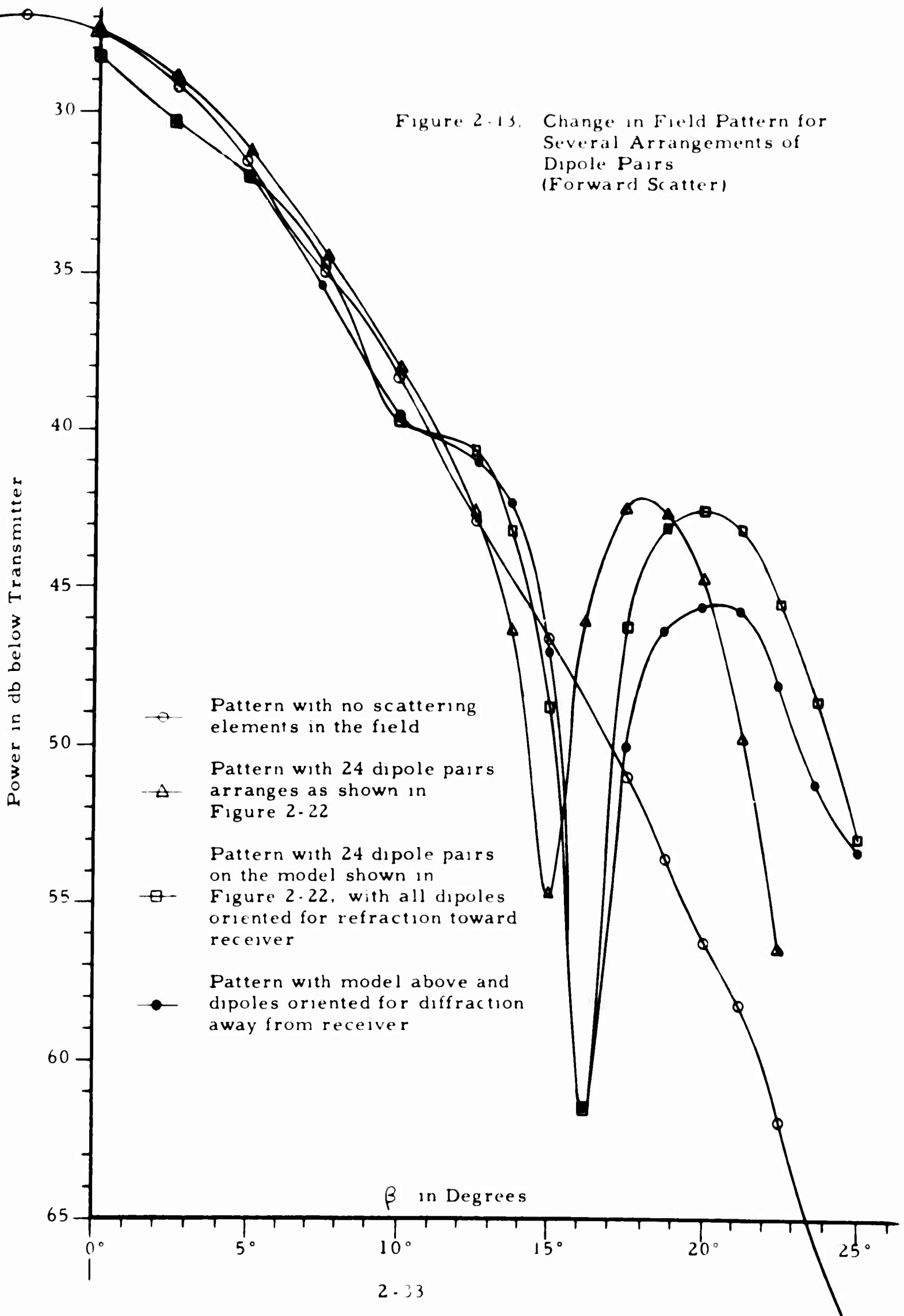
It should be noted that the direct diffractive propagation from the transmitter to the receiver was not sufficiently reduced to be ineffective on the measurement of the scatter path. Where both transmission paths are about equal, destructive interference can take place; this explains the deep depression of the curves in Figure 2-13 around  $\beta = 16$  degrees. The shortcomings of the indoor model experiments can be overcome by an outdoor test over greater distances and height, whereby hills should serve as propagation barriers.

#### F. Scatter Experiments

Scatter experiments on the various elements of interest were conducted in a room approximately 10' x 12' with the walls and ceiling lined with microwave adsorber to minimize background reflections. The experimental work was performed at a frequency of 10 kmc with horizontal polarization of the E field to simulate vertical polarization in the actual forward scatter case.

A block diagram of the X-band facility is shown in Figure 2-14. The null-loop method of measurement employed 1000-cycle square wave amplitude modulation of the klystron, a detector, and a band pass amplified for the null indicator. Scatter signal strengths of approximately 80 db below the klystron power output can be measured by comparison of both the amplitude and phase of the scatter signal with the background reflections.

Figure 2-13. Change in Field Pattern for Several Arrangements of Dipole Pairs (Forward Scatter)



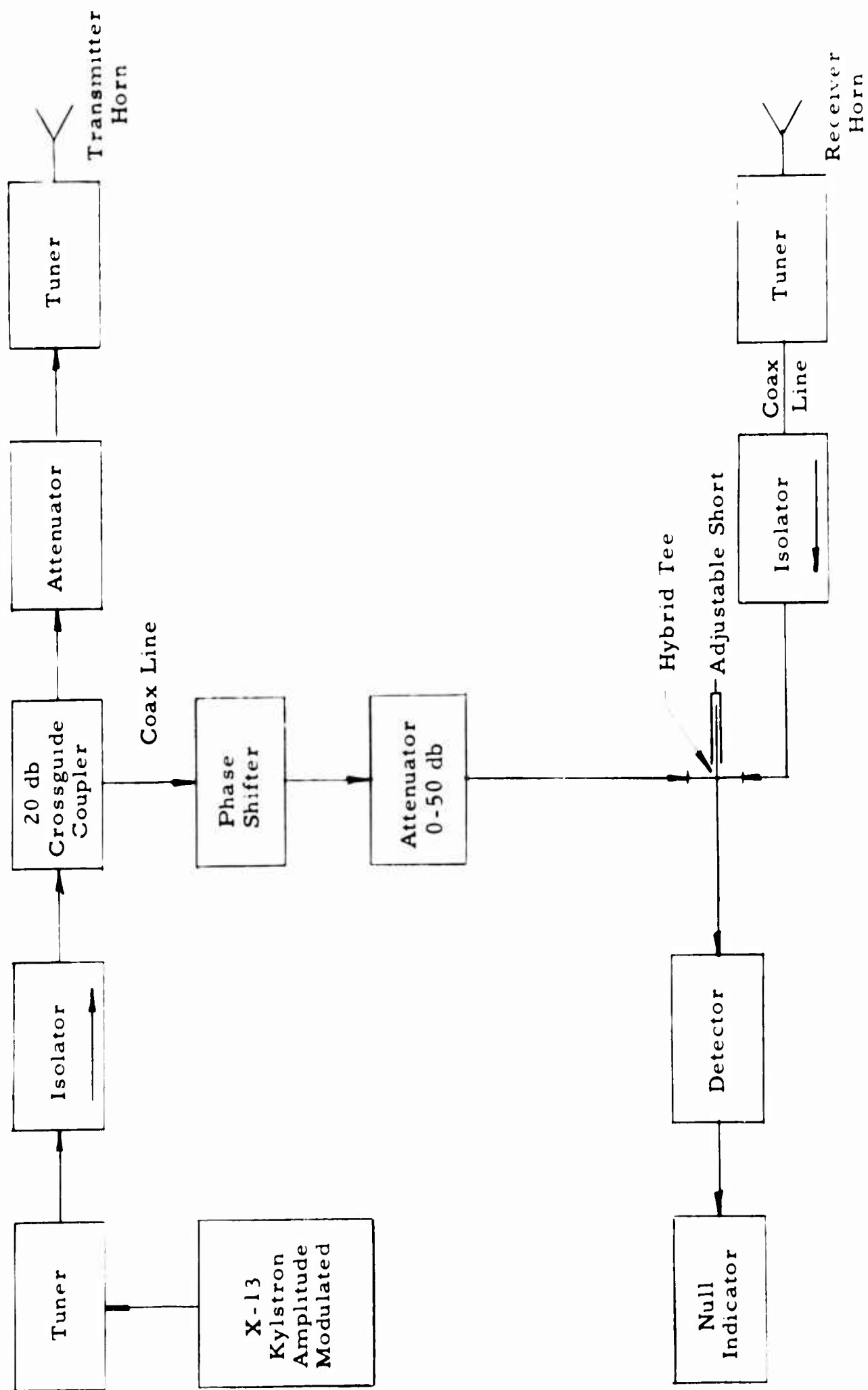


Figure 2-14. Block Diagram of X-Band Electromagnetic Scattering Facility

## 1. Backscatter from Spheres

Backscatter measurements were made on 3/8-inch diameter metal spheres for various configurations. The diagram of Figure 2-15 depicts the arrangement of the microwave equipment. The target consisting of the spheres supported in polystyrene foamed plastic was located at a distance of 8 feet from the transmitter and receiver horns. The transmitter and receiver were separated by an angle of 19.5 degrees and the array of spheres was rotated through approximately  $\pm 60$  degrees about the bisector between transmitter and receiver. An absorbing barrier between transmitter and receiver horns prevented direct transmission by way of the side lobes.

Four sets of backscatter measurements were made from the 3/8-inch spheres. The first consisted of the backscatter versus the number of spheres in the support with the spheres randomly spaced in a plane perpendicular to the bisector between transmitter and receiver. The results are shown in Figure 2-16. The second measurement is scatter signal versus the orientation in angle ( $\theta$  of Figure 2-15) of a randomly spaced plane array of forty 3/8-inch spheres. The results are indicated in Figure 2-10. The two other curves in Figure 2-10 indicate backscattering versus orientation angle for the same random arrangement of forty spheres except that they are now arranged with random depth as well as random spacing. The relative placements and depths of the spheres is indicated in Figures 2-17 and 2-18 for the two arrangements. The straight line of Figure 2-10 indicates the average backscatter signal theoretically expected from the number of scatterers used.

## 2. Forward Scatter from Spheres

The diagram of Figure 2-19 shows the arrangement of the microwave equipment for forward scatter measurements. The curved absorbing barrier was constructed to approach, as nearly as possible, the actual

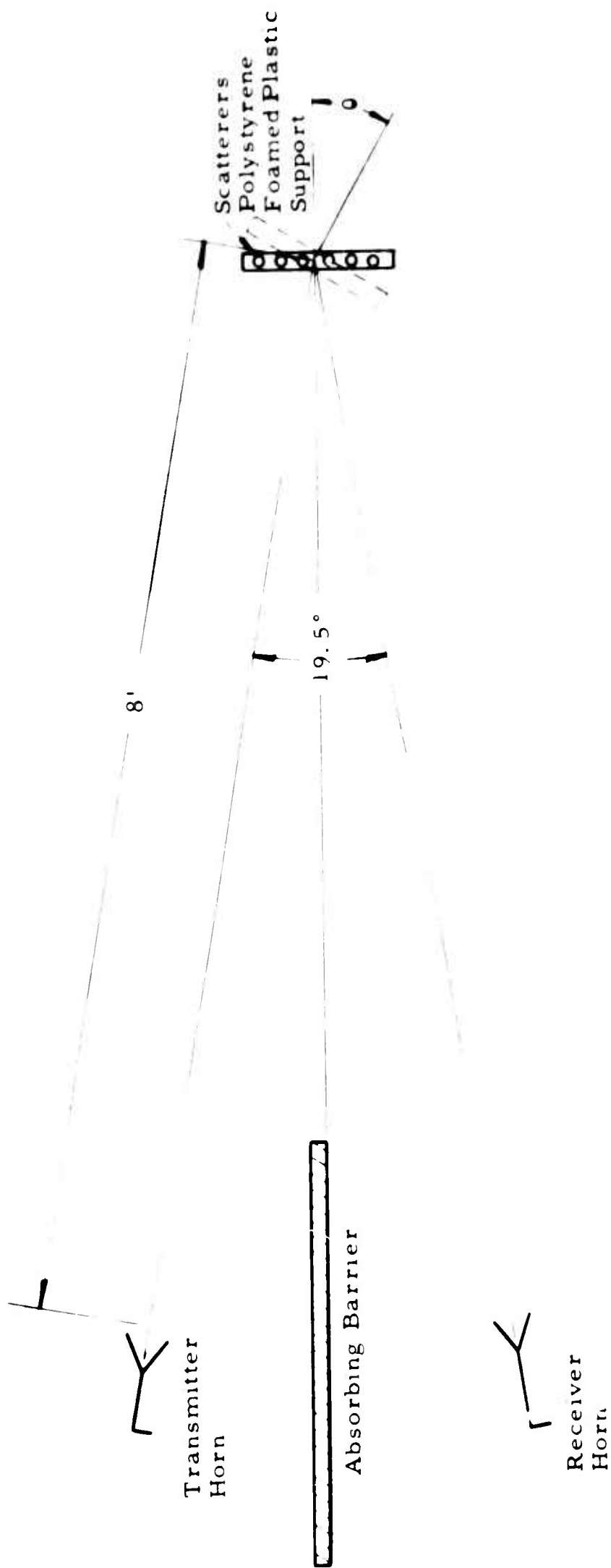
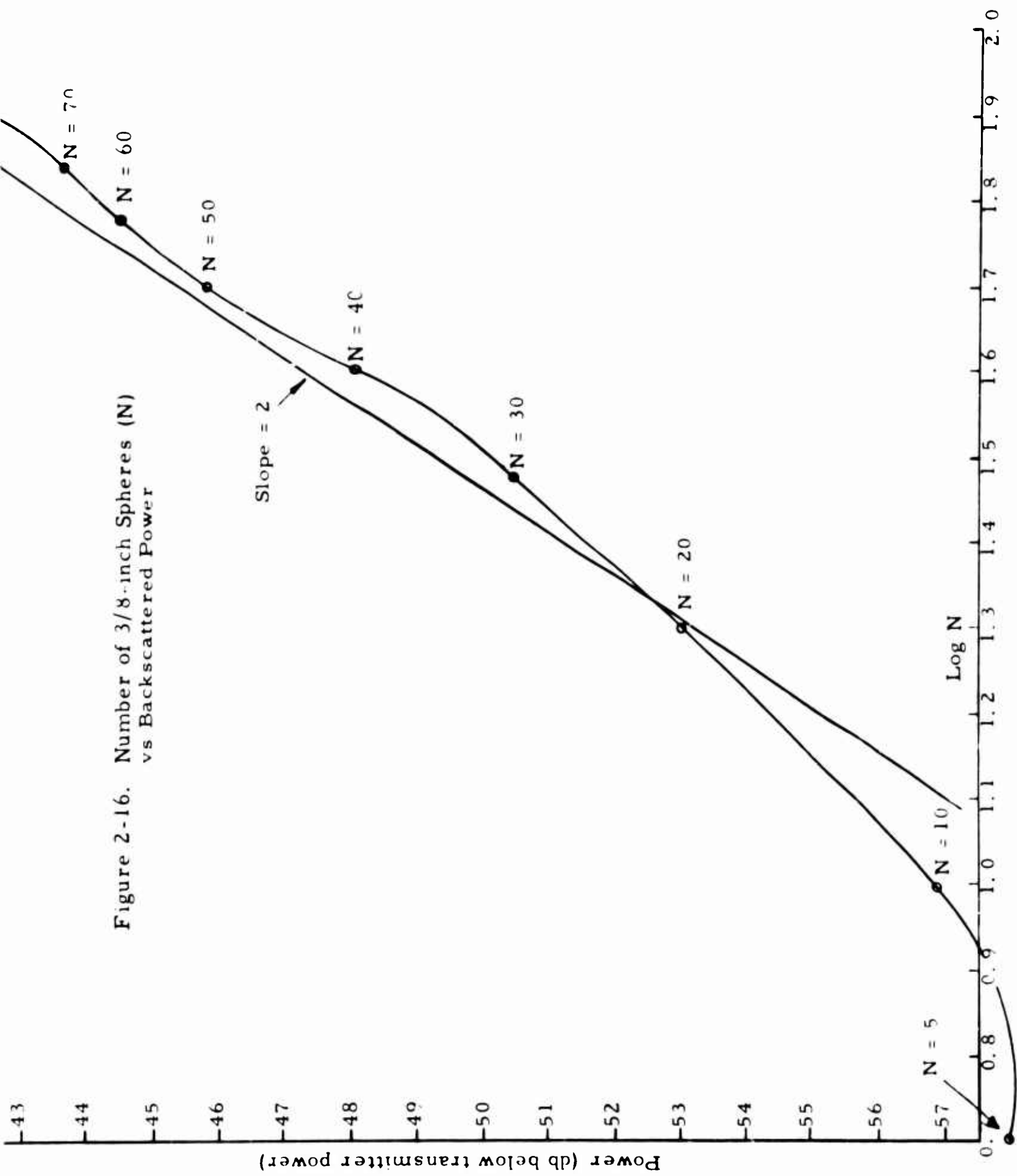
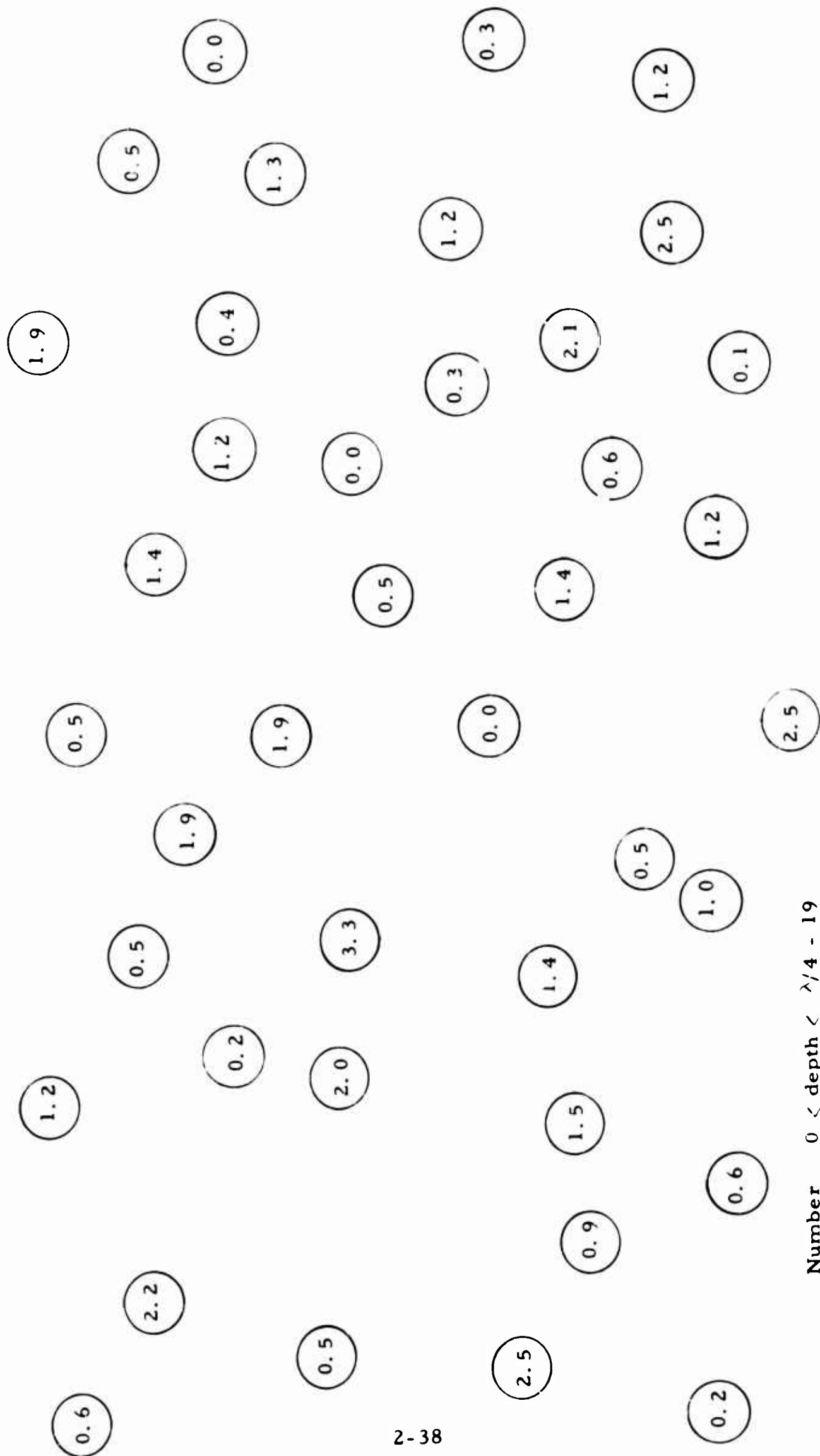
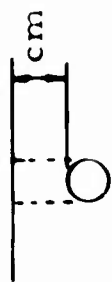



Figure 2-15. Diagram of Backscatter Measurement Facility



Figures indicate depth of spheres below surface



**Number**       $0 < \text{depth} < \lambda/4$  - 19  
 $\lambda/4 < \text{depth} < \lambda/2$  - 11  
 $\lambda/2 < \text{depth} < 3\lambda/4$  - 7  
 $3\lambda/4 < \text{depth} < \lambda$  - 3

Figure 2-17. Arrangement No. 1

Figures indicate depth of spheres below surface

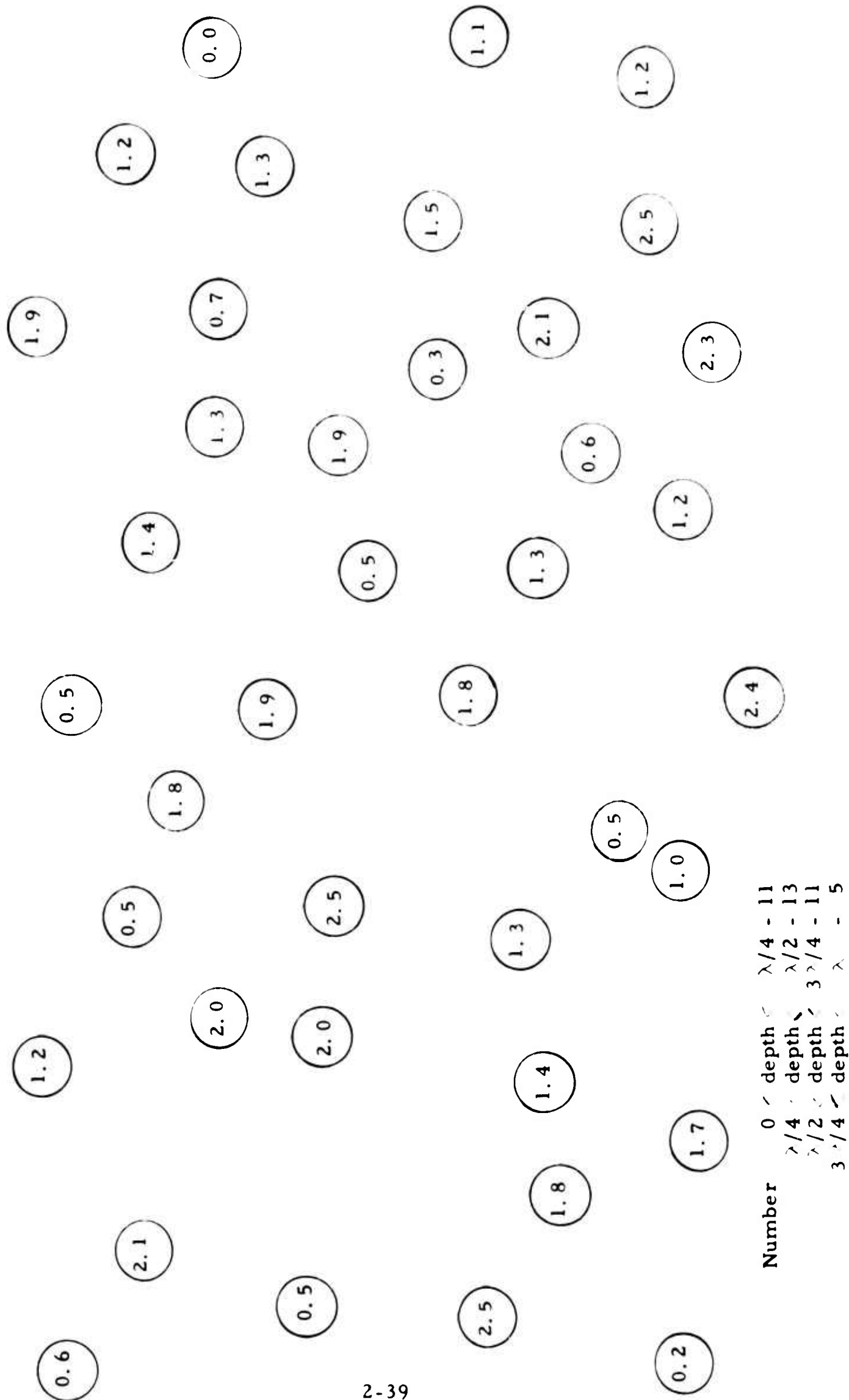


Figure 2-18. Arrangement No. 2



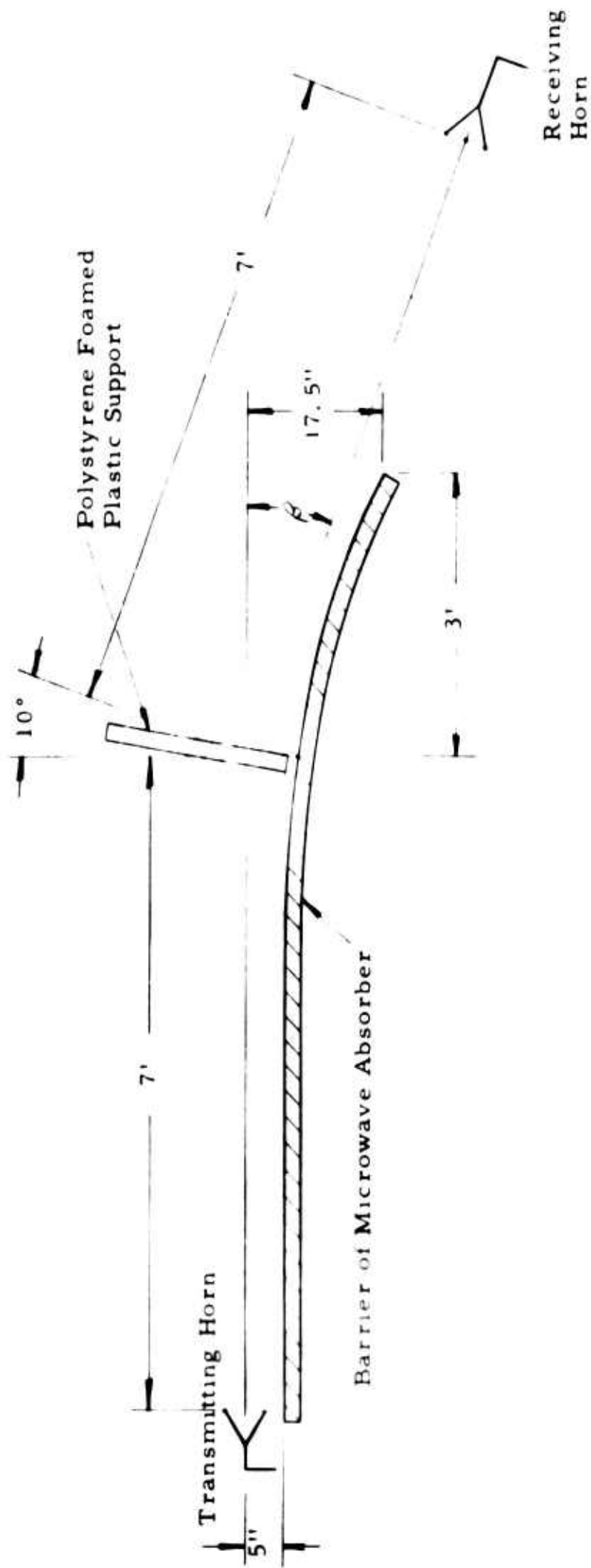


Figure 2-19. Diagram of Forward Scatter Facility

forward scatter problem where only a small amount of power reaches the receiver antenna. The power at the receiver antenna at an angle  $\beta$  from -5 to 22.5 degrees without scatterers in the field is shown in Figure 2-12.

The first arrangement of the spheres was a random pattern of 90 spheres located in the foam support so as to fill up the 3 db beamwidth of the transmitter antenna pattern at the position of the support. This resulted in location of the spheres in a circular area of 9-inch radius flattened to 7 inches at the barrier side. The resultant antenna pattern is shown in Figure 2-12. In order to show the effect of a smaller number of scatterers optimally placed, one-half of the spheres were removed with the remaining ones located in the crosshatched areas shown in Figure 2-20. The remaining curve on Figure 2-12 shows the reinforcement of signal strength at an angle of 20 degrees for which the positions of the layers of scatterers were calculated.

To increase the effect of optimum placement of scattering elements for phase reinforcement, the spheres removed from the support were added for a total of 90 spheres in the position shown by the crosshatched area in Figure 2-20. The results of this test are shown in Figure 2-11 with an increase of about 2 db. The effect of a random depth of the scatter cloud of spheres is also shown in Figure 2-11, indicating the forward scatter is insensitive to the depth of the cloud if no shielding of the scatterers takes place.

The condition for phase reinforcement by optimum placement of scatterers is that the layers form segments of concentric circular ellipsoids with foci at transmitter and receiver rather than plane surfaces. To simulate this condition the shape of the layers was modified as shown in the diagram of Figure 2-20. The scattering characteristics of this arrangement are shown in Figure 2-11 with approximately 3 db improvement over the case of scattering elements located between plane surfaces.

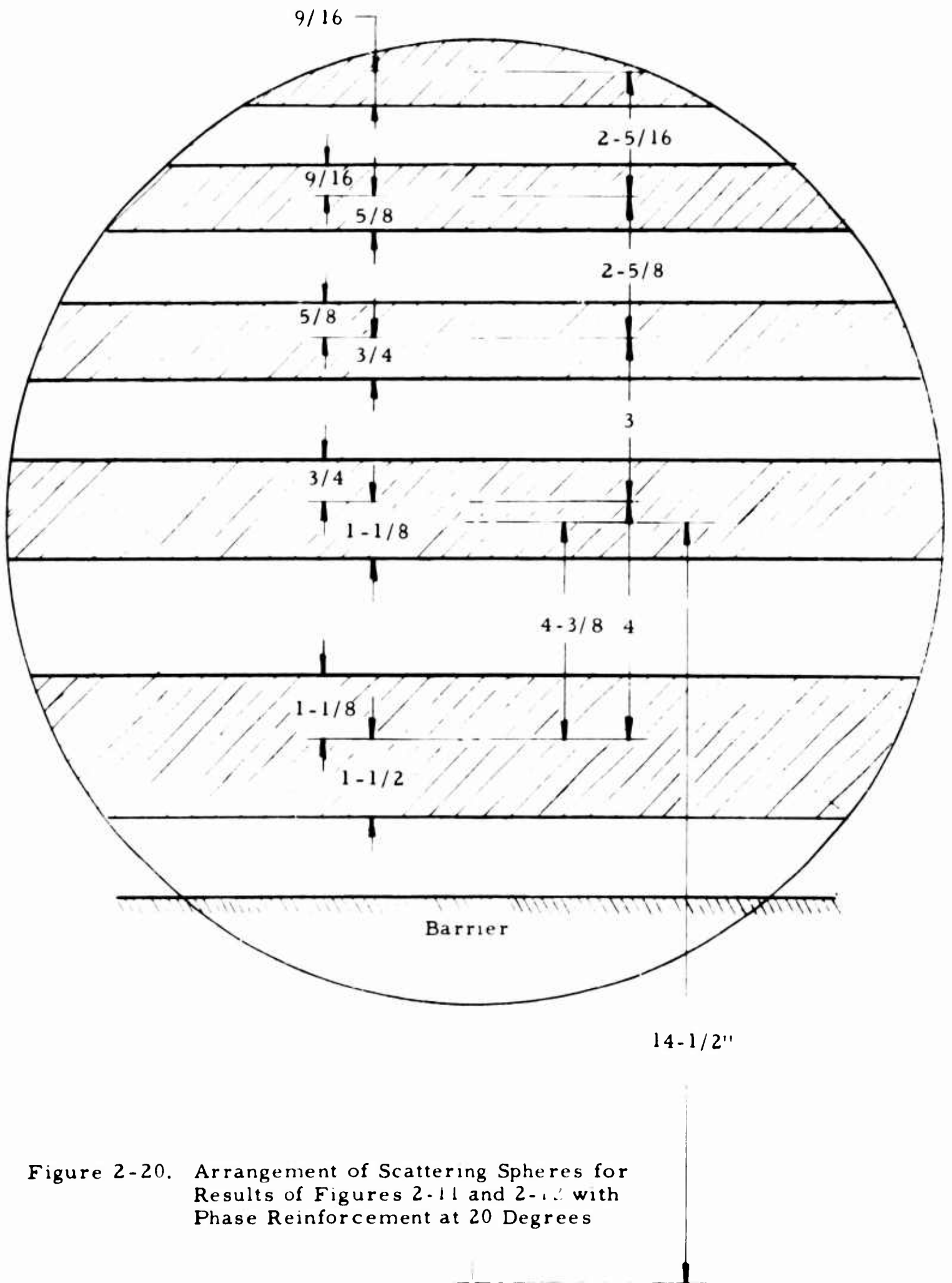


Figure 2-20. Arrangement of Scattering Spheres for Results of Figures 2-11 and 2-12 with Phase Reinforcement at 20 Degrees

### 3. Forward Scatter from Dipole Arrays

Reference to Figure 2-19 is again invited since the arrangement of microwave equipment and absorbing barrier is the same as for forward scattering from spheres. The dipoles were cut from #38 copper wire to lengths which when paired resulted in a refraction of the incident wave front due to the phase shift resulting from dipoles tuned above and below the operating frequency. Cellophane tape supported the dipoles on the foamed plastic structure. In the first test 24 dipole pairs were placed in the 3 db beamwidth of the transmitter as shown in Figure 2-21. Again, spacing on arcs of concentric circles is for phase reinforcement at a predetermined angle of receiver with respect to transmitter, in this case 20 degrees. The forward scatter enhancement is illustrated by the curve in Figure 2-13 where the field pattern without scatterers in the field is again inserted for comparison.

A second foamed plastic model was constructed to hold the dipoles in a cylindrical arrangement to simulate attaching them to a balloon. There were 24 dipole pairs attached in a 4-inch diameter in three rings about the model as shown in Figure 2-22. The field pattern modification for this arrangement is shown in Figure 2-13 in the case where the refractive effect of the dipole pairs was both away from and toward the receiver. The rotation of the model about an axis through the center of the cylinder resulted in an oscillation of signal strength of 1 db with the receiver in the 20-degree position. This showed the effect of shielding of some of the dipoles by others as the cylinder was rotated.

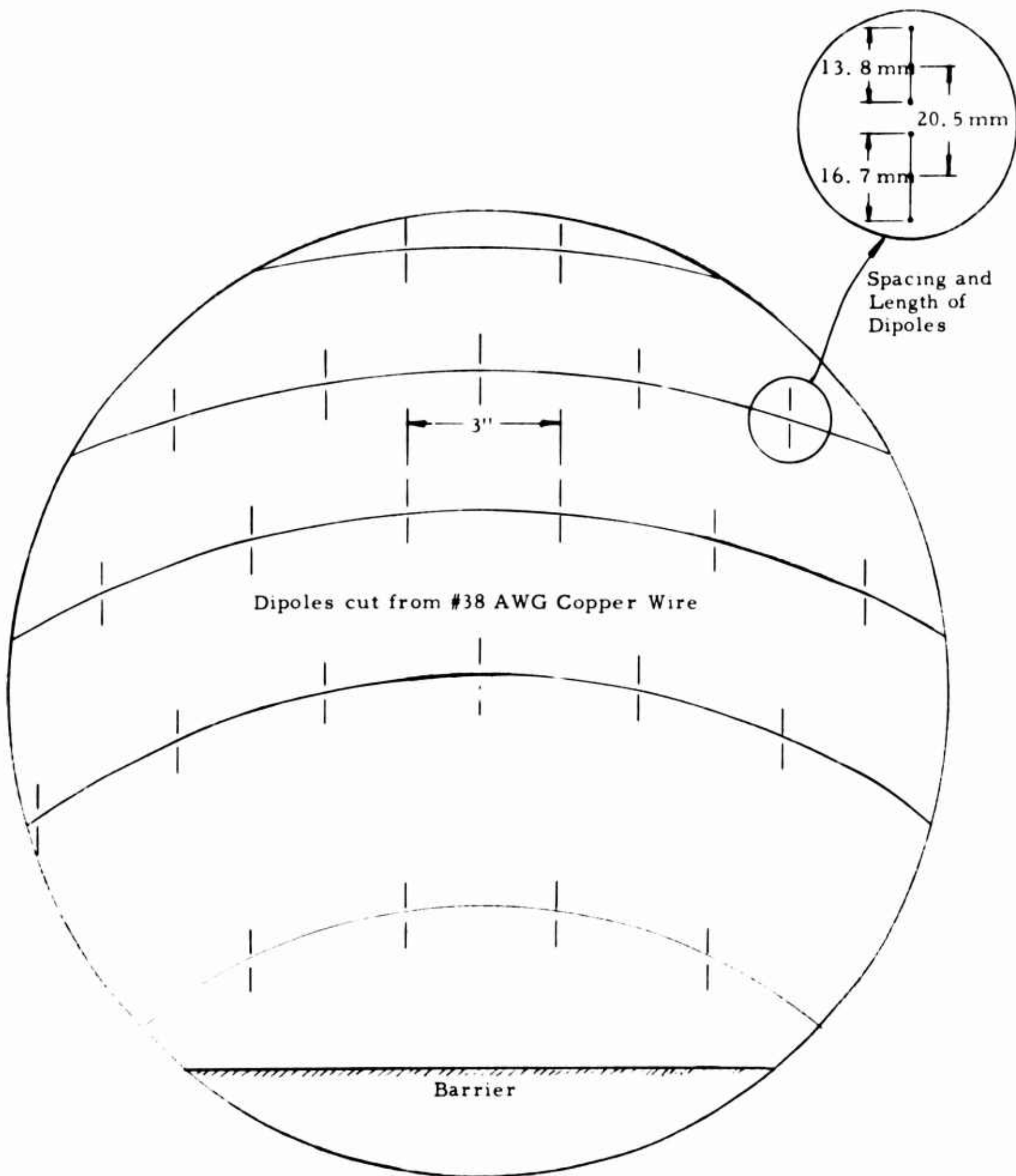


Figure 2-21. Placements of Dipoles for Phase Reinforcement at 20 Degrees

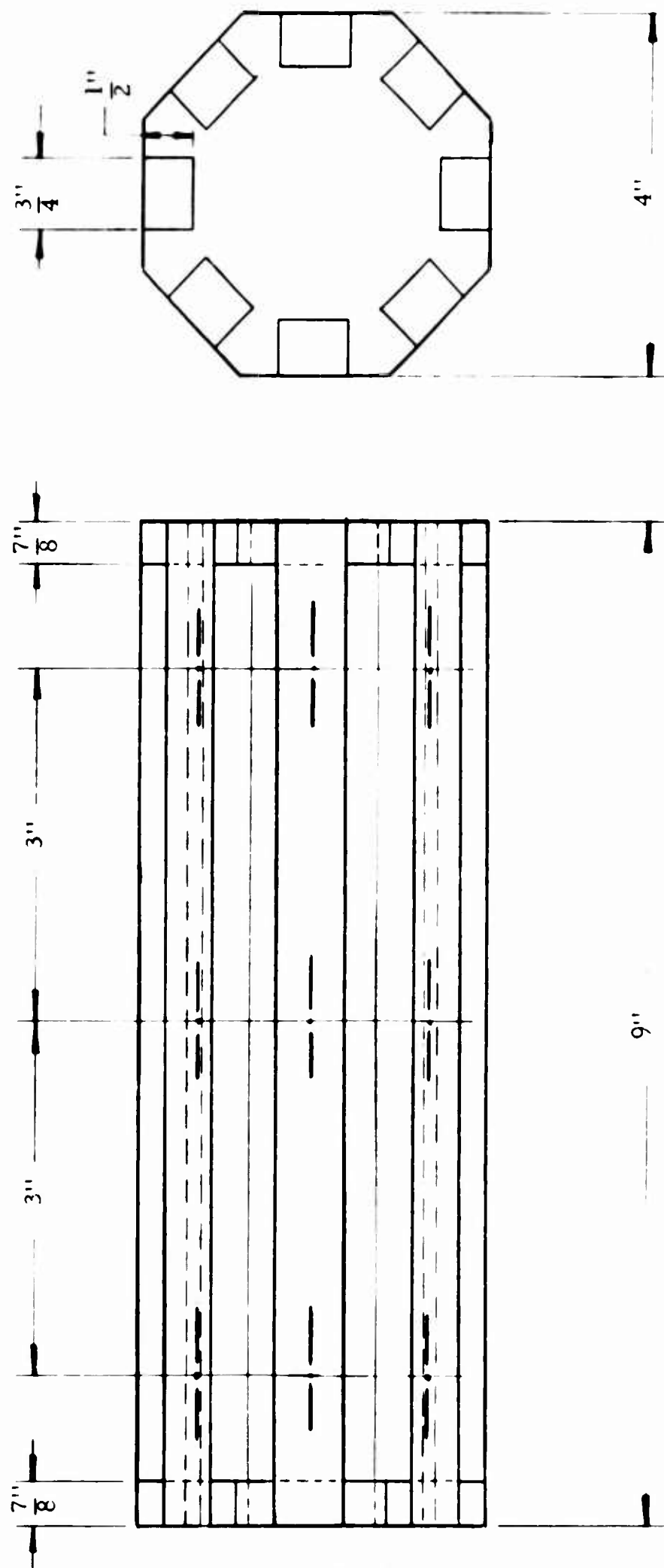


Figure 2-22. Cylindrical Polystyrene Foamed Plastic Model for Mounting of 24 Dipole Pairs

## G. Conclusions

- 1) Small untuned metallized spheres would not be feasible as artificial scatterers at the wavelengths considered (1 to 50 meters).
- 2) Metallized balloons could provide a scatter path but the large numbers of balloons required coupled with the necessity for constant replenishment make this approach economically undesirable.
- 3) It has been demonstrated that properly spaced tuned dipoles are very efficient. A single dipole array supported by a balloon system can be made to provide a scatter communication path over the maximum range as determined by path geometry. Balloon size (10 to 30 meters) is not much larger than the minimum size required to be self-supporting at 30 km.
- 4) An experimental investigation of the possibilities of artificial scatterers which are small with respect to the wavelength would be of great interest.

### III. DELIVERY AND SUPPORT OF SCATTERING ELEMENTS

#### A. Experimental Study of the Radiometer Effect to Prevent or Retard Gravitational Settling of Small Particles in the Stratosphere

##### 1. Natural Settling of Small Particles

Small particles which might be placed in the stratosphere will settle out in time. The rate of removal from the stratosphere from natural settling will depend on the particle radius  $a$ , its effective density  $d_p$ , the air viscosity and density  $\eta$  and  $d_a$ , and the mean free path  $\bar{\lambda}$ . In general, the settling velocity  $V_s$  of solid spherical particles is given by the relation:

$$V_s = \frac{2 (d_p - d_a) a^2 g C}{9 \eta} \quad (3-1)$$

The parameter  $C$  is the Cunningham slip correction which becomes significant only when the particle size is of the same order as the mean free path.

The slip correction factor is given by:

$$C = 1 + k \frac{\bar{\lambda}}{a} \quad (3-2)$$

where  $k$  depends to some extent on  $(\bar{\lambda}/a)$  as shown in Figure 3-1. At the low densities of the upper atmosphere, molecular slip has a very pronounced effect in increasing the settling velocity of small particles, as may be seen in Figure 3-2.

Since the settling velocity of a particle is directly proportional to its density (neglecting air density), consideration was given to the use of hollow spheres, possibly filled with a light gas, to retard settling. In this case, the particle will exhibit a net reduction in density to  $d_p'$  which is given by:



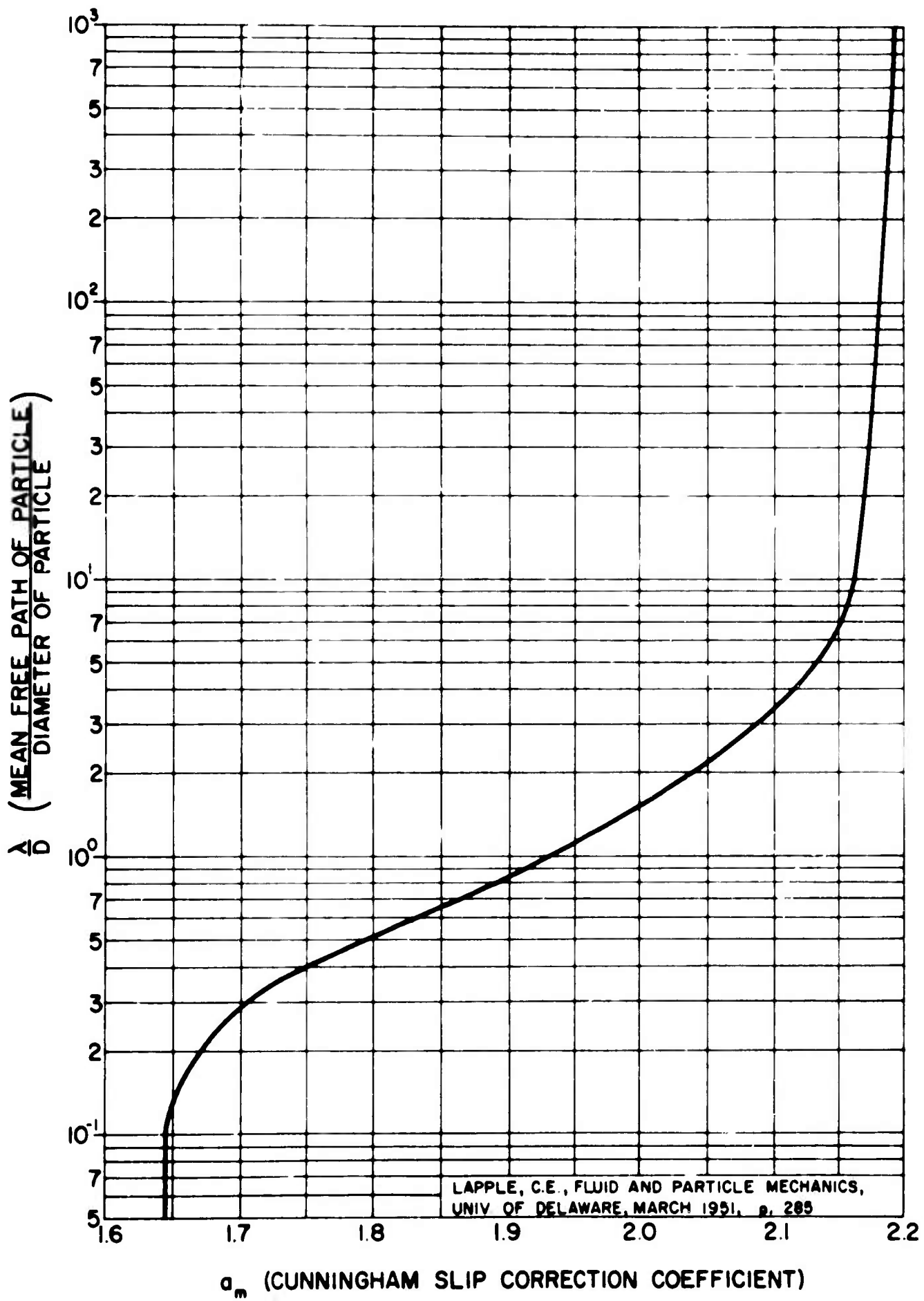


Figure 3-1. Variation of Slip Coefficient

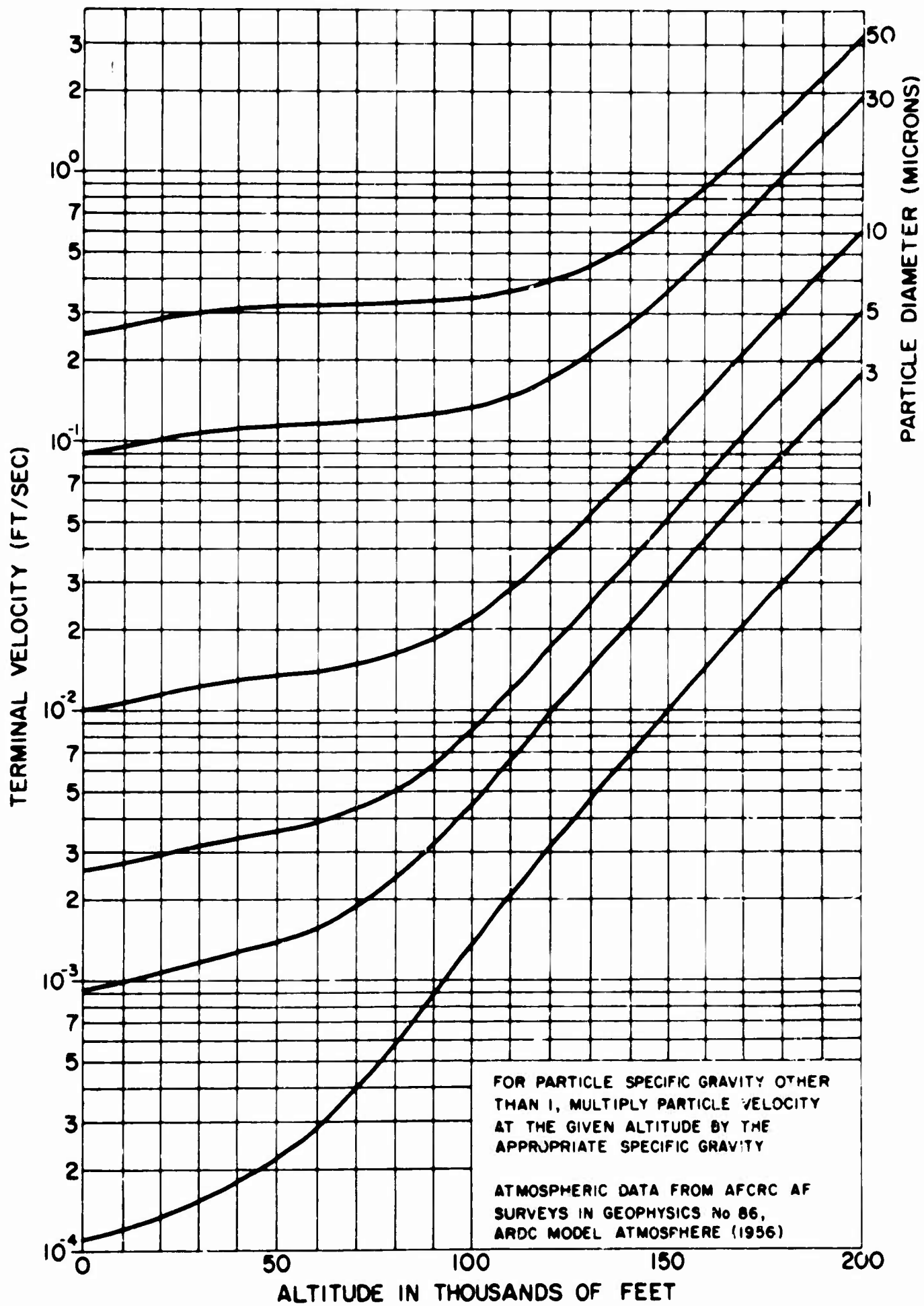


Figure 3-2. Settling Velocity in the Stratosphere

$$d_p' = \frac{3 d_s \delta}{a} \quad (3-3)$$

where  $d_s$  is the density of the skin and  $\delta$  is the skin thickness. Equation (3-3) neglects the weight of gas inside the particle and, therefore, represents the apparent density when the particle contains the lightest possible gas or a perfect vacuum. Combining (3-3) with (3-4) settling velocity of a hollow spherical particle becomes:

$$V_s = \frac{2}{3} \frac{g d_s \delta a C}{\eta} \quad (3-4)$$

Equation (3-4) applies to small particles where for any reasonable skin thickness (of the order of one micron) and skin density (assumed to be unity)  $d_a'$  is large compared with the density of air. It can be shown that a sphere with a skin of this thickness and density must be of the order of centimeters in diameter to float when filled with hydrogen or helium. In addition, the rate of loss of such a light gas by diffusion through a one-micron skin would be exceedingly high.

In addition to spherical particles, consideration has also been given to cylindrical filaments. The settling velocity of a cylinder is given by:

$$V_s = \frac{g (d_p - d_a) a^2 C'}{4 \eta} (2 - \ln R_e) \quad (3-5)$$

where

$$R_e = \frac{2 a d_a V_s}{\eta} = \text{Reynolds number} \quad (3-6)$$

The slip correction factor  $C'$  for cylinders has the same form as  $C$  but is less than  $C$  for a given  $\bar{\ell}/a$  ratio.<sup>4</sup> Equation (3-5) is valid where  $Re < 0.1$  and the fiber is assumed to fall broadside-on.

A comparison of settling velocities for hollow spheres, solid spheres, and cylindrical filaments as a function of particle size for 30 km altitude is shown in Figure 3-3.

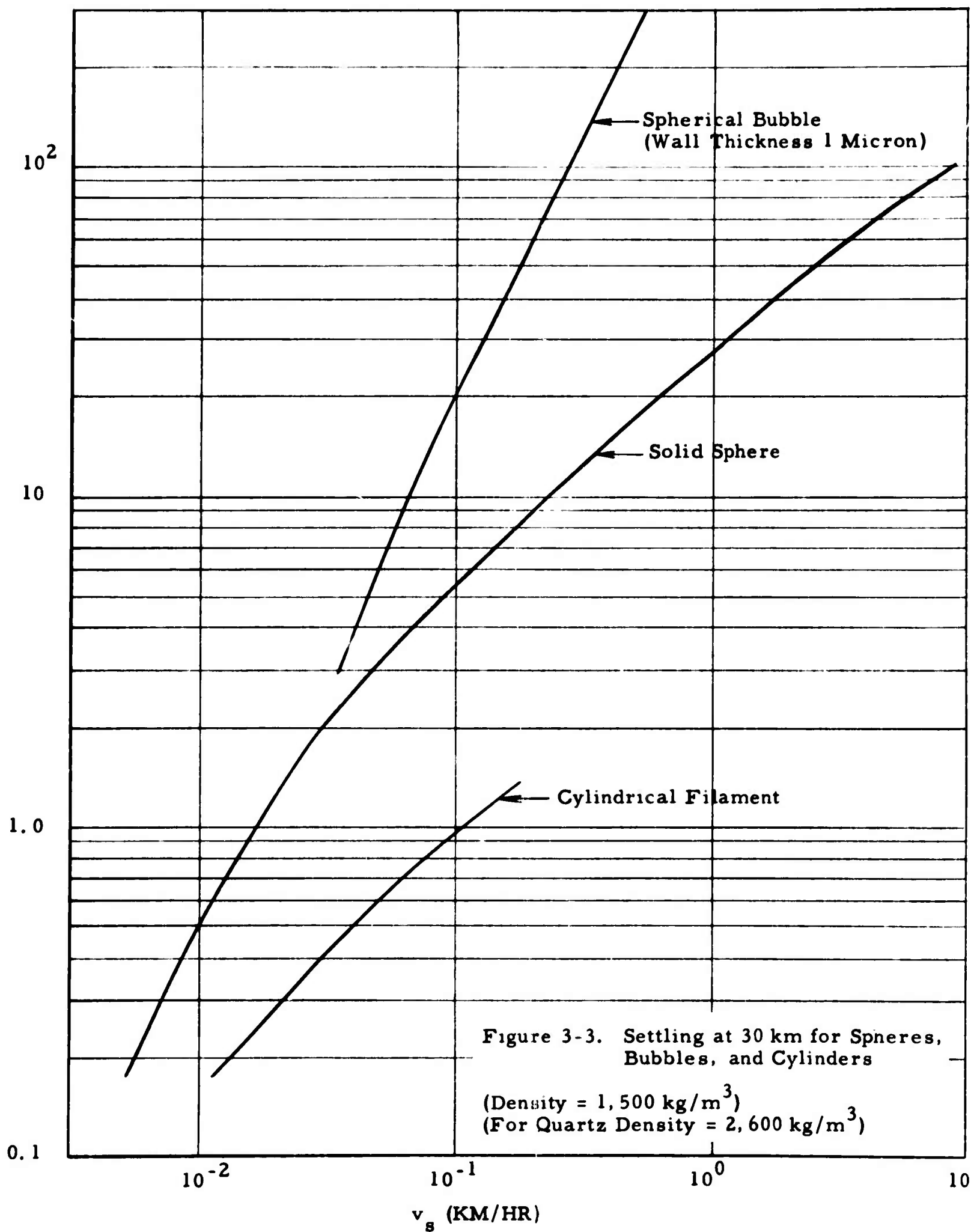
## 2. Studies on the Radiometer Effect

### a. Background

Since small particles placed in the stratosphere for electromagnetic propagation purposes would settle out more or less rapidly, depending on their size, this program has included a study of the radiometer effect as a possible method to prevent or retard settling. It has been known for over a century that a body suspended in a gas and exposed to a radiation source is acted upon by a force acting away from that source.<sup>5</sup> This apparently accounts for the dust-free space around a heated wire and the migration of particles suspended in a thermal gradient.<sup>6</sup> Photophoresis, which is the migration of particles with respect to a strong light source, appears to be a closely related effect.

The radiometer force is associated with differential heating of a particle and consequent gas dynamic effects. From the theoretical work of Epstein<sup>7</sup>, Sexl<sup>8</sup>, and Hettner<sup>9</sup> two regimes exist. When  $\bar{\ell}/a \ll 1$  the force is inversely proportional to pressure, while when  $\bar{\ell}/a \gg 1$  it is directly proportional to pressure.

In the regime where  $\bar{\ell}$  is large compared to  $a$ , an unevenly heated particle will give rise to a force due to the difference in temperature and therefore kinetic energy of the gas molecules striking or rebounding from the hot and cold surfaces, respectively. Thus, if it is assumed that a



uniform temperature gradient exists across a spherical particle giving a temperature differential between the poles of the particle of  $\Delta T$ , then a first approximation calculation reveals the force to be:

$$F = - \frac{a^2 P \Delta T}{6 T} \quad (3-7)$$

where  $P$  is the absolute pressure and  $T$  the absolute temperature.

The case where  $\bar{l}$  is small compared to  $a$  is considerably more difficult because the dominant effect is due to fluid stresses arising from conduction of heat to the surrounding gas. For the photophoresis phenomenon at high gas pressures, Sexl<sup>6</sup> and Hettner<sup>7</sup> derived the equation:

$$F = - \frac{k P \bar{l}^2 \Delta T}{T} \quad (3-8)$$

This equation agrees in form with that of A. Einstein<sup>10</sup> and Epstein<sup>7</sup> who worked on the theory of the conventional radiometer; however, the value of the constant  $k$  differs for all of these authors since it evidently depends upon the specific conditions, including the physical properties of the particle and the gas. In any case, the value of the constant is somewhat academic, since for very small particles it is virtually impossible to determine the temperature differential  $\Delta T$  across the particle.

Although they studied a slightly different case than that of photophoresis, the work of Rosenblatt and LaMer<sup>6</sup> is the nearest approach to quantitative measurement of the radiometer effect with small particles. They measured the force on small particles suspended in a gas which had a uniform thermal gradient. In the absence of other data, however, their results have been used to estimate the order of magnitude of the force produced when the gas receives its heat from the particle.

An analysis of the Rosenblatt data reveals it does fit the form of Equation (3-8) as shown in Figure 3-4. The equation has been rearranged to the form:

$$\frac{F}{\pi a^2 \Delta T} = - \frac{k P}{\pi T} \left( \frac{D}{a} \right)^2 \quad (3-9)$$

and  $\frac{F}{\pi a^2 \Delta T}$  plotted against  $P \left( \frac{D}{a} \right)^2$  (see Figure 3-4). Over most of the range of experimental data, a linear relationship is observed.

Based upon the Rosenblatt data and Equation (3-7), Figure 3-5 has been derived to show the order of magnitude of the radiometer force to be expected for small particles.

#### b. Special Particles having a Radiometer Effect

Particles in the high stratosphere exposed to solar radiation might be expected to experience heating. If, however, the side of the particle exposed to the sun became warmer, the result would be a force acting away from the sun or in the same direction as gravity. The opposite effect or negative photophoresis is known. A particle which might exhibit negative photophoresis is shown in Figure 3-6.

If a particle transparent to infrared were coated on one side with a strong absorber such as graphite, the effect would be achieved. The fluid stresses resulting from the temperature gradient should produce a torque tending to keep the particle oriented with the warmer side away from the sun, thus producing a radiometer force toward the sun or opposing gravity.

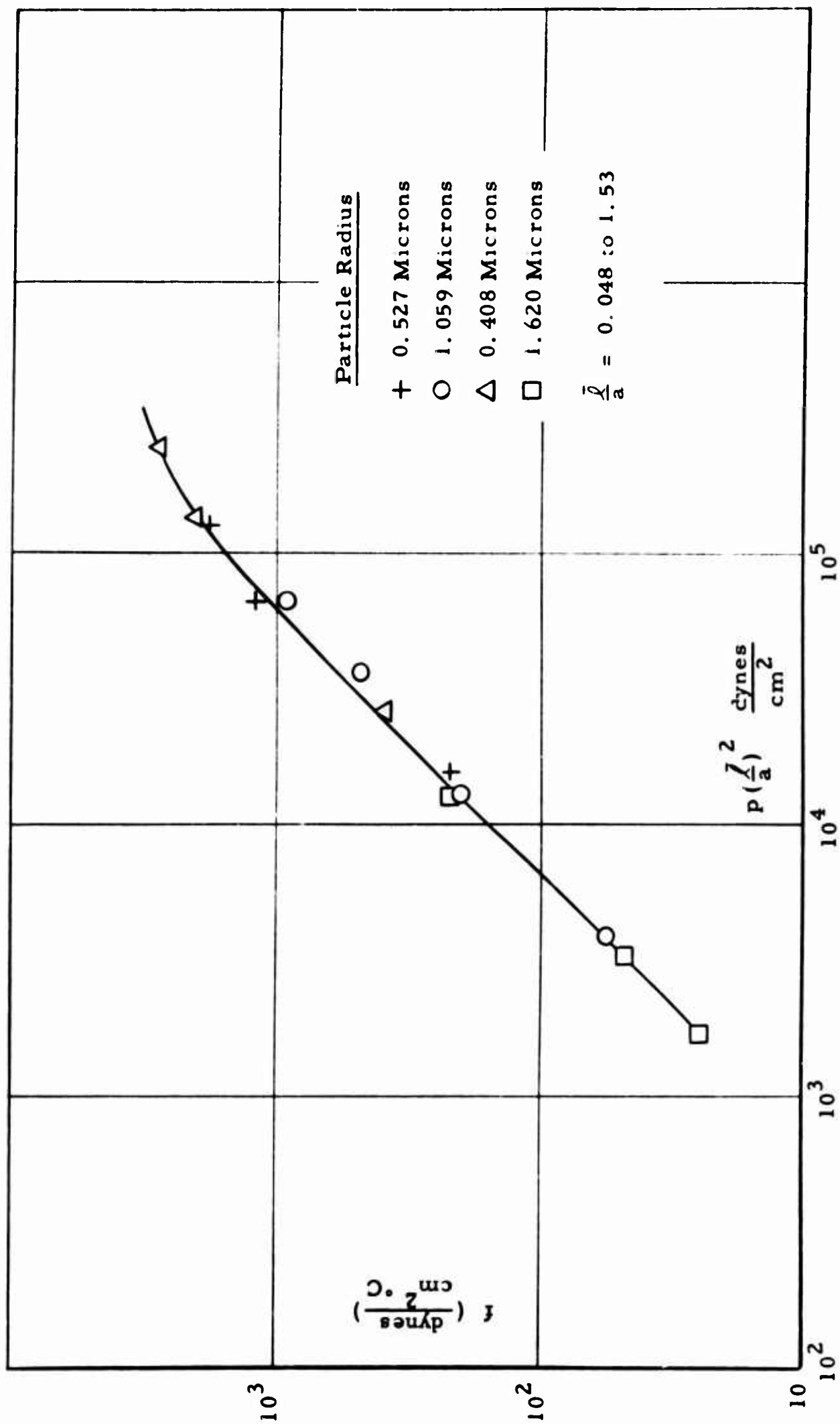


Figure 3-4. Radiometer Effect on Micron-Size Particles.  
Data taken from Rosenblatt.



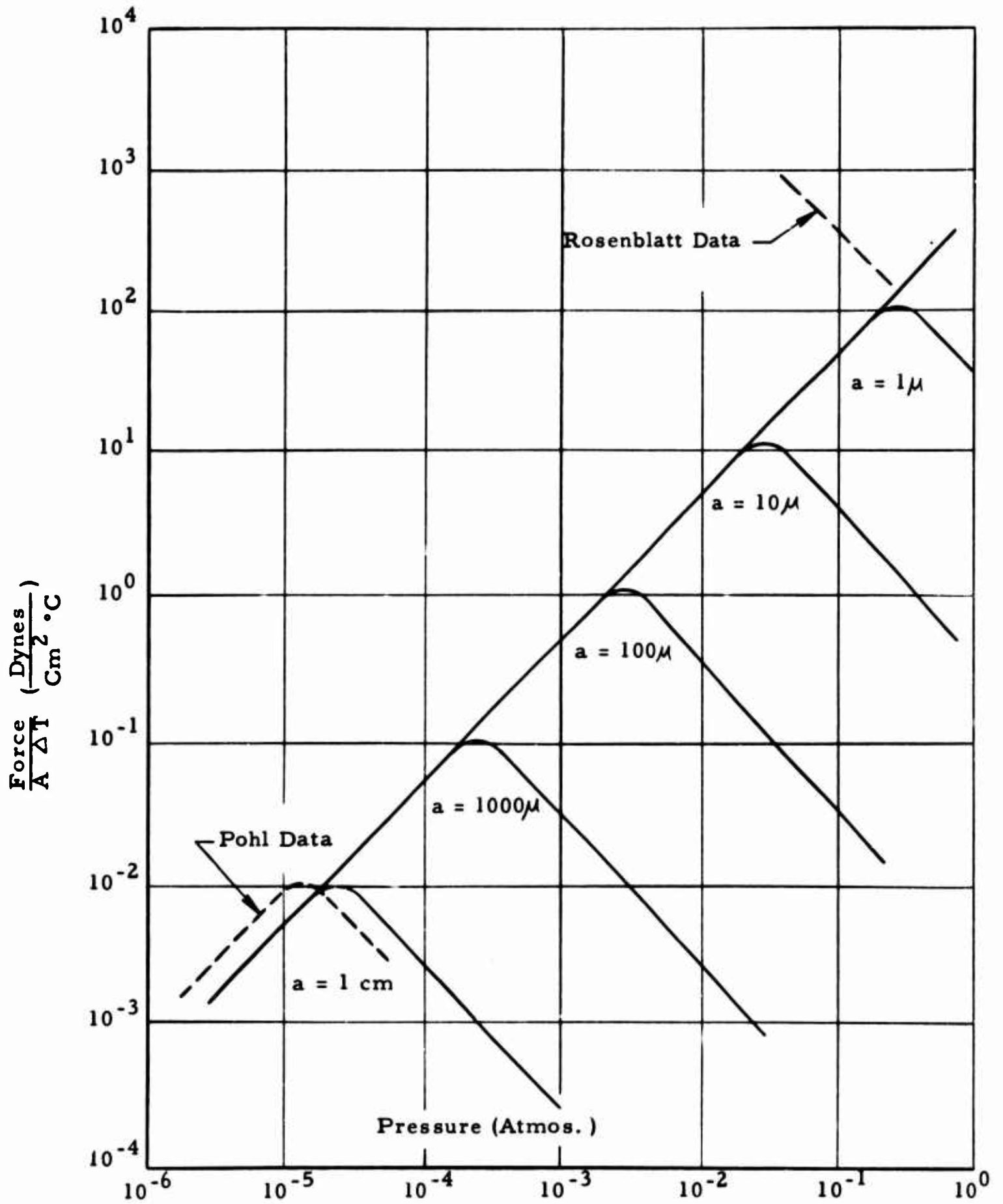


Figure 3-5. Radiometer Force on Particles of Various Sizes

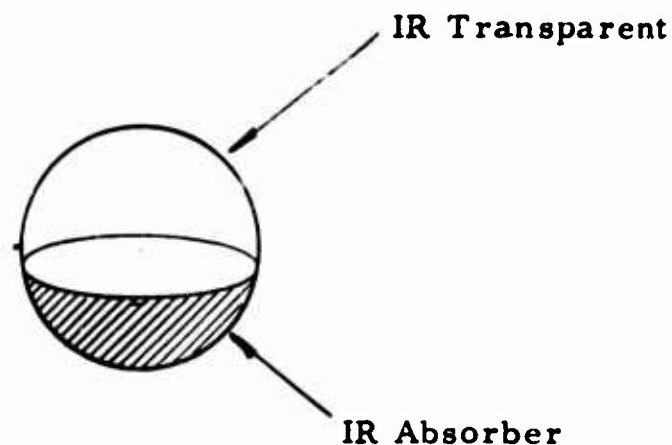


Figure 3-6. Particle which would Exhibit Negative Photophoresis or Motion toward the Sun

#### c. Experimental Study

Because little or no quantitative data exists on the forces produced by differential heating of small particles, an experimental program was undertaken. Figure 3-7 shows the experimental set-up photographically and Figure 3-8 is a schematic diagram of the set-up. The apparatus is essentially a torsion balance suspended in a vacuum system. The system is evacuated by means of a Welch Duo-Seal vacuum pump and a Consolidated Vacuum Corp. air-cooled oil diffusion pump. An Alphatron vacuum gage and controller indicates the system pressure. A check calibration of the Alphatron gage was made against an "Octoil S" manometer. A cathetometer was used to determine level changes in the manometer. It was found that each set of readings were within the limits of the Alphatron ( $\pm 2\%$ ) and the experimental limits of the test method.

As shown in Figure 3-8, an 80-micron diameter quartz fiber, approximately 22 cm long is suspended in the center of a vacuum chamber. The end of the fiber is attached to the center of a quartz rod such that the rod is perpendicular to the fiber. At each end of the quartz rod is a test sphere or vane. The torsion coefficient of the fiber was determined for each new set of test spheres or vanes.

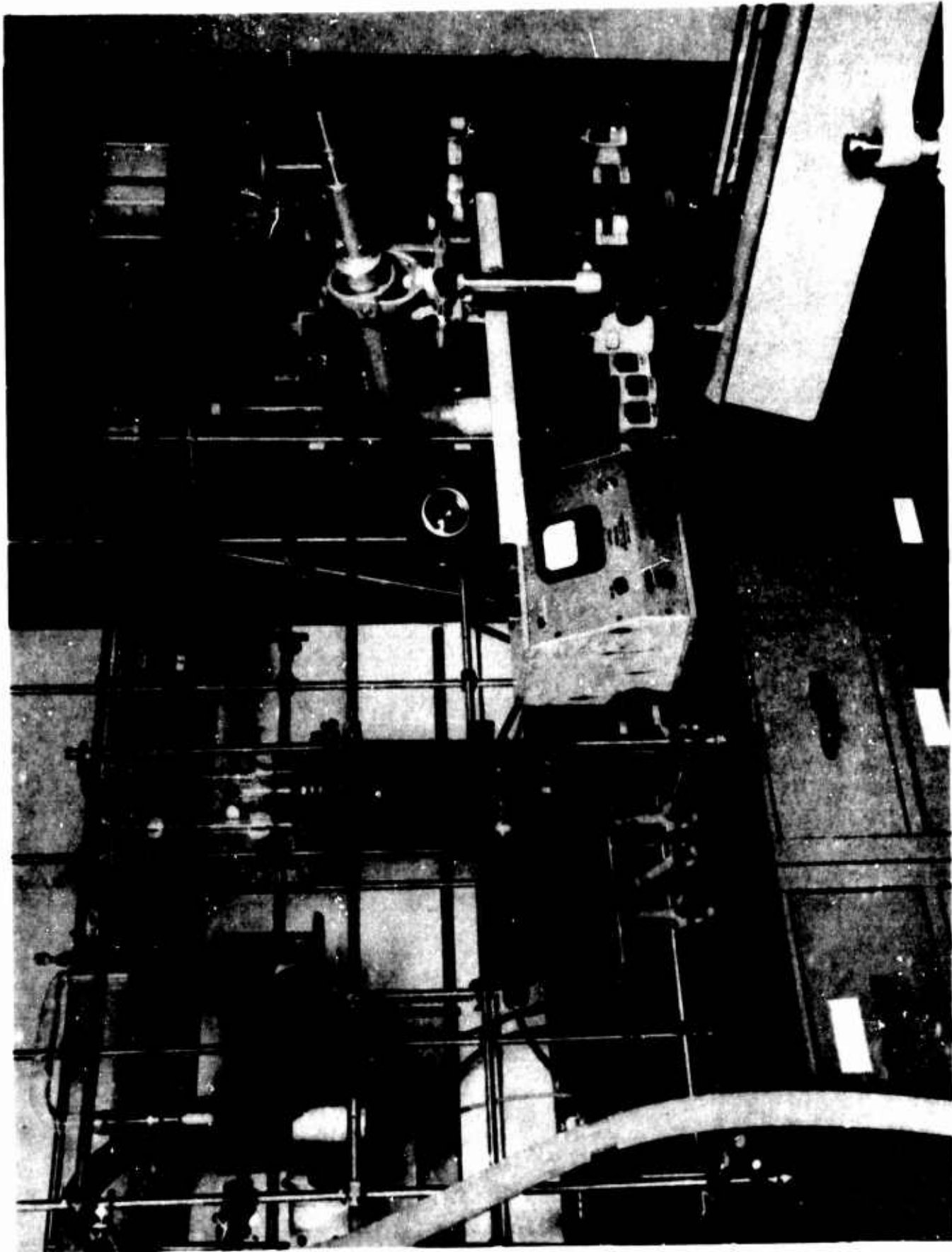


Figure 3-7. Experimental Set-Up Used to Study the Radiometer Effect

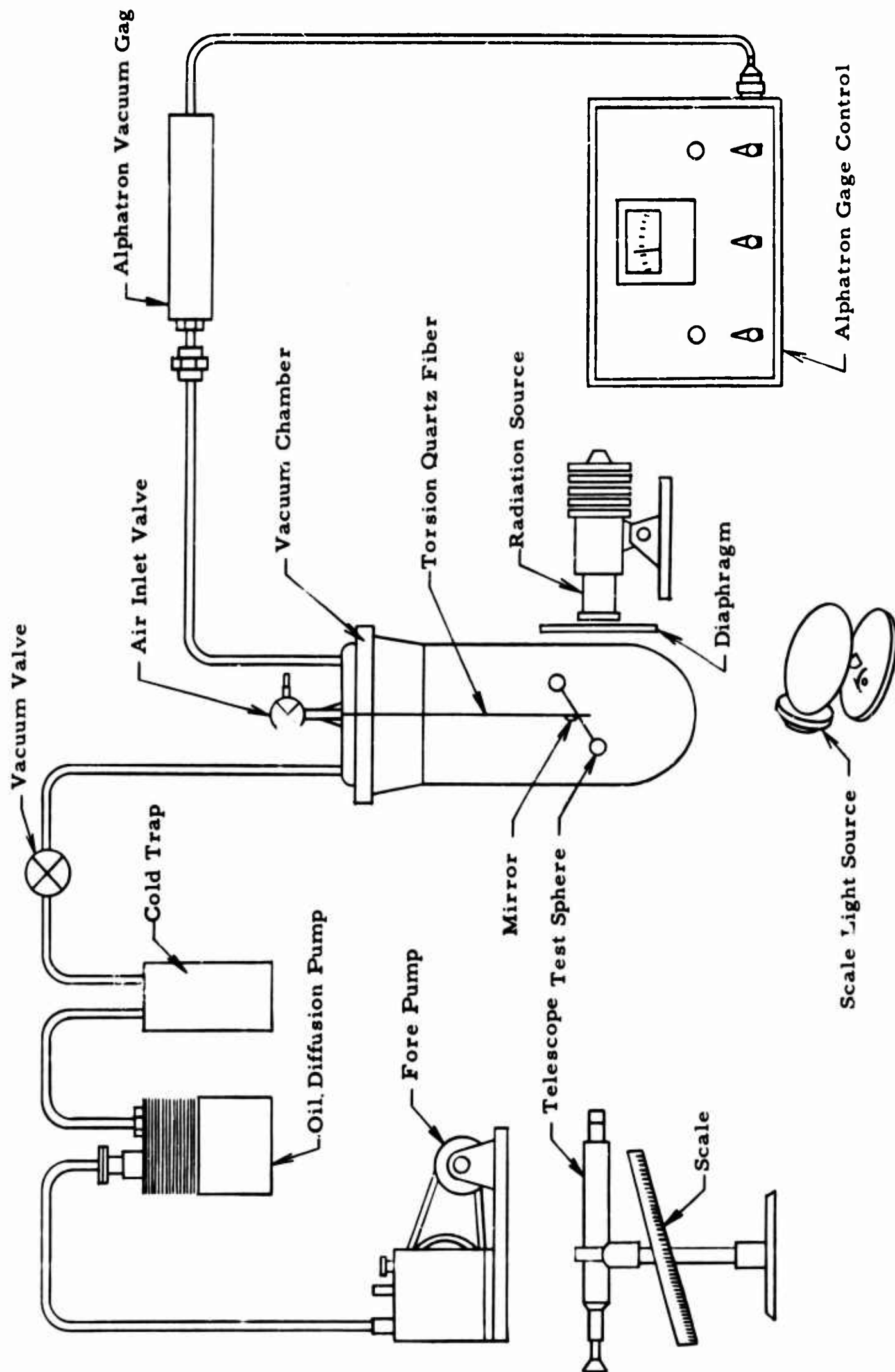


Figure 3-8. Schematic Diagram of Experimental Set-Up Used to Study the Radiometer Effect

The test items were: 1) a 13-mm diameter, thin-walled, hollow quartz sphere, 2) a 6-mm diameter, thin-walled, hollow quartz sphere, and 3) an 0.01-mm diameter, 1.502 m long glass fiber wound on a 1 cm<sup>2</sup> quartz supporting vane. Each sphere had a hole and thus the interior of the sphere was at the same pressure as the environment. The spheres were blackened on one side by exposing the spheres to a carbonizing flame and then wiping 1/2 of the sphere clean. The fibers were more difficult to blacken. It was accomplished by vacuum depositing carbon on a properly masked vane containing the fibers.

Two different radiation sources were used. The first was a 3-position Westinghouse microscope illuminator lamp (18 amps, 6 volts). All the reported data on the spheres and fiber were obtained with this lamp. In addition, for the fibers an attempt was made to use a zirconium arc source. However, it was found that the fiber vanes moved when exposed to this source whether or not fibers were present. The area of radiation was controlled by means of a variable diaphragm.

The radiation flux received by the samples was determined by the use of a foil calorimeter. A platinum foil, 1 cm<sup>2</sup> and 50 microns thick, was blackened on one side by a carbonizing flame. To the other side, a differential copper-constantin thermocouple was attached. This calorimeter was calibrated by utilizing as a standard a Barnes Engineering Co. black body source.

In order to observe and measure the deflection of the torsion system, a telescope, scale, and reflecting mirror were utilized. The mirror was placed at the point of attachment of the torsion fiber and the quartz rod. An illuminated scale reflected in the mirror and observed through a Gaertner Scientific Co. telescope gave a measure of the deflection.

To prevent interference from outside radiation and reflections, the vacuum chamber was enclosed with black paper. There were only openings for the radiation source and for viewing the mirror as can be seen in Figure 3-7.

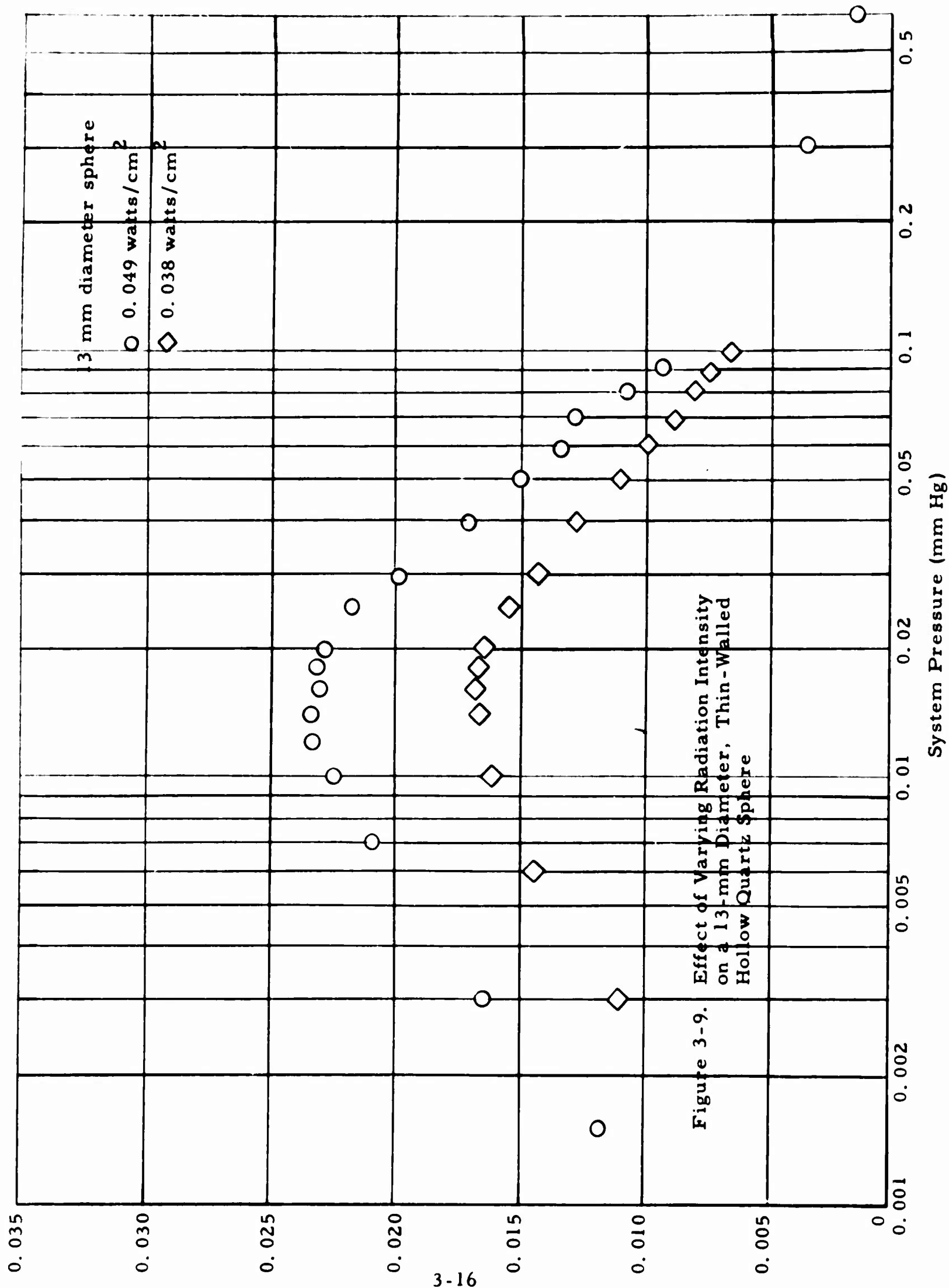
#### d. Results of the Experimental Study

The experimental results are summarized in Figure 3-9, Figure 3-10, and Table 3-1. Figure 3-9 gives the force per unit cross-sectional area over a range of system pressures for the 13-mm diameter sphere at two different radiation intensities. As expected, in the region of maximum force, the greater radiation flux gave the larger force per unit cross-sectional area. However, as can be seen in Table 3-1, which gives values at maximum deflection, the force per unit radiation flux is almost the same. If one takes into consideration the probable experimental error involved in the measurements and calibration, the two values 0.477 dynes/watt and 0.442 dynes/watt are in experimental agreement.

A reduction in the size of the spheres from 13-mm to 6-mm diameter appeared to increase the force per unit radiation intensity from 0.477 to 0.673 dynes/watt. This may be due to non-uniform radiation intensity. The outer portion of the radiation beam is probably weaker than the center; therefore, the small sphere would receive a larger intensity per unit area.

The rather low force per unit radiation intensity, 0.096 dynes/watt, exhibited by the 0.01-mm diameter glass fiber is probably due to the relatively higher rate of thermal conductivity across the small diameter solid fiber. Since, as previously discussed, a temperature differential between the two halves of the body is required, it is therefore expected in this instance that a relatively small force, if any, would be exerted.

Figure 3-10 gives the force per unit cross-sectional area over a range of system pressures for the 13-mm and 6-mm diameter spheres for exposure to the same radiation intensity of 0.049 watts/cm<sup>2</sup>. In addition, there is a relationship for the 0.01-mm diameter fiber exposed to a radiation flux of 0.059 watts/cm<sup>2</sup>. This figure indicates that there is a change in system pressure (which is related to the mean free path) at which the maximum force is exerted for each size sample. However, the change is not as dramatic as would be expected from the theoretical considerations.



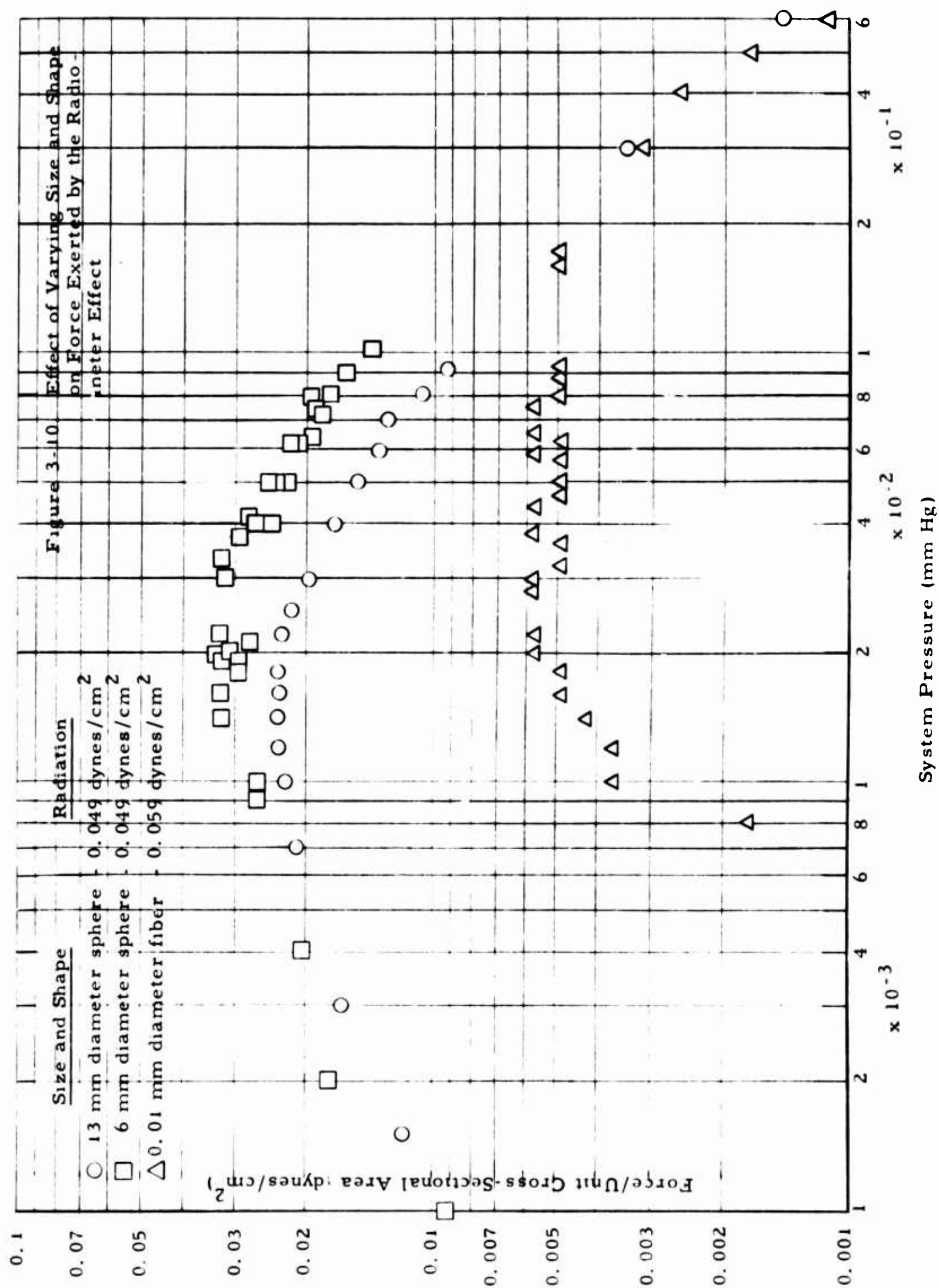




Table 3-1. Summary of Data at Maximum Exhibited Force

Material and Shape	Diameter mm	Radiation Flux * watts/cm <sup>2</sup>	Maximum Force Exerted		Pressure at Max. Force mm Hg	Mean Free Path at Pressure mm	Altitude Corresponding to Pressure km
			dynes/cm <sup>2</sup>	dynes/watt			
thin-walled hollow quartz spheres	13	0.049	0.0233	0.477	0.015	3.4	77
		0.038	0.0168	0.442	0.015	3.4	77
thin-walled hollow quartz spheres	6	0.049	0.0330	0.673	0.020	2.5	75
glass fiber	0.01	0.059	0.0057	0.096	0.02-0.17	2.5-0.30	75-61

\* Solar Radiation - 0.138 watts/cm<sup>2</sup>

#### e. Conclusions of the Experimental Study

It was concluded that at the altitude of 30 km. the area of our proposed operation, there would be no discernible force due to radiometer effect. Using the data obtained on the 6-mm diameter sphere and assuming the following:

- 1) a linear force per unit radiation intensity relationship
- 2) a solar radiation intensity of  $0.138 \text{ dynes/cm}^2$
- 3) an insulating material of poor thermal conductivity with a density of 1
- 4) the material can be made into a hollow sphere with a shell thickness of 0.001 mm
- 5) no other settling force is acting on the sphere other than gravity,

calculations showed it would require a 4-mm diameter sphere at an altitude of about 75 km to obtain suspension due to the radiometer effect phenomenon.

#### B. Delivery and Support of Large Scattering Elements

##### 1. Introduction

This section covers studies of techniques for delivery and support of large scattering elements for improvement of electromagnetic propagation.

Several different types of large scattering elements have been studied including 1) metalized balloons 2) conventional linear dipoles, and 3) special dipole configurations. The discussions presented in the following paragraphs deal with the problems involved in the delivery of these elements to altitudes between 30 and 40 kilometers so they will be properly located and maintain the effectiveness of the scattering system for a practical duration.

At this point it is convenient to divide the problem into two areas  
1) the support of the scattering elements and 2) the delivery of the elements and required supporting system to the required location. Because the physical characteristics of the supporting system have a strong influence on the delivery approach selected, the problem of support will be discussed first.

## 2. Support of the Scattering System in the Atmosphere

Methods have been considered for supporting the scatterers in the atmosphere to provide a useful duration over which time scattering elements will be available to improve communication. The factors involved in the limitations on the useful duration of the system are the rate of vertical descent (due to gravity) of the scattering elements, and the horizontal velocity of travel of these elements due to atmospheric circulations.

Studies of atmospheric circulation, found in Appendix B, have determined that this consideration will limit the useful duration of any free-floating scattering elements to approximately 1 to 6 hours, depending on the local wind velocity. Therefore, no incentive exists to provide a dipole supporting system capable of a duration longer than approximately 6 hours.

Systems depending on 1) aerodynamic forces and 2) buoyancy appear to offer the most reasonable solutions.

### a. Aerodynamic Systems

The function of an aerodynamic system would be to limit the rate of descent of the scattering elements so that for periods of 1 to 6 hours they are contained within altitude limits which are compatible with the communication requirements.

The simplest form of such a system would be one depending on aerodynamic drag, basically the parachute approach. A more elaborate approach would be to employ aerodynamic surfaces which will yield a

smaller descent rate such as the glider concept. The potentialities of these approaches are discussed separately in the following paragraphs.

(1) Parachutes. - The settling rate of a parachute is given<sup>11</sup> by:

$$V_s = \sqrt{\frac{2W}{d_a (C_D S)}} \quad (5-10)$$

where

$W$  = weight of the suspended load and parachute

$d_a$  = air density

$C_D$  = drag coefficient

$S$  = cross-sectional area of the parachute

Conventional parachute practice is to design for descent rates of approximately 5 to 15 meters per second. For the support of dipoles, the maximum tolerable descent rate would be approximately 3 m/sec, which would result in the loss of 12-km/hr altitude.

The canopy loading (mass/area) required for this velocity at sea level is approximately 580 gm/m<sup>2</sup>. Since the air density at 30-km altitude is approximately 1/70 of that at sea level, the required loading would be 8 gm/m<sup>2</sup>. The lightest Mylar parachutes which can be envisioned for this purpose would weigh approximately 15 gm/m<sup>2</sup> for the parachute alone. Therefore, the conclusion is that the descent rate of parachute systems at 30-km altitude will be too high to provide useful support of the dipoles.

(2) Gliders. - Gliders, being more efficient aerodynamically than parachutes, deserve consideration. A typical figure-of-merit for a conventional low-speed glider is a 20-to-1 glide ratio. Assuming that this could be maintained in a light-weight, high-altitude glider, and that the flight velocity could be limited to 40 m/sec, the descent rate would be 2 m/sec, which is within the range of interest in this application.

In order to maintain the low-flight speed mentioned previously, it will be necessary to develop an extremely light-weight structure, where the wind loading is reduced radically (factor of 10 or more) from conventional practice. A likely method of construction would be a shaped, constrained, inflated body. Small aircraft with inflatable wings have been successfully demonstrated. Such a glider could conceivably be launched from a small rocket, such as the Arcus rocket. However, the problem of inflating the glider is basically the same as delivering a balloon system, which has the advantage of the buoyant gas and constant altitude maintenance over longer period. Therefore, it appears that the glider system would not be a preferred approach.

b. Buoyancy Systems

(1) General. - Consideration has been given to supporting scatterers by balloons. Such a system could take the form of many balloons, either with a conductive coating or carrying one or more dipoles, or one larger balloon carrying many dipoles in an ordered array. The latter system appears to be the best for the following reasons:

- 1) The relative position of the dipoles is maintained so the dipoles may be used most efficiently.
- 2) At altitudes of 30 km or higher, the size of the balloon required to carry an ordered array of dipoles will not be greatly different than that of a balloon for a single dipole. This situation occurs because the mass of the dipoles will be small compared to the balloon, so a small increase in volume will permit the system to be in equilibrium.
- 3) Proper delivery and inflation of a single balloon is more easily accomplished than placement of a large number of balloons to serve the same purpose.

(2) Arrangement of Dipoles. - In the single-balloon system discussed in paragraph (1), the dipoles could be arranged in several ways. The three arrangements that appear most practical are:

- 1) dipoles suspended in a long chain below the balloon
- 2) dipole conductors fastened to the balloon skin at selected points to maintain the desired arrangement
- 3) dipoles placed directly on the balloon skin, by employing printed circuit techniques.

Of these arrangements, the first configuration appears to be the most flexible because the dimensions of the dipoles are independent of the size, shape, material and method of fabrication of the balloon. However, the latter two configurations also have attractive features, such as compactness and a minimum chance that the desired array of dipoles will be displaced by wind-shear effects.

The electronic performance of the dipoles is discussed extensively in Section II of this report.

(3) Size of the Required Balloons. - The volume of a balloon which will float in equilibrium at a given altitude is directly proportional to the total mass of the system, including the balloon itself and the payload. In this case the total mass equals the buoyancy produced which is equal to the mass of the air displaced minus the mass of the lifting gas;

$$W_B + W_L = V_B ( \rho_a - \rho_g ) \quad (3-11)$$

where:

$W_B$  = the mass of the balloon

$W_L$  = the mass of the payload

$V_B$  = the volume of the balloon

$\rho_a$  = the density of the air at the altitude in question

$\rho_g$  = the density of the lifting gas at the floating condition.

Equation (3-11) may also be written in the form

$$W_B + W_L = \left( \frac{P_a M_a}{R T_a} - \frac{P_g M_g}{R T_g} \right) \quad (3-12)$$

where:

$P_a$  and  $P_g$  = the absolute pressures of the air and the lifting gas, respectively.

$M_a$  and  $M_g$  = the molecular weight of the air and the lifting gas, respectively.

$T_a$  and  $T_g$  = the absolute temperatures of the air and lifting gas, respectively.

$R$  = the universal gas constant.

In determining the size of stratospheric constant level balloons, it is generally assumed that  $P_a$  and  $P_g$  are equal and  $T_a$  and  $T_g$  are equal. It is well known that there are common exceptions to both of these assumptions, but they have a minor influence on the required size. Equation (3-12) becomes.

$$W_B + W_L = V_B \left( \frac{P_a}{R T_a} \right) (M_a - M_g) \quad (3-13)$$

The lifting gases commonly used in balloons are helium ( $M=4$ ) and hydrogen ( $M=2$ ). It can be seen that, although hydrogen is one-half as dense as helium, the net effect on the size of a balloon system is small, since

$$\text{hydrogen, } M_a - M_g \cong 27$$

$$\text{helium, } M_a - M_g \cong 25$$

Recognizing this small difference, helium is selected most frequently because it is safe to handle. At standard sea level conditions, Equation (3-13) reduces (for helium) to

$$W_B + W_L = 0.94 V_B \text{ (in Kg/m}^3 \text{ at sea level)}$$

If we introduce a term,  $\sigma$ , which is the dimensionless ratio of the air density at any altitude in question to that at sea level, we have

$$W_B + W_L = 0.94 \sigma V_B \quad (3-14)$$

where  $W_B$  and  $W_L$  are in kilograms and  $V_B$  is in cubic meters.

(a) Spherical Balloons. - To investigate an example system we will assume:

- 1) Altitude 30 km, where  $\sigma \cong 1/70$
- 2)  $W_L$  negligible compared to  $W_B$
- 3) Spherical balloon shape, for which

$$W_B = 4 \pi r^2 t d_m$$

and

$$V_B = 4/3 \pi r^3$$

where:

$r$  = the balloon radius

$t$  = the thickness of the skin

$d_m$  = the density of the balloon material



then:

$$4 \pi r^2 t d_m = \frac{0.94}{70} (4/3 \pi r^3)$$

$$t d_m = \frac{0.94}{210} r$$

and

$$r = 223 t d_m$$

For a minimum weight balloon, two common materials are

$$\text{Mylar } d_M \cong 1.4 \times 10^3 \text{ kg/m}^3$$

$$\text{minimum thickness, } t = 6.3 \times 10^{-6} \text{ m}$$

and

$$\text{polyethylene } d_M \cong 0.9 \times 10^3 \text{ kg/m}^3$$

$$\text{minimum thickness, } t = 12.6 \times 10^{-6} \text{ m}$$

Therefore, for the Mylar balloon at 30-km altitude,

$$r = 223 t d_M = 223 (6.3 \times 10^{-6}) (1.4 \times 10^3)$$

$$\cong 2.0 \text{ meters}$$

For the polyethylene balloon at 30-km altitude

$$r = 223 t d_M = 223 (12.6 \times 10^{-6}) (0.9 \times 10^3)$$

$$\cong 2.5 \text{ meters}$$

(b) **Natural-Shape Balloons.** - Balloons which are vented to the atmosphere (at the lowest point while they are floating) assume a "natural" shape, as shown in Figure 3-11.

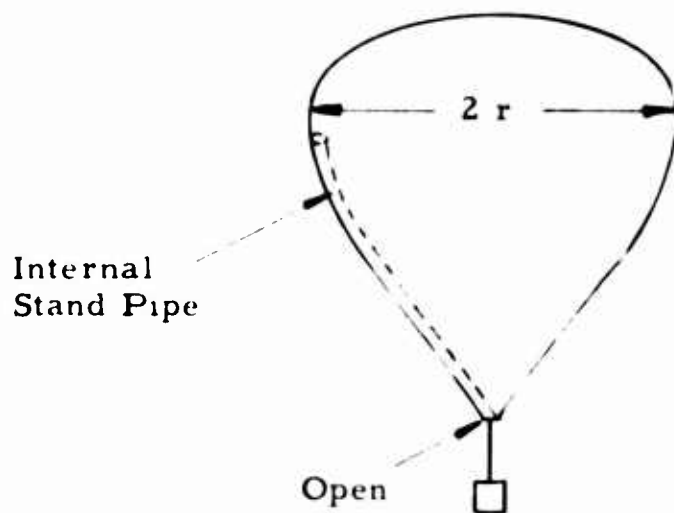


Figure 3-11. Natural-Shape Balloon

This shape results from the combined effects of the weight of the skin, the load, and the pressure distribution caused by the gas. Although the shape varies somewhat with variations in these parameters, the volume is approximately

$$V_B = 3.8 r^3$$

For the spherical balloon,

$$V_B = 4/3 \pi r^3 = 4.2 r^3$$

It can be seen from the above that for a given volume the radius of the natural-shape balloon will be slightly larger. However, this difference is so small that the main findings are not altered.

(c) **Conclusion Relative to Balloon Size.** - As shown in paragraph (a), spherical balloons of approximately 2.0 meters (Mylar) or 2.5 meters (polyethylene) theoretically meet the minimum requirements for supporting a negligible load at 30 km. In actual fabrication of balloons, the seams and end-fittings increase the weight slightly, so that a modest increase in the required size results.

(4) **Balloon Flight Duration.** -

(a) **Unpressurized Balloons.** - The flight duration of a vented, free-floating balloon is limited by diffusion through the skin and thermodynamic effects. The main thermodynamic effects of interest to us are associated with sunset and sunrise.

During a daytime flight the gas inside the balloon is heated somewhat by the sun. Expansion drives some of the gas (~10%) out of the balloon, through the open vent at the base of the balloon. The immediate effect of this is only to make the balloon rise slightly because of the reduced density of the lifting gas. However, at sunset, the gas contracts which upsets the equilibrium. If no correction action is taken, this causes the balloon to descend. In the case of the vented (unpressurized) balloon this effect is the main consideration and normally limits the flight duration to less than 24 hours. Two techniques are commonly employed to counteract this effect and extend the flight duration. They involve the use of ballasted balloons or pressurized balloons.

(b) **Ballasted Balloons.** - Ballasted balloons are capable of flight at reasonably constant (but increasing) altitude for periods of several weeks. However, for long duration rather large balloons are required which carry a large fraction of the gross system mass as ballast. At each sunset, ballast (amounting to about 10% of the gross system mass) must be released in order to counteract the cooling of the gas. Thus, by doubling the mass

of the system by adding ballast, a duration can be extended to several days. The operating altitude increases modestly each day as a result of the change in system weight.

(c) **Pressurized Balloons.** - It has been shown that the sunset effect can be counteracted with a pressurized balloon. In this technique a nearly constant volume system is maintained in contrast to the vented balloon which contracts at night by storing energy in the highly-stressed skin. At sunrise, the tendency for the (sealed) balloon to expand is counteracted by strong balloon skin, usually made of Mylar. Thus, the internal pressure rises, and the skin-stress increases, but the weight of air displaced and the mass of the lifting gas stay essentially constant. At sunset, the balloon returns to its original condition with no (theoretical) change in altitude.

Pressurized balloons are not extremely reliable in practice because of the high (daytime) stresses in the skin and the high differential pressure which will cause leakage through small imperfections in the balloon. The ballasted balloons discussed in paragraph (b) are considerably more reliable.

(d) **Conclusions on Balloon Flight Duration.** - In the typical meteorological situation, the wind velocity will be high enough to limit the useful life (due to horizontal travel) to a few hours. Therefore, the unpressurized balloons, discussed in (a), will be adequate. However, it may be worthwhile to also develop ballasted balloons, capable of longer duration, for use when low stratospheric wind velocities prevail.

### 3. Delivery of Balloon-Supported Scattering Systems

Three possibilities for delivery of this type of system have been investigated. These include first, the launch of the balloon from shipboard, secondly, the launch of the balloon from an aircraft, and third, rocket-launched balloons. Shipboard-launched balloons would be practical only if

a launching ship were available in the approximate area over which the scattering elements were required. For this case simple procedures could be employed to deliver balloons to an altitude of 30 km, rising in a period of approximately two hours due to their natural buoyancy. As balloons carrying scattering elements are displaced from the area of interest by the wind, additional balloons could be launched from the same ship as replacements.

Perhaps the most promising approach is the use of rockets carrying balloon systems. This approach would permit repeated delivery of the scattering elements to the required location and continuous support thereafter (if required) by repeated launchings of the same type. In order to employ simple rockets such as the Arcus, which has a payload capacity of approximately 25 pounds when operating in this altitude range, a ship-board launching situation would again be required. The major item in the rocket payload will be the inflation gas container, which can be expected to weigh approximately five times the mass of the balloon system it launches.

Long range delivery of balloon systems by rockets is entirely possible but would require considerably more elaborate rocket vehicles. In the case where it is necessary to deliver scattering elements to a location near the midpoint of a very long communication link, larger rockets delivered in a parabolic trajectory would be required. The economics of the approach are questionable except under emergency conditions.

The use of aircraft for delivery of the balloon system appears to be reasonable only in the case where the meteorological situation will permit a long useful duration of the balloon system. That is, it would be practical to deliver the system several hundreds of miles from the home base only during periods where balloons would stay in the area of interest for many hours. It is believed that adequate launching systems could be developed for this case.

As stated earlier, delivery of balloon-supported dipoles by rockets appears to be the best approach. For the case of a vertical rocket trajectory, the balloon would be inflated and ejected while the rocket was moving

at low velocity near the top of the trajectory. Where longer range and a parabolic trajectory are required, it is believed that a capsule must be released from the rocket which is equipped with a drag system (or retro-rockets in the most sophisticated system) for deceleration of the balloon package before inflation.

With respect to a field test of a system of this type for improvement of communication, we believe that a vertical rocket trajectory should be employed. The performance of the delivery system could be demonstrated in connection with experiments to evaluate the effectiveness of the scattering elements.

### C. The Effect of Meteorology on the Useful Life of Scattering Elements

#### 1. Introduction

Mean monthly maps of zonal winds, for the Arctic, North Atlantic, and North America, given in Appendix B, are used to describe the probable duration of tuned dipoles released at 30 km. Frequencies of wind direction are not discussed here in detail because for a given instance the direction will be known and an appropriate launch can be made. The time to transit the area is a function only of wind speed. The maps are excerpts from those prepared for Contract ONR 1589(20), supplemented by all data available at Asheville, North Carolina within the past five years for the areas of special interest. The map coverage includes areas of experimental and operational interest.

#### 2. Discussion of Zonal Wind Speeds at 30 km

In January strong westerlies (80 to 100 knots) prevail from 50°N to 90°N over the North Atlantic, while weaker westerlies (20 to 40 knots) are present over the continental United States. The pattern of zonal winds is

much the same in February with the exception that the speed of the westerlies decrease over continental North America and the Arctic. In March, although the frequency of westerlies remains high, their speed has been reduced over the entire area. Polar and tropical easterlies appear in April on the respective sides of a band of westerlies extending from  $30^{\circ}\text{N}$  to  $60^{\circ}\text{N}$ . The maximum speed of the westerlies is 30 knots while that of the easterlies is 20 knots. By May the westerlies have vanished and weak easterlies prevail throughout the region encompassed by the map. In June, July, and August, easterlies prevail, their speed gradually increasing to 40 knots over the southern half of the continental United States. The westerlies suddenly appear in September north of  $50^{\circ}\text{N}$ . Their maximum speed is 25 knots in a belt extending from  $50^{\circ}\text{N}$  to  $60^{\circ}\text{N}$ . South of  $50^{\circ}\text{N}$ , the winds are easterly with representative speeds of 20 knots. In October and November westerlies prevail north of  $30^{\circ}\text{N}$ . Speeds of 30 to 40 knots are representative of the Arctic and North Atlantic regions while over the continental United States, the speed of the westerlies is between 20 and 30 knots. Strong westerlies appear over Alaska in November reaching a speed of 60 knots. In December the pattern resembles that of January with 80-knot westerlies prevailing over the North Atlantic between  $60^{\circ}\text{N}$  and  $80^{\circ}\text{N}$  and winds of 20 to 40 knots occurring over the continental United States.

These zonal wind patterns may be summarized by saying the winter (October to February) has variable but generally strong prevailing westerly winds, and the summer has relatively constant, light easterly winds. It is to be realized that large variations in wind speed and direction may occur from September to May depending upon the orientation and movement of transient pressure centers and their associated gradients. The smaller features do not usually recur in a given area each year nor is the timing of the formation and breakdown of the large-scale seasonal vortices constant. One can expect, however, that the summer easterly circulation at highest latitudes is organized not later than the latter half of May and is destroyed not later than mid-September.

The present patterns at this level are sufficiently large scale and develop slowly enough so that forecasting winds over a given region is in many instances more reliable than at surface levels.

Table 3-2 gives estimates of the time in hours that a balloon carrying tuned dipoles can be expected to remain within an area of effective communication 128 km wide (Appendix A) at 10 mb (30 km) for three locations.

These estimates should be considered maximum average durations as:

- 1) The maximum trajectory across the effective relay volume has been used.
- 2) Zonal component speeds were used rather than scalar speeds which are slightly higher.

If release is made at 40 km, the winds will be stronger, but as the distance will also be greater, the useful duration within the volume should not be much different.

Table 3-2. Estimated time to the nearest one-half hour that an object will remain within a belt 128 km wide at 30 km altitude

Month	<u>Location</u>		
	Iceland	Port Barrow (Alaska)	Omaha, Nebraska
January	1	1.5	2
February	1	2	3
March	1.5	2.5	2.5
April	5	5	3
May	4	6	5
June	3	4.5	3
July	3.5	5.5	2.5
August	7	7	3
September	4.5	5	10
October	2	2	3.5
November	1.5	2	3
December	1	1	2



#### IV. BRIEF DESCRIPTION OF THE PROPOSED SYSTEM

While incomplete in that tuned scatterers much smaller than a wavelength were not investigated, our studies have led to an intermediate system which we consider economically feasible and useful in many situations. It has been theoretically demonstrated in this report that it would be possible to create a useful scatter propagation path over 1430 km by placing a configuration of about 50 tuned dipoles at 30 km altitude at a point midway between the receiver and transmitter.

Because replacement of the scattering system will often be necessary every few hours due to weather conditions, a rocket delivery system appears to be the most feasible (alternate delivery systems are discussed in paragraph III. B. 3). A ship near the center of the desired communication path would fire a rocket similar to those used in meteorological soundings, in the upwind end of the volume of interest (see Appendix A). The balloon and scatterers would be released at altitude and drift through this volume with the wind. When the scatterers drift out of the critical volume of space, the system would be destroyed on command of the launching ship and be replaced with a new scattering system.

Placing the scatterers at the path midpoint is necessary only when communication over the maximum range of 1430 km is required. For ranges less than 715 km, the scatterers could be launched by the party wishing to establish the communication link.

Because this system employs so few airborne elements, the control of these elements becomes much simpler. Each scattering system would carry a simple self-destruction unit to operate on command from the ground or from an internal timer. The chances that these scatterers would offend friendly or neutral nations or fall into the hands of unfriendly nations would be remote.

## V. PROPOSED PROGRAM

The first step in a program designed to equip the Navy with the ability to improve electromagnetic propagation would be to prove the elements of the system. Work to be conducted would include.

- 1) Field testing of the dipole configuration described in paragraph II. A over a range great enough for suppression of the direct propagation path.
- 2) Investigation of techniques of packaging the dipole configurations with supporting balloons.
- 3) Development of methods of deploying the balloon and dipoles from the rocket payload housing while ensuring proper balloon inflation at altitude.

Concurrent with the practical development of the necessary techniques a study would be conducted for the development of optimum dipole configurations for other frequencies.

After development and testing of the various techniques, field testing of the entire system should be carried out at sea. Dipole arrays would be built for the specific frequencies of interest and rocket launched at sea. The scatter communication path could then be evaluated under actual conditions.

## VI. REFERENCES

- 1) Hogg, D. C. and W. W. Mumford, The Effective Noise Temperature of the Sky, The Microwave Journal, Vol. 3 No. 3 p. 80.
- 2) Jordan, E. C., "Electromagnetic Waves and Radiating Systems" New York, Prentice-Hall, 1950 p. 459.
- 3) Lapple, C. E., Fluid and Particle Mechanics, Univ. of Delaware, March 1951 p. 285.
- 4) Stern, S. C., et al, J. Coll. Sci. 15, 546-61 (1960).
- 5) Fresnel, Amer. Chem. Phys. 29, 57 (1825).
- 6) Rosenblatt, P., et al, Phys. Rev. 70, 385 (1946).
- 7) Epstein, P. S., Zeits f. Physik 30, 258 (1924).
- 8) Sexl, T. Zeits f. Physik 52, 261 (1928).
- 9) Hettner, G. et al, Zeits f. Physik 30, 258 (1924).
- 10) Einstein, A., Zeits f. Physik 27, 1 (1924).
- 11) United States Air Force Parachute Handbook, WADC Technical Report 55-265, ASTA Document No. AD 118036, Wright Air Development Center, December 1956, pp 5-2-2.

## APPENDIX A

### GEOMETRY OF SPACE WITHIN WHICH SCATTERERS WOULD BE USEFUL

In order to estimate deployment feasibility and probable useful life due to settling and meteorological conditions, the space within which a scattering system would be useful must be defined. This space would have an ultimate upper altitude limitation at the bottom of the "D" layer of the ionosphere (about 50 km), and may also be limited practically by the deployment or lifting technique employed. As previously mentioned, the scattering system must be above both the plane tangential to the earth's surface at the receiver and the plane tangential to the earth's surface at the transmitter. This geometry is illustrated in Figure A-1. The heavy lines enclose the discussed space of interest. The dimensions of this space in terms of minimum altitude (h), maximum altitude (h+Δh) and the earth's radius (ρ) follows. This spherical section has a depth of (Δh), its short dimension (a) is along the propagation path and its long dimension (b) is perpendicular to the propagation path.

The dimensions of this space for two cases are given in the following examples.

#### Example 1:

$$\rho = 8500 \text{ km}, \quad h = 30 \text{ km}, \quad \Delta h = 5 \text{ km}$$

$$\cos \alpha = \frac{\rho}{\rho + h}$$

$$= \frac{8500}{8530}$$

$$\alpha = 0.0840$$

$$\cos \beta = \frac{\rho}{\rho + h + \Delta h}$$

$$= \frac{8500}{8535}$$

$$\beta = 0.0915$$

$$\cos \gamma = \frac{\rho + h}{\rho + h + \Delta h}$$

$$= \frac{8530}{8535}$$

$$\gamma = 0.0346$$

$$d = 2 \alpha \rho$$

$$= 2(0.0840) (8500) \text{ km}$$

$$= 1,428 \text{ km}$$

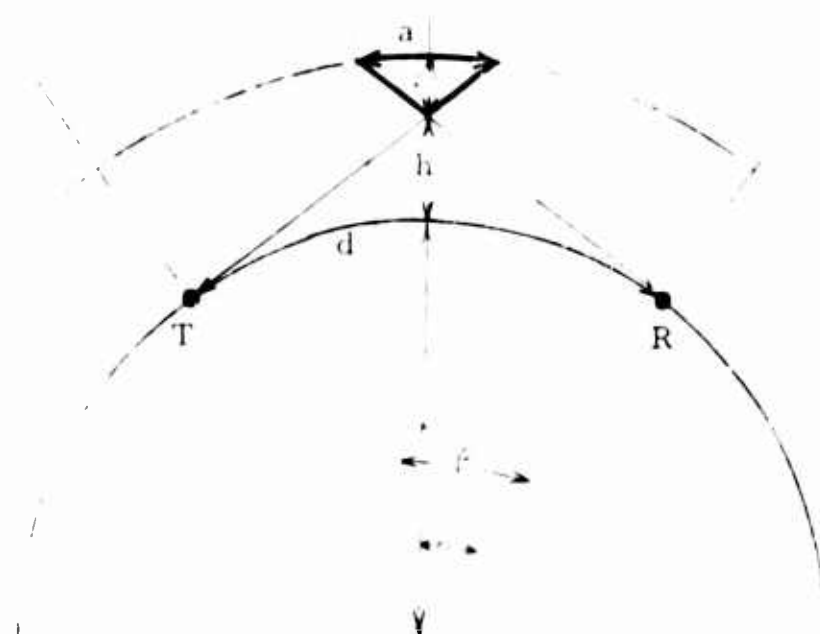
$$a = 2(\beta - \alpha) (\rho + h + \Delta h) \quad b = 2 \gamma (\rho + h + \Delta h)$$

$$= 2(0.0075) (8535) \text{ km}$$

$$= 128 \text{ km}$$

$$= 2(0.0346) (8535) \text{ km}$$

$$= 591 \text{ km}$$



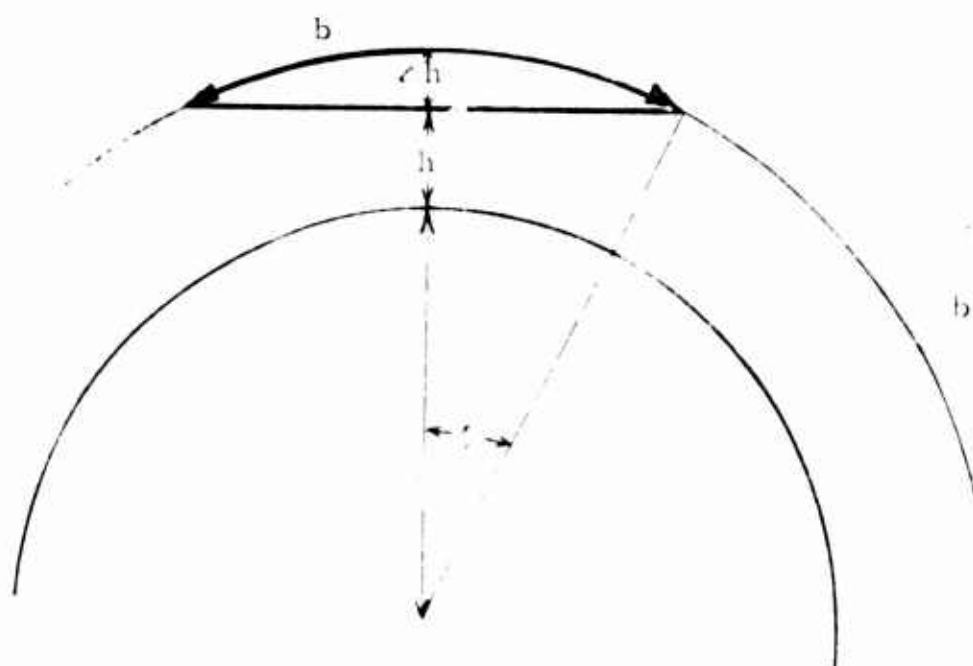
$$\theta = \arccos \frac{R}{R+h}$$

$$\phi = \arccos \frac{R}{R+h+d}$$

$$\alpha = 2(\theta - \phi)$$

$$a = 2(R \sin \theta \cos \phi) \quad (1)$$

Plane defined by the earth's center, the transmitter (T), and the receiver (R)



$$\theta = \arccos \frac{R}{R+h+h}$$

$$b = 2(R \sin \theta \cos \theta)$$

Plane normal to above plane at the midpoint of the communication path

Figure A-1. Geometry of Space Useful for Scattering

Example 2

$$\rho = 8500 \text{ km}, \quad h = 30 \text{ km}, \quad \Delta h = 20 \text{ km}$$

$$\cos \alpha = \frac{\rho}{\rho + h}$$

$$= \frac{8500}{8530}$$

$$= 0.0840$$

$$\cos \beta = \frac{\rho}{\rho + h + \Delta h}$$

$$= \frac{8500}{8550}$$

$$= 0.1081$$

$$\cos \gamma = \frac{\rho + h}{\rho + h + \Delta h}$$

$$= \frac{8530}{8550}$$

$$= 0.0683$$

$$d = 2 \alpha \rho$$

$$= 2(0.0840)(8500) \text{ km}$$

$$d = 1,428 \text{ km}$$

$$a = 2(\beta - \gamma)(\rho + h + \Delta h)$$

$$= 2(0.0241)(8550) \text{ km}$$

$$a = 412 \text{ km}$$

$$b = 2\delta(\rho + h + \Delta h)$$

$$= 2(0.0683)(8550) \text{ km}$$

$$b = 1,168 \text{ km}$$

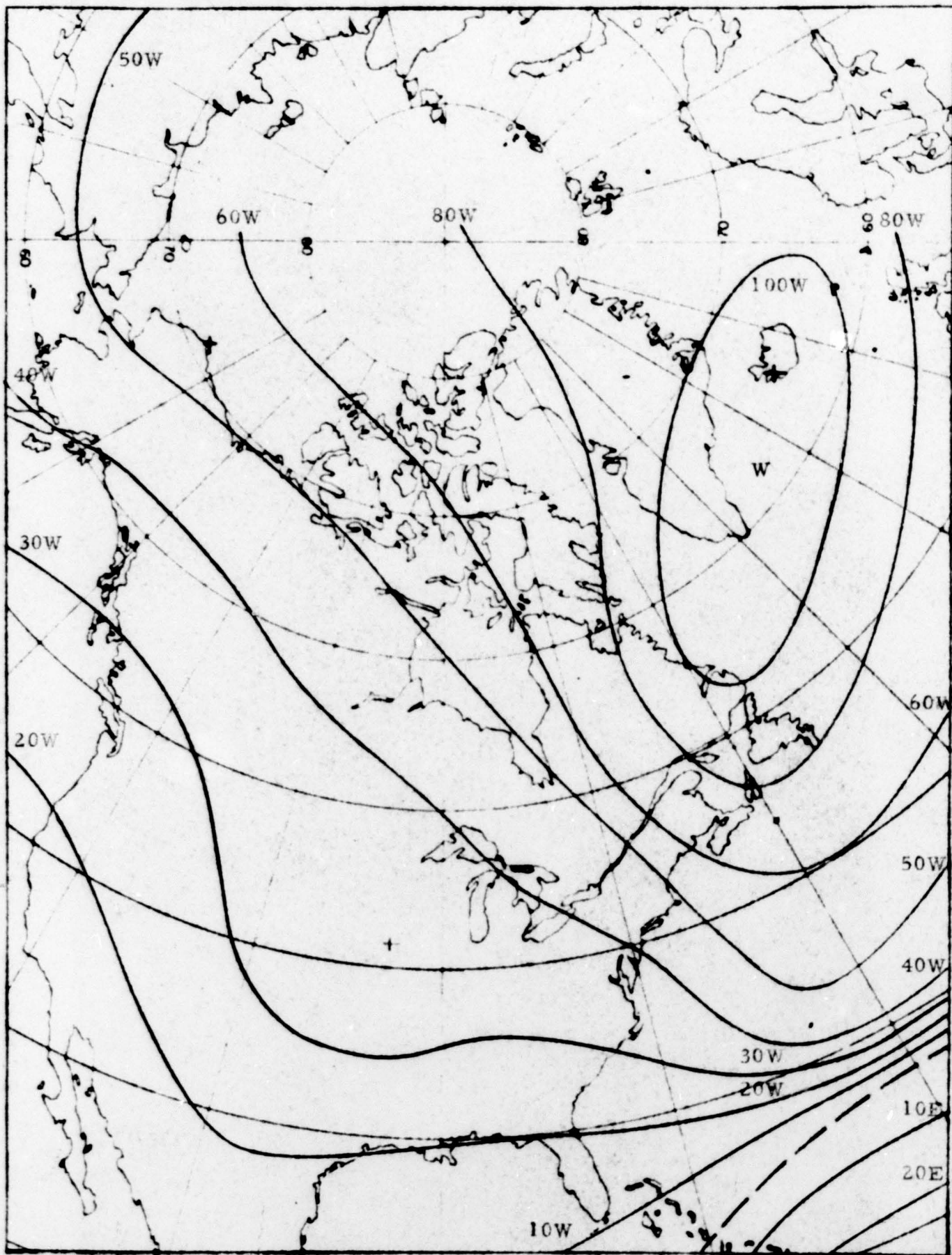
## APPENDIX B

### AVERAGE ZONAL COMPONENT OF PREVAILING WIND IN KNOTS BY MONTH AT 10 mb (30 km)

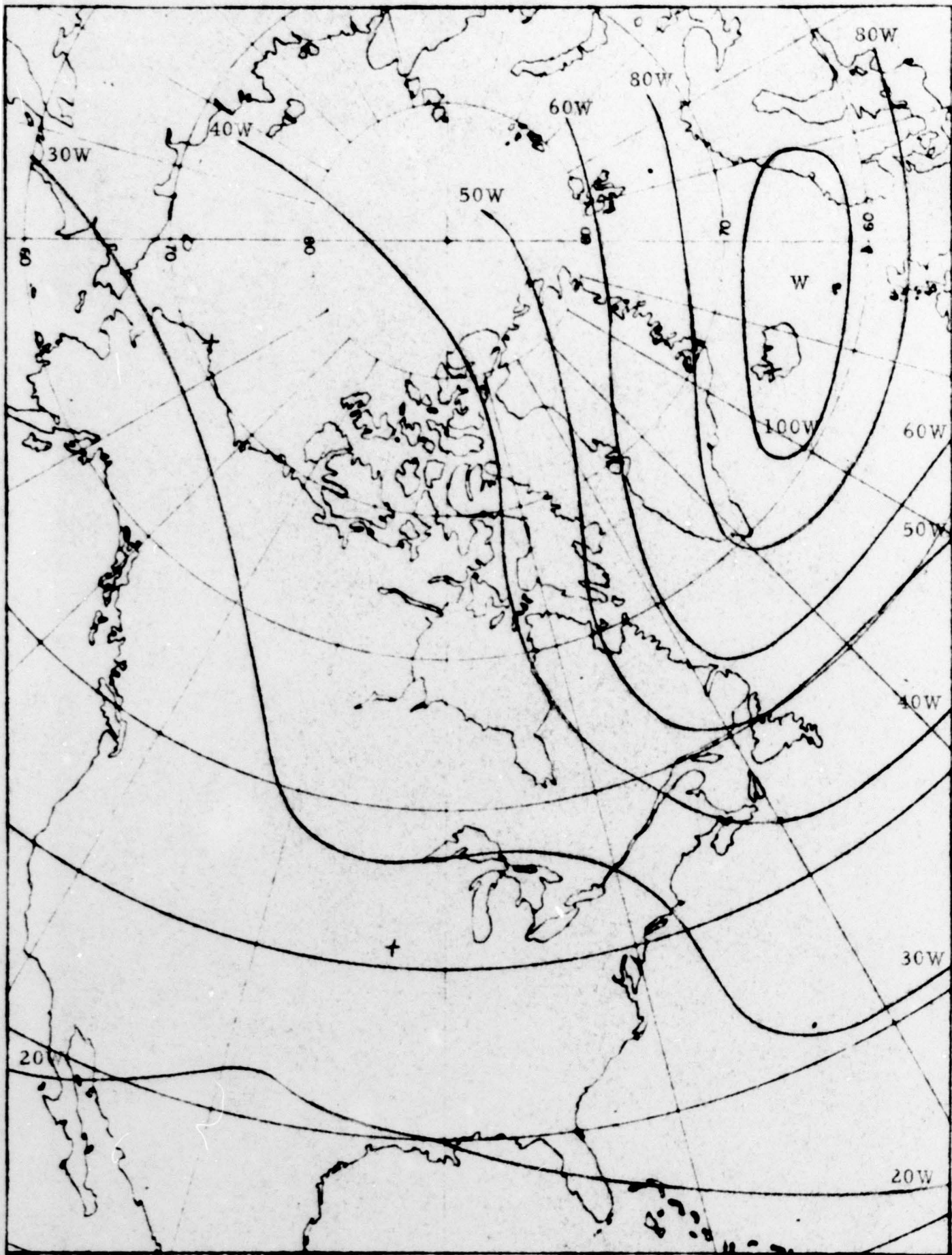
.



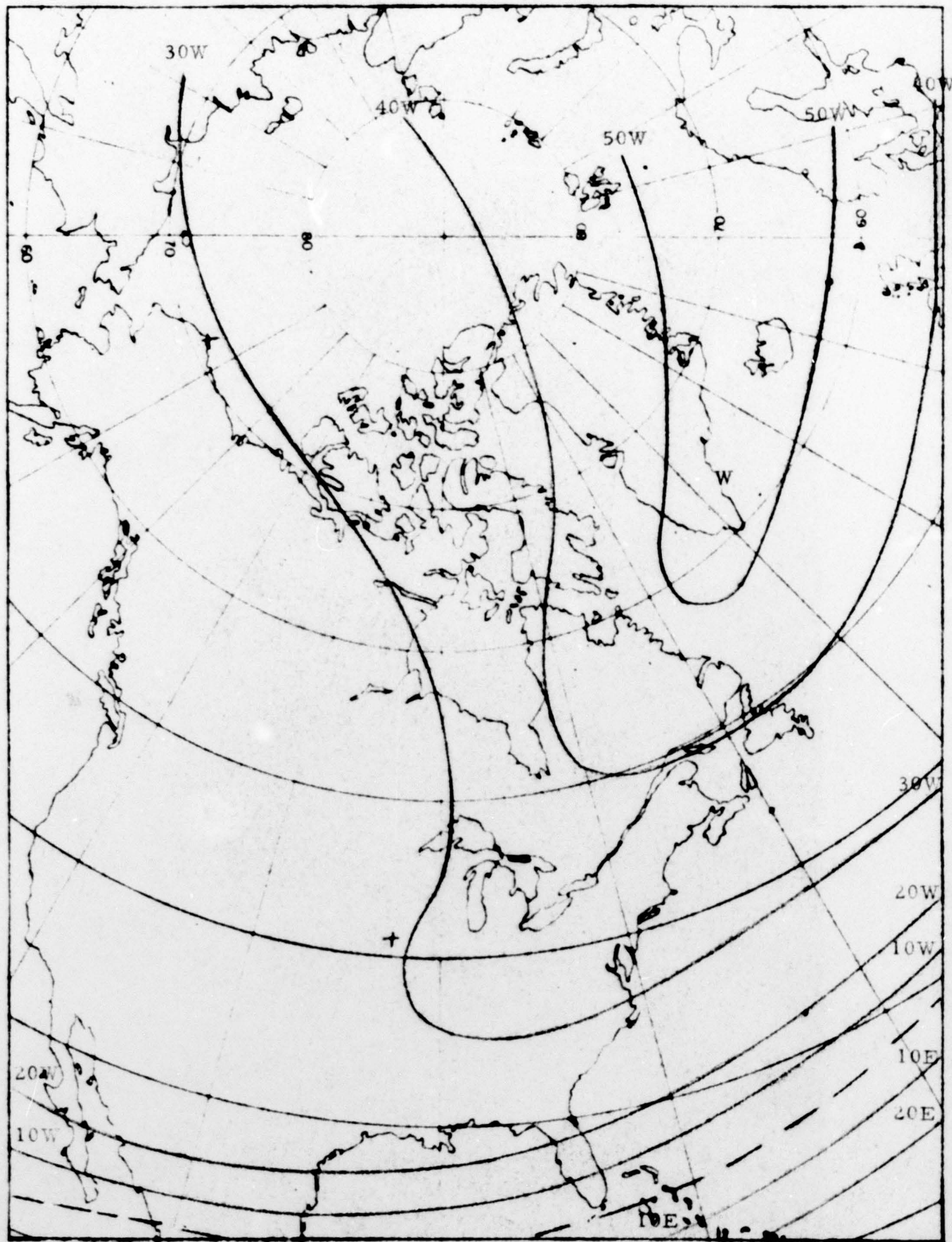
The graphs in this appendix show the zonal component of prevailing wind in knots at 10 mb (30 km) for each of the twelve months of the year. The dashed line represents the boundary between the prevailing east and west wind.



JANUARY

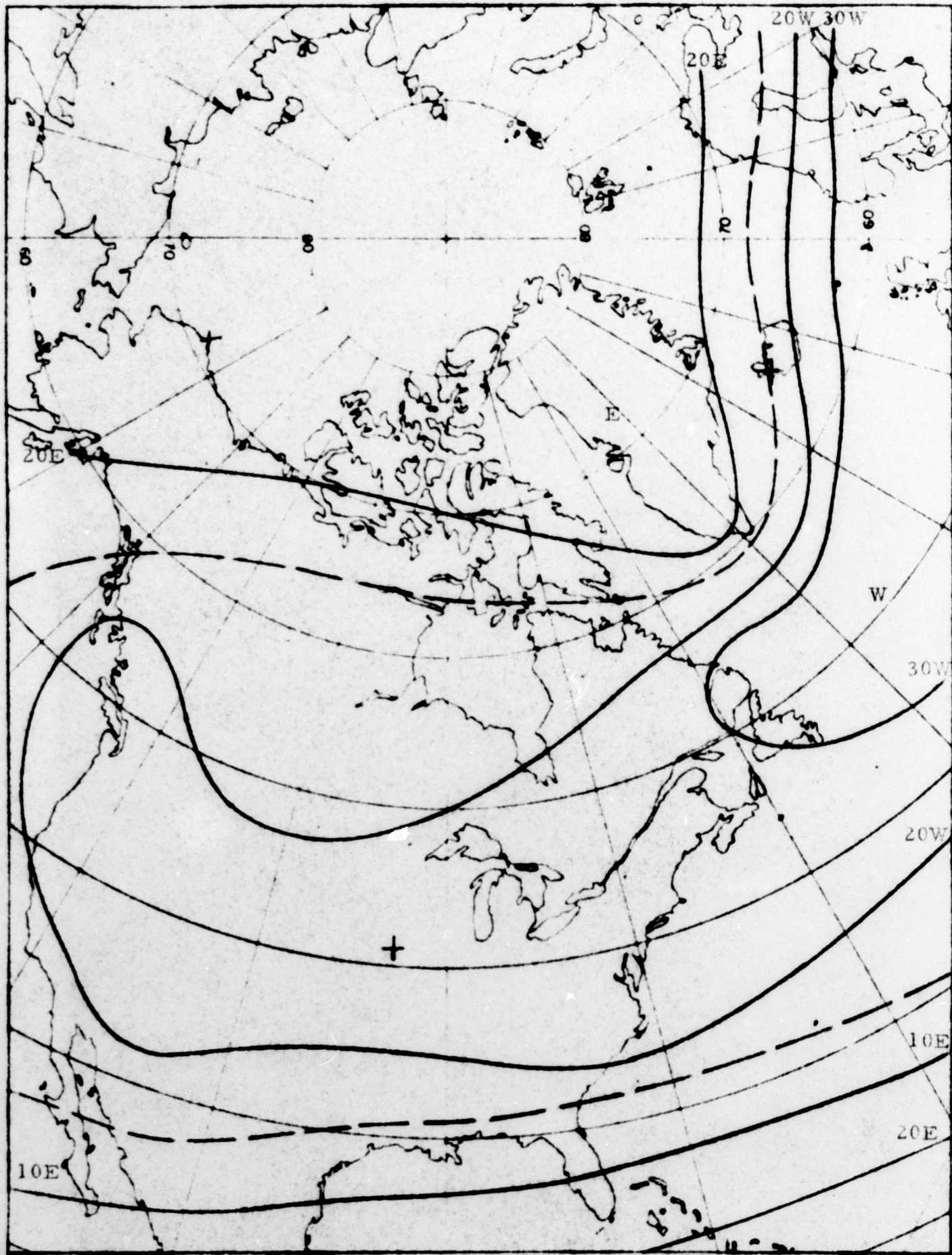


FEBRUARY

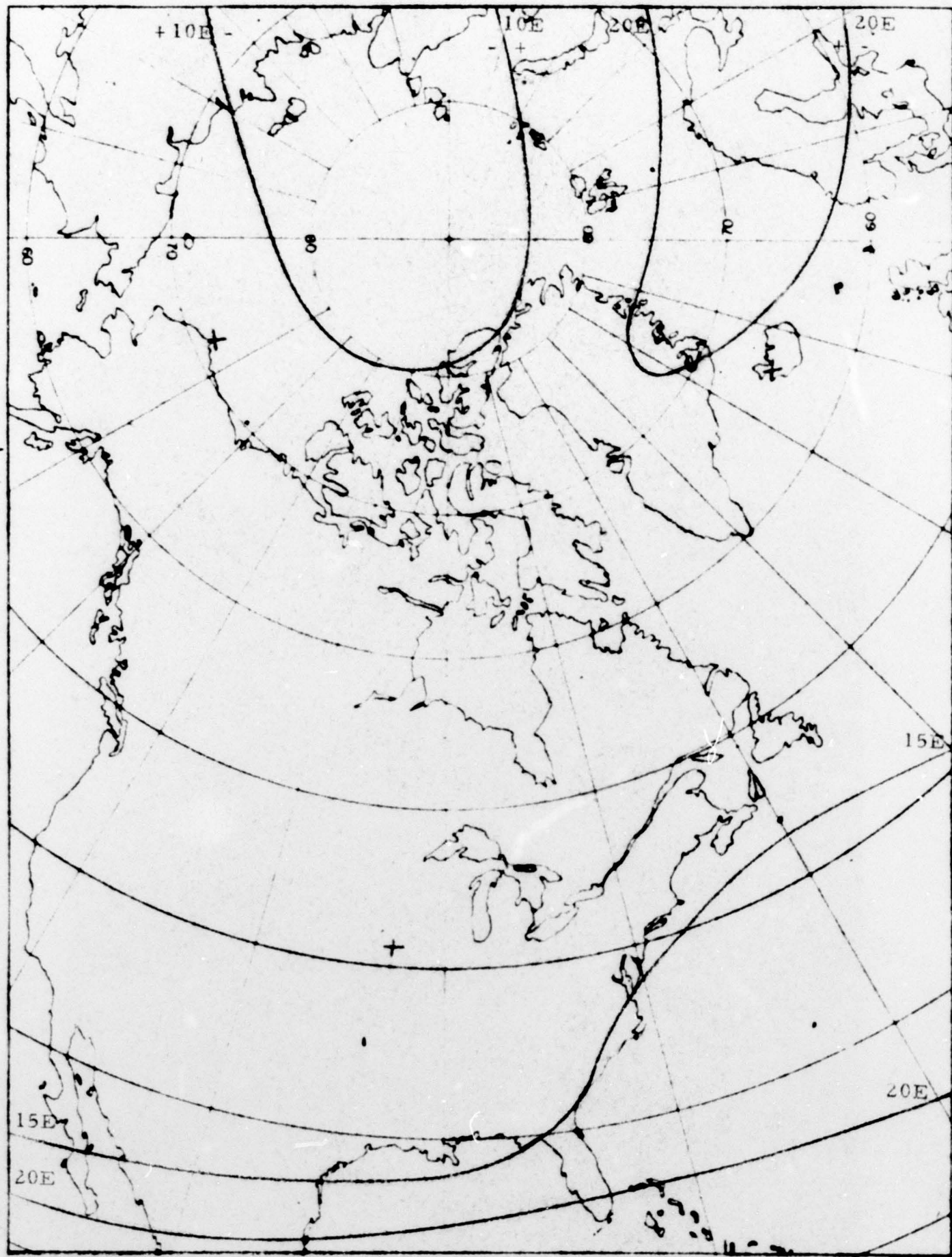


MARCH

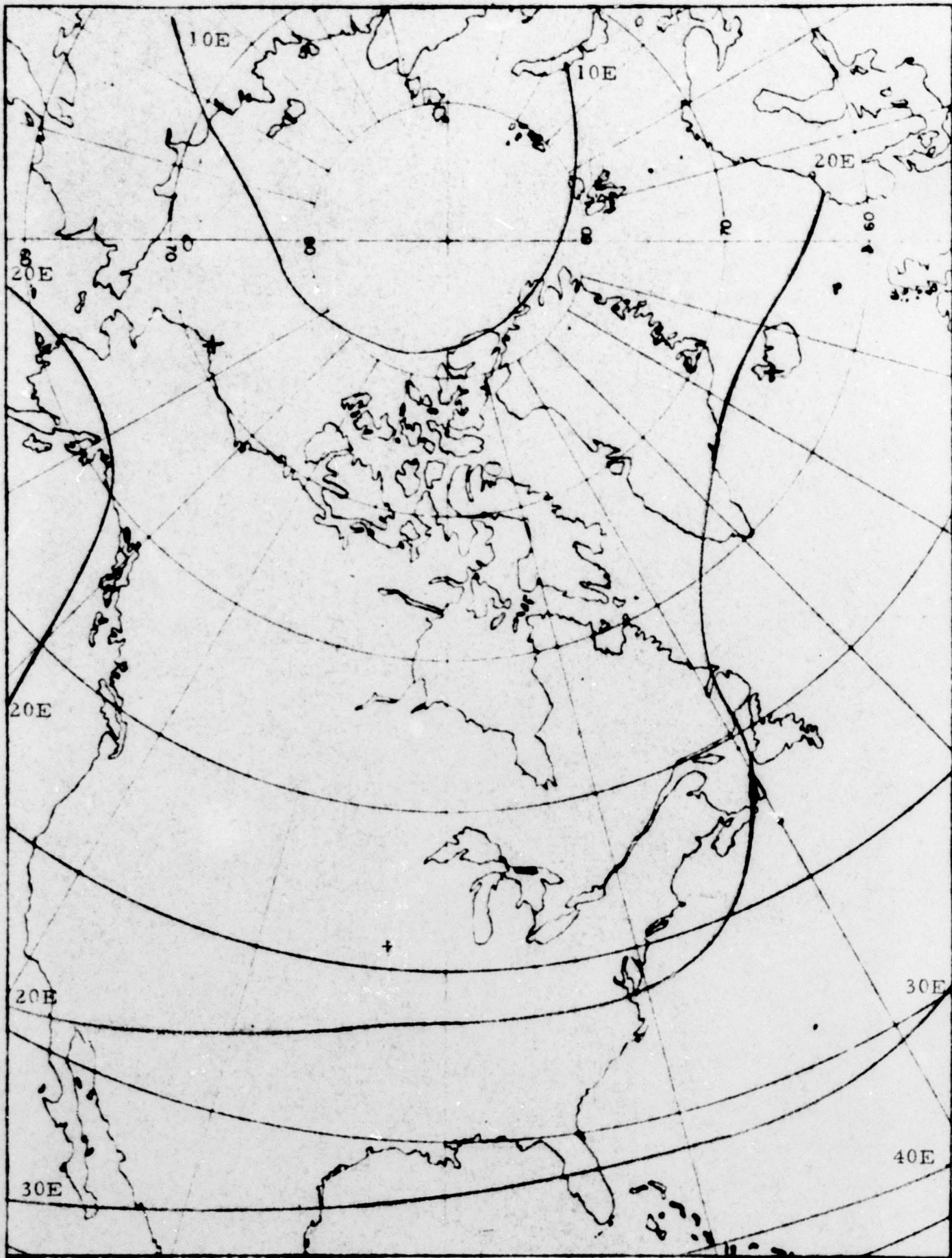




APRIL

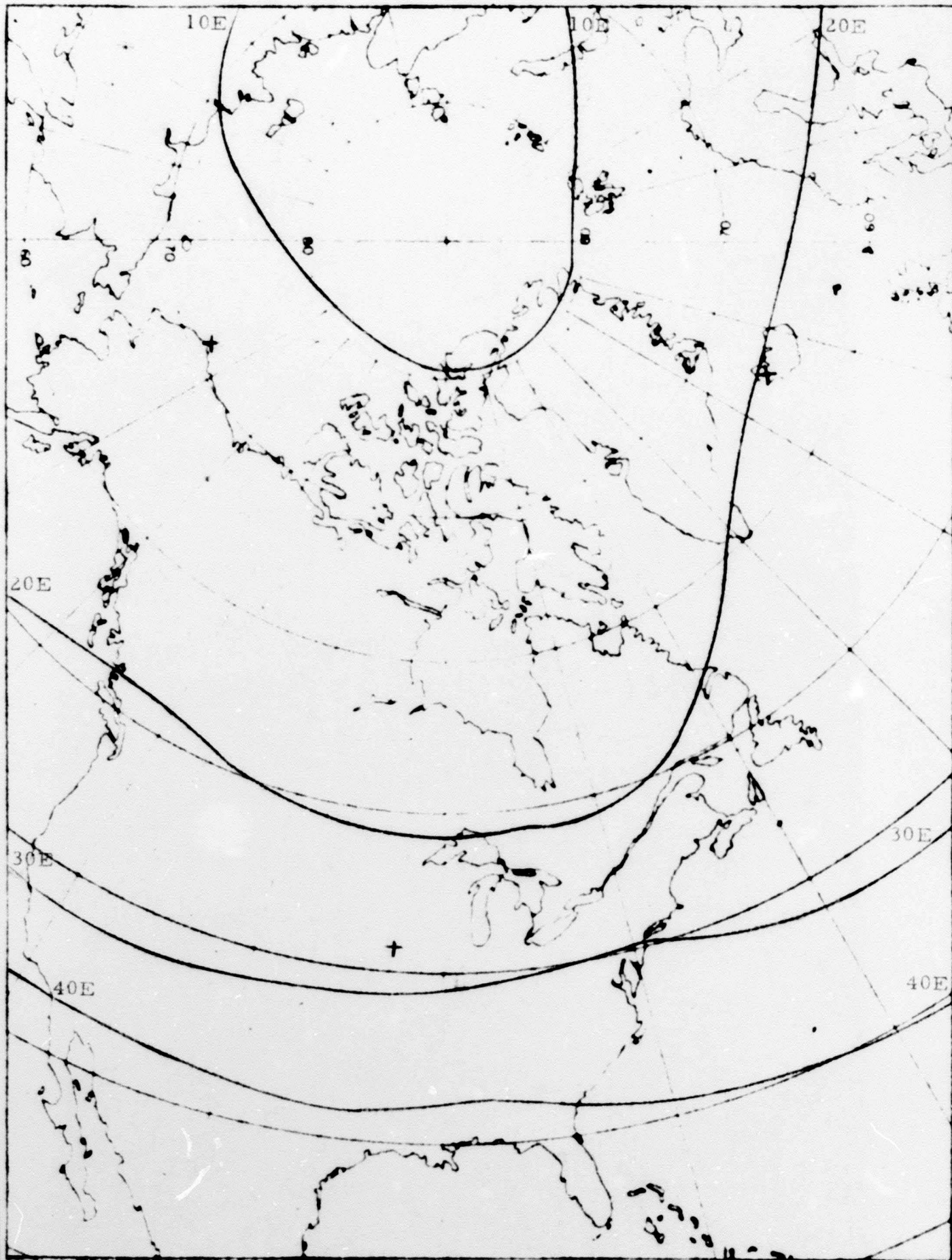


MAY



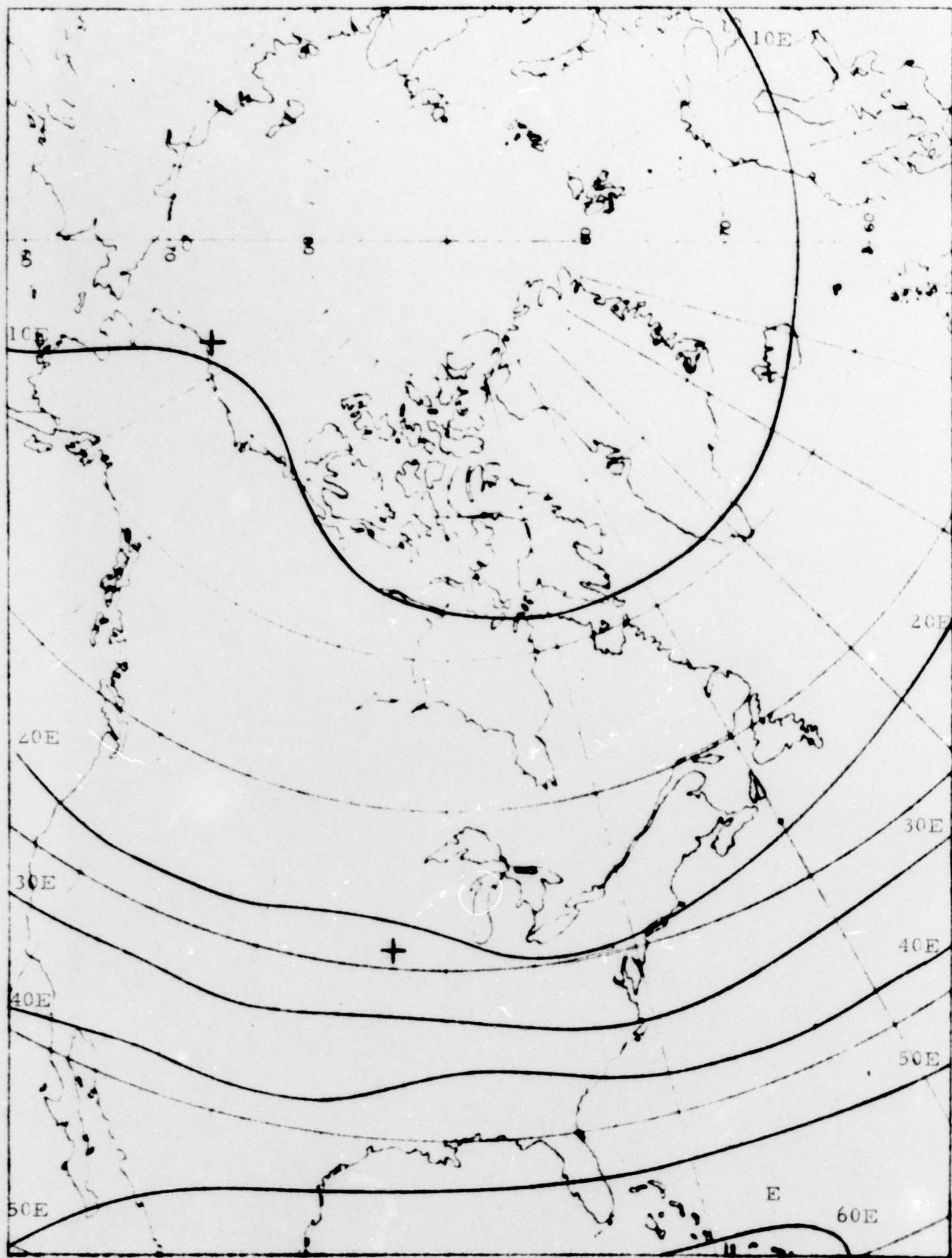
JUNE



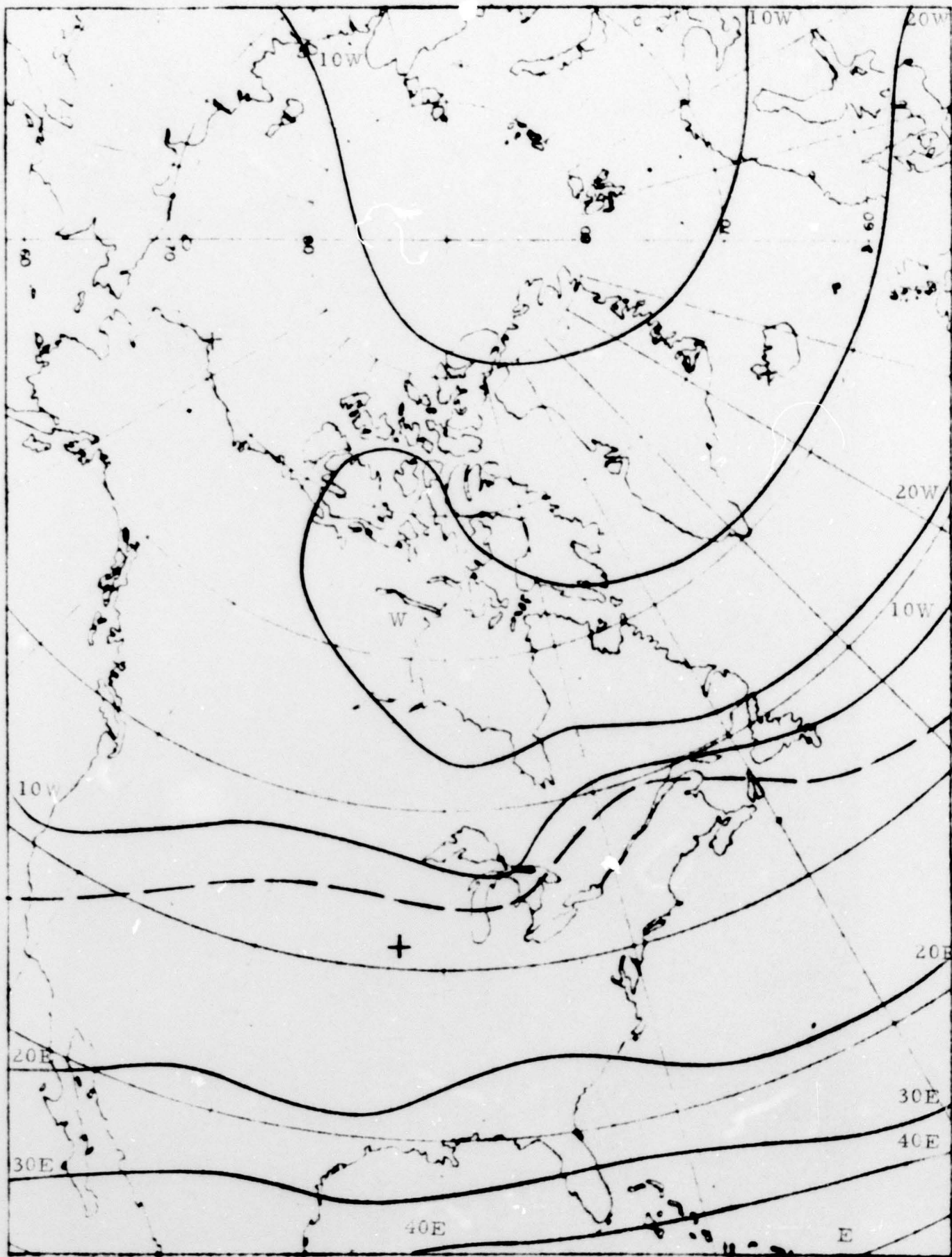


JULY

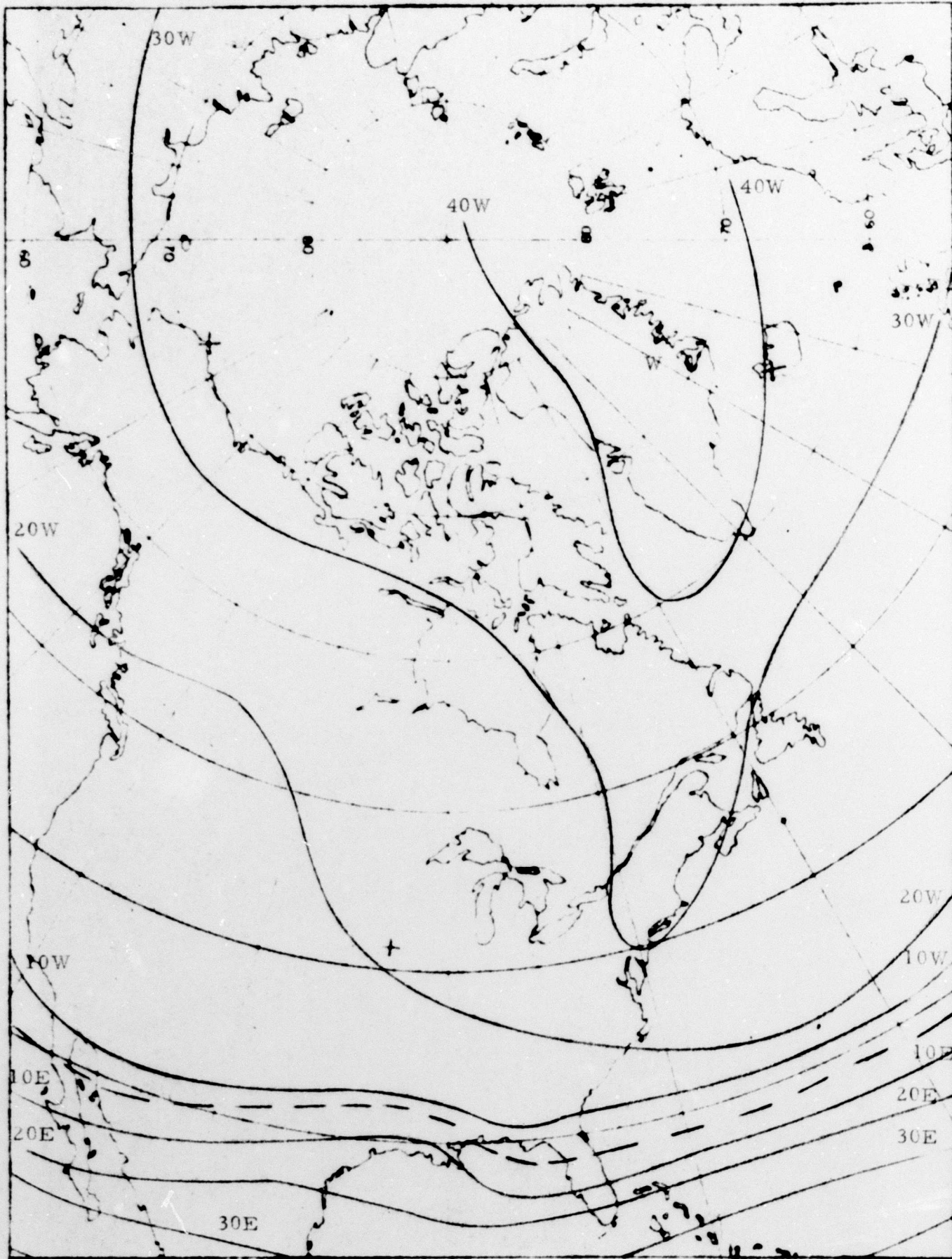




AUGUST

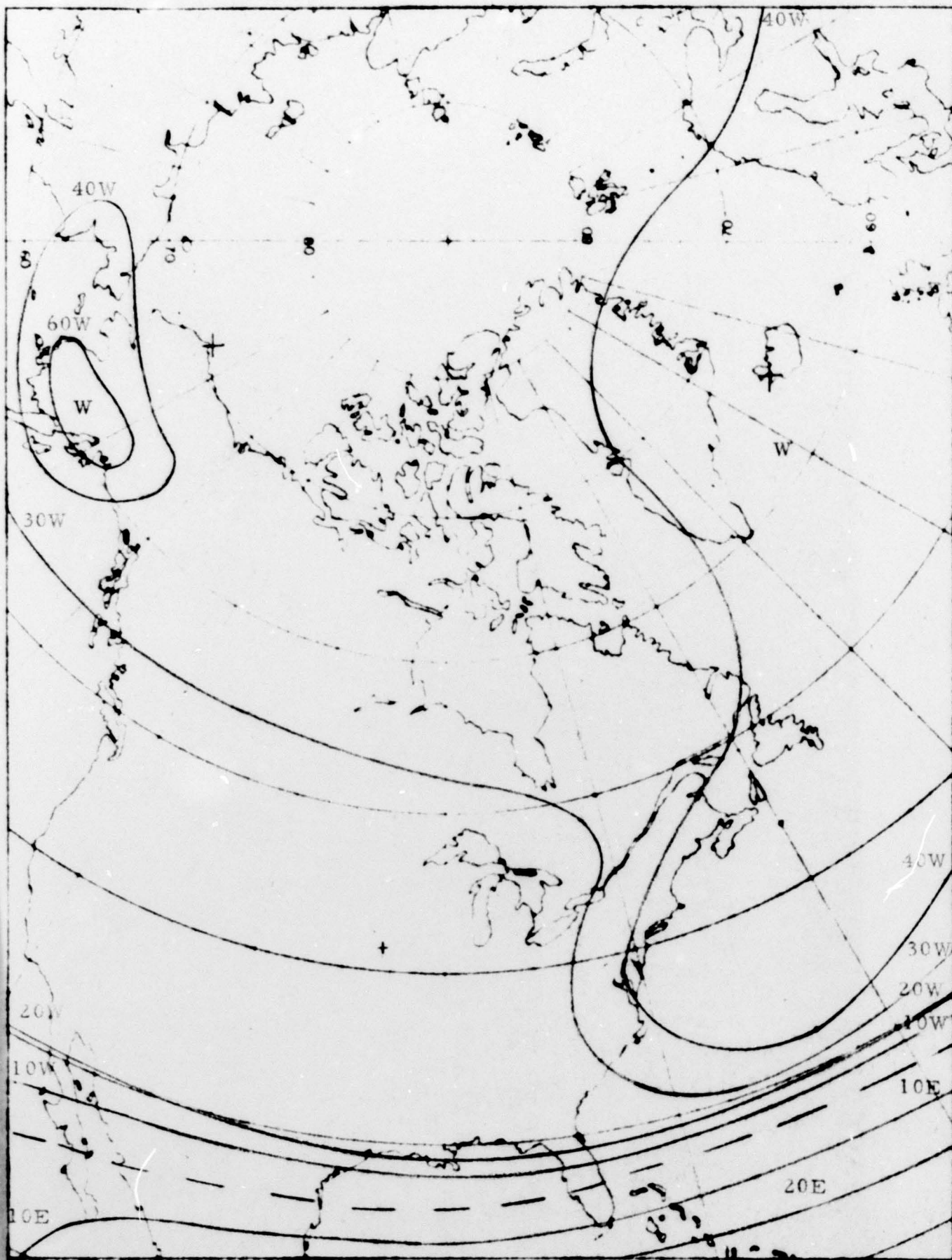


SEPTEMBER

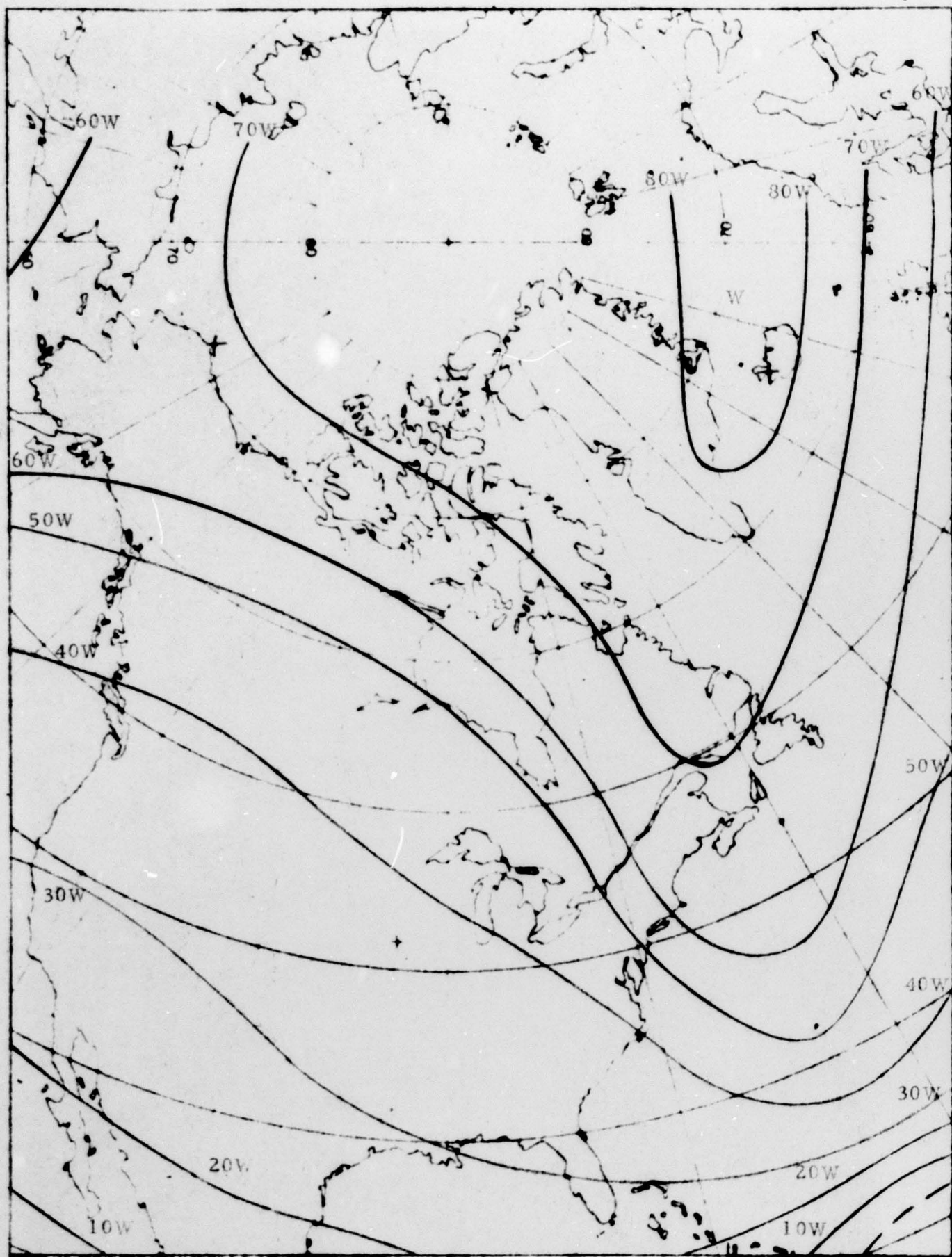


OCTOBER





NOVEMBER



DECEMBER